OPEN ACCESS

KING'S College LONDON

King's Research Portal

DOI:
10.1016/j.biopsych.2018.11.026

Document Version
Peer reviewed version

Link to publication record in King's Research Portal

Citation for published version (APA):
Peterson, B. S., Zargarian, A., Peterson, J. B., Goh, S., Sawardekar, S., Williams, S. C. R., Lythgoe, D. J., Zelaya, F. O., & Bansal, R. (2018). Hyperperfusion of Frontal White and Subcortical Gray Matter in Autism Spectrum Disorder. *Biological psychiatry*. https://doi.org/10.1016/j.biopsych.2018.11.026

Citing this paper
Please note that where the full-text provided on King's Research Portal is the Author Accepted Manuscript or Post-Print version this may differ from the final Published version. If citing, it is advised that you check and use the publisher's definitive version for pagination, volume/issue, and date of publication details. And where the final published version is provided on the Research Portal, if citing you are again advised to check the publisher's website for any subsequent corrections.

General rights
Copyright and moral rights for the publications made accessible in the Research Portal are retained by the authors and/or other copyright owners and it is a condition of accessing publications that users recognize and abide by the legal requirements associated with these rights.

•Users may download and print one copy of any publication from the Research Portal for the purpose of private study or research.
•You may not further distribute the material or use it for any profit-making activity or commercial gain
•You may freely distribute the URL identifying the publication in the Research Portal

Take down policy
If you believe that this document breaches copyright please contact librarypure@kcl.ac.uk providing details, and we will remove access to the work immediately and investigate your claim.

Download date: 05. May. 2023

Accepted Manuscript

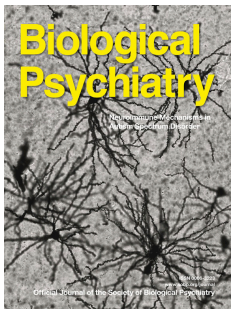

Hyperperfusion of Frontal White and Subcortical Gray Matter in Autism Spectrum Disorder

Bradley S. Peterson, Ariana Zargarian, Jarod B. Peterson, Suzanne Goh, Siddhant Sawardekar, Steven C.R. Williams, David J. Lythgoe, Fernando O. Zelaya, Ravi Bansal

PII: S0006-3223(18)32090-0

DOI: https://doi.org/10.1016/j.biopsych.2018.11.026

Reference: BPS 13719

To appear in: *Biological Psychiatry*

Received Date: 10 September 2018

Revised Date: 21 November 2018

Accepted Date: 27 November 2018

Please cite this article as: Peterson B.S., Zargarian A., Peterson J.B., Goh S., Sawardekar S., Williams S.C.R., Lythgoe D.J., Zelaya F.O. & Bansal R., Hyperperfusion of Frontal White and Subcortical Gray Matter in Autism Spectrum Disorder, *Biological Psychiatry* (2019), doi: https://doi.org/10.1016/j.biopsych.2018.11.026.

This is a PDF file of an unedited manuscript that has been accepted for publication. As a service to our customers we are providing this early version of the manuscript. The manuscript will undergo copyediting, typesetting, and review of the resulting proof before it is published in its final form. Please note that during the production process errors may be discovered which could affect the content, and all legal disclaimers that apply to the journal pertain.

ACCEPTED MANUSCRIPT

HYPERPERFUSION OF FRONTAL WHITE AND SUBCORTICAL GRAY MATTER IN AUTISM SPECTRUM DISORDER

Bradley S. Peterson,[a,b] Ariana Zargarian,[b] Jarod B. Peterson,[a] Suzanne Goh,[c] Siddhant Sawardekar,[a] Steven C. R. Williams,[d] David J. Lythgoe,[d] Fernando O. Zelaya,[d] Ravi Bansal[a,b]

[a]Institute for the Developing Mind, Children's Hospital Los Angeles, Los Angeles, CA 90027; [b]Keck School of Medicine at the University of Southern California, Los Angeles, CA 90033; [c]*Cortica* healthcare, San Diego, CA 92121; [d]Department of Neuroimaging, Institute of Psychiatry, Psychology and Neuroscience, King's College London, UK.

Running Head: Hyperperfusion in Autism Spectrum Disorder

Corresponding Author: Bradley S. Peterson, M.D., Children's Hospital Los Angeles, 4650 Sunset Blvd MS# 135, Los Angeles CA 90027. Phone: 323-361-3654; Email: bpeterson@chla.usc.edu

KEY WORDS: Autism, Magnetic Resonance Imaging, Arterial Spin Labeling, white matter, glia, cerebral blood flow

Number of Words in Abstract: 250

Number of Words in Main Text: 3956

Number of Figures: 4

Number of Tables: 1

Number of Supplemental Information: 1

ABSTRACT

Background: Our aim was to assess resting cerebral blood flow (rCBF) in children and adults with Autism Spectrum Disorder (ASD). **Methods:** We acquired pulsed arterial spin labeling MRI data in 44 generally high functioning ASD simplex participants and 66 typically developing (TD) controls with comparable mean full-scale IQ's. We compared rCBF values voxel-wise across diagnostic groups and assessed correlations with symptom scores. We also assessed the moderating influences of participant age, sex, and IQ on our findings and the correlations of rCBF with NAA (N-acetylaspartate) metabolite levels. **Results:** We detected significantly higher rCBF values throughout frontal white matter and subcortical gray in ASD participants. rCBF correlated positively with socialization deficits in regions where ASD hyperperfusion was greatest. rCBF declined with increasing IQ in the TD group, a correlation that was absent in ASD participants because their rCBF values were elevated across all IQ levels. rCBF in the ASD group correlated inversely with NAA metabolite levels throughout frontal white matter, with greater rCBF accompanying lower and increasingly abnormal NAA levels relative to TD controls. **Conclusions:** These findings taken together suggest the presence of altered metabolism, likely of mitochondrial origin, and dysfunctional maintenance processes that support axonal functioning in ASD. These disturbances in turn likely reduce neural efficiency for cognitive and social functioning, and trigger compensatory responses from supporting glial cells, which subsequently increase rCBF to affected white matter. These findings, if confirmed, suggest cellular and molecular targets for novel therapeutics that address axonal pathology and bolster glial compensatory responses in ASD.

INTRODUCTION

Regional cerebral blood flow (rCBF) is a surrogate measure of brain metabolism, because blood flow and metabolism are usually tightly coupled(1-5). Arterial Spin Labeling (ASL) provides absolute and reproducible measures of rCBF(6, 7) by magnetically labeling water in arterial blood as a diffusible tracer, analogous to the use of ^{15}O water in PET scanning(8). Unlike PET, ASL does not require the use of a radioactive tracer and therefore can be used in children, and it is a less costly and procedurally less complicated set of procedures. Moreover, because perfusion signals are obtained by pair-wise subtraction of adjacently acquired tagged and control images, ASL is less prone to motion artifact, low frequency physiological noise, and baseline drift than more conventional BOLD-based functional imaging(9). Finally, perfusion maps quantify rCBF at every voxel in the brain, whereas task-based BOLD imaging quantifies neural activity only in locations that the task activates, often confounded by systematic biases in task performance across participants(10).

We are aware of only one previous preliminary study employing ASL in persons with Autism Spectrum Disorder (ASD) and typically developing (TD) controls, which had a limited sample size, included only children, and reported abnormalities (increased rCBF) only in cortical gray matter of the ASD group(11). PET metabolism studies and SPECT rCBF studies in ASD have had small numbers of participants, and some have either employed sedation or compared against atypically developing patient controls; most have interrogated only gray matter, and their findings have been rather inconsistent. Nevertheless, FDG PET studies generally have reported reduced metabolism in cortical gray matter (anterior cingulate, parietal(12, 13), and temporal(14-16) cortex) and increased metabolism in occipital(17, 18) and other cortical regions(19). One preliminary PET study reported hyperperfusion of basal ganglia and posterior cingulate cortex in

ASD(20), whereas larger ^{18}FDG PET studies have found reduced basal ganglia and thalamus metabolism(21, 22). One FDG PET study assessed white matter metabolism explicitly, reporting higher metabolic rates that were greatest in prefrontal regions and internal capsule in 25 ASD compared with 55 TD adults during a verbal learning task(23). SPECT blood flow studies have generally reported reduced rCBF in temporal(24-31), parietal(25, 30, 31), and frontal(26, 27, 29-33) cortices and basal ganglia(28, 31, 33). Prior resting state functional MRI (fMRI) studies have generally reported long-range underconnectivity and local overconnectivity(34-45), suggesting the presence of axonal pathology in ASD.

We aimed to exploit some of the advantages of ASL to compare rCBF across a large sample of children and adults with ASD and age-, sex-, and IQ-matched TD controls. We also assessed the voxel-wise associations of ASL-based measures of rCBF and brain metabolism with MR spectroscopy-based measures of NAA (N-acetylaspartate)(46, 47) to understand how rCBF associates with this index of mitochondrial functioning(48-50), cellular metabolism(51), and neuronal abundance and viability(49, 50). Based on the prior metabolism and blood flow findings in ASD, we hypothesized *a priori* that we would detect reduced cortical and increased white matter rCBF. We also assessed the moderating effects of age, sex, and IQ on rCBF values in an effort to use rCBF values to parse the phenotypic heterogeneity of ASD. Finally, we assessed the voxel-wise correlation of rCBF with measures of NAA in ASD participants.

ACCEPTED MANUSCRIPT

METHODS

Sample Ascertainment & Characterization

This was a subset of 110 participants(44 ASD,66 TD) drawn from a larger MRI study of 200 ASD (simplex cases) and TD controls(36, 46); the ASL pulse sequence was not available for the earliest recruited participants in the larger study. ASD participants were recruited through the Developmental Neuropsychiatry Clinic at Columbia University and community awareness events. Because screening of participants occurred prior to the publication of DSM 5 diagnostic criteria for ASD, screening was based on DSM-IV-TR criteria for PDD. Potential participants were required to have a previous clinical DSM-IV-TR(52) diagnosis of Pervasive Developmental Disorder (PDD) and a score >15 on either the Social Communication Questionnaire Lifetime Version(53) or Autism-spectrum Quotient(54). Exclusion criteria specific to ASD were known medical conditions associated with autism (e.g., Fragile-X syndrome, tuberous sclerosis). The final consensus diagnoses were established by a physician or clinical psychologist with established reliability by administering Module 3(n=16) or Module 4(n=25) of the Autism Diagnostic Observation Schedule(ADOS-G)(55). The revised algorithm was used for all modules(56, 57). Diagnoses for younger participants were also aided by administering the parent Autism Diagnostic Interview-Revised(ADI-R)(58)(n=17). In our final sample, 12 (27%) met DSM-IV-TR criteria for Autistic Disorder, 23 (52%) for Asperger's Disorder, and 8 (18%) for PDD-NOS. Because substantial evidence suggests that most individuals with DSM-IV-based PDD diagnoses also meet DSM 5 criteria for a diagnosis of ASD(59), for ease of reference we herein used the DSM 5 designation.

TD participants were recruited through flyers, online advertisements, and random sampling from a telemarketing list of local households eligible for participation, group-matched

to ASD participants on age, sex, and ethnicity. TD controls participated after a clinical interview including the Kiddie Schedule for Affective Disorders and Schizophrenia Present and Lifetime Version for those under age 18(60) or the Structured Clinical Interview for DSM-IV Axis I Disorders for those ≥age 18(61). Additional exclusion criteria for all participants included contraindications to MRI, a history of premature birth(<36 weeks), low birth weight(<2000g), birth complications or injury, prior head trauma with loss of consciousness, seizures, or chronic medical illness. The Institutional Review Board of the New York State Psychiatric Institute approved the study procedures. An independent clinical monitor assessed the capacity for all adult ASD participants to provide informed consent. One participant was deemed to lack that capacity and therefore designated a surrogate to provide it. All children provided written assent.

Intelligence quotient(IQ) for 1 ASD participant was assessed using the Wechsler Intelligence Scale for Children(62) and 1 using the Wechsler Adult Intelligence Scale(63); all other ASD and TD participants were assessed using the Wechsler Abbreviated Scale of Intelligence(64). As all ASD participants had fluent speech, full-scale IQ was available for all. The Edinburgh Inventory assessed laterality of handedness(65), and Hollingshead's four-factor index estimated socioeconomic status(66).

MRI Scanning & Processing

All participants were unsedated for the scan. Details for scanning procedures, MRI pulse sequences, scan times, and image processing methods are provided in Supplementary Materials.

Statistical Analyses

All group-level statistical analyses employed a general linear model(GLM) at each voxel of the spatially normalized, individual rCBF maps, while covarying for age and sex, applying a False Discovery Rate (FDR) procedure at FDR=0.05 to control for false positives and color-

coding voxels on the T1 template where *P*-values survived the FDR procedure. All statistical models were hierarchically well-formulated, with any interaction terms including the component main effects. Our *a priori* hypothesis assessed the main effect of diagnosis on rCBF in all participants with no other covariates or interactions in the model. We also assessed the influences of FSIQ and medication use on our findings in post hoc analyses by covarying separately for FSIQ and psychotropic medication use and by applying again our model for *a priori* hypothesis testing while excluding any ASD participants who were taking psychotropic medications at the time of scan.

Secondary analyses assessed the moderating effects of age, sex, and FSIQ on group differences in separate models that included the respective interactions with their component main effects. These interactions assessed whether the slopes of the correlations differed across the ASD and TD control groups. In addition, within the ASD group we assessed the correlations of rCBF with Total and Domain scores on the developmentally appropriate ADOS module and with standardized Total and Subscale scores on SRS, while covarying for age and sex. We also assessed the voxel-wise correlations of rCBF with MRS-based measures of NAA metabolite levels as a continuous variable, and we compared rCBF values in the 6 ASD participants in whom we previously detected the presence of lactate with 30 ASD participants in whom we did not detect the presence of lactate.

ACCEPTED MANUSCRIPT

RESULTS

Sample Characteristics

The ASD and TD samples did not differ significantly in age, sex, ethnicity, FSIQ, handedness, or socioeconomic status(Table 1). By design, all SRS domain scores were higher in the ASD sample (all $P<10^{-11}$), reflecting more severe social symptoms(Table 1). Fourteen of the 44 ASD participants (and no TD participants) were taking psychotropic medication at the time of scan: stimulants(n=5), antidepressants(n=7; includes SSRIs and SNRIs), lithium(n=2), anticonvulsants/mood stabilizers(n=1), antipsychotics(n=4), benzodiazepine(n=2), MAOI(n=1), and non-stimulant ADHD medication(n=2) (these total >n=14 because some were taking multiple medications).

[Table 1]

Group Comparisons of rCBF

ASD compared with TD participants had higher rCBF values throughout large expanses of white matter, primarily in frontal regions comprising the centrum semiovale(CS), corona radiata(CR), and internal capsule(IC) bilaterally. They also had greater rCBF bilaterally in gray matter of the caudate(Cd) and lenticular nucleus(L) more dorsally, the ventral striatum(VS), orbitofrontal cortex(OFC), and amygdala(Am).

[Figure 1]

Correlations of rCBF with ASD Symptom Measures

Within the ASD group, rCBF correlated positively with the Total ADOS score in much of the same frontal white matter regions where a main effect of diagnosis was located(CS,CR), as well as within the hypothalamus, hippocampus, and middle temporal gyrus(Fig.1). The social affect domain score of the ADOS almost exclusively contributed to this correlation, with little or

no contribution from the repetitive behaviors domain score(Supplemental Figs.S22-S23). Of the various SRS subscale scores, social awareness correlated most robustly with rCBF measures, both within more dorsal white matter of the frontal lobe(CS), as well as in gray matter of the hypothalamus, hippocampus, middle temporal gyrus, basal ganglia(Cd,L,VS), amygdala, hippocampus, and brainstem(Supplemental Figs.S24-S28).

Moderators of Diagnosis Effect

Age significantly moderated the effects of diagnosis in the subgenual, pregenual, and dorsal ACC, inferior frontal gyrus, DLPFC, occipital gyrus, middle and inferior temporal gyrus, and amygdala(Fig.2), with the effects deriving in each instance from a steeper inverse correlation of rCBF with age in the ASD group than in TD controls(Fig.3).

Sex significantly moderated the effect of diagnosis, though localized almost exclusively to the subgenual and pregenual ACC and small portions of the caudate, ventral striatum, and amygdala(Fig.2), with the effects deriving in each case from a reversal in the ASD group of the female>male rCBF differences present in TD controls(Fig.3).

FSIQ also significantly moderated the effect of diagnosis within frontal white matter(CR,CS,IC), hypothalamus, and insular cortex(Fig.2), with the effect in each case deriving from a steeper decline in FSIQ with increasing rCBF, and more broadly throughout frontal white matter and subcortical gray matter, in the TD controls than in the ASD participants(Fig.3).

[Figures 2&3]

Correlations of rCBF with MRS Metabolites

In the ASD and TD groups separately and combined, rCBF correlated inversely with NAA metabolite levels throughout frontal white matter, as well as in white matter of the internal and external capsules(Fig.4). The 6 ASD participants who had detectable lactate in their brains,

compared with the 30 who did not, had significantly lower rCBF in the white matter of the CC genu and posterior CS, and in gray matter of the DPFC and pregenual ACC. They also had higher rCBF values in the midcingulate cortex(Fig.4).

[Figure 4]

Post Hoc Analyses

We conducted post hoc analyses to assess the effects of potential confounds on our findings. Covarying for FSIQ in our models had negligible effects on our findings(Supplemental Figs. S29-S31). Likewise, covarying for the use of psychotropic medications at the time of MRI scan had negligible effects, as did excluding from analyses those ASD participants taking psychotropic medications, though maps were overall somewhat less statistically significant because of reduced statistical power associated with fewer participants(Supplemental Figs.S32-S37). Covarying for total cortical gray matter or total white matter volumes also had no discernible effects on our findings(Supplemental Figs.S38-S39). Finally, we also conducted our primary analyses (shown in Fig.1) separately in youth($\leq$ 21 years; N=20) and adults(>21 years; N=24); despite reduced statistical power, hyperperfusion was present in both groups, with the frontal locations most prominent in youth and dorsal parietal location more prominent in the adults(Supplemental Fig.S40). rCBF correlations with ADOS total scores were stronger in ASD adults, whereas SRS Awareness correlations were stronger in ASD youth(Supplemental Figs.S41-S42).

ACCEPTED MANUSCRIPT

DISCUSSION

To the best of our knowledge, this is the first report of widespread hyperperfusion in ASD, and the first to report voxelwise correlations of rCBF with NAA metabolite concentrations throughout the brain.

Hyperperfusion in ASD

Hyperperfusion was present throughout frontal white matter (WM) and subcortical gray in ASD participants of all ages and in both sexes. rCBF correlated positively with measures of socialization deficits within the ASD group, including social affect domain scores on the ADOS and the social awareness subscale of the SRS, in regions where ASD hyperperfusion in group comparisons of rCBF were greatest.

Our findings of WM hyperperfusion are consistent with one prior FDG PET brain metabolism study reporting higher metabolic rates in the WM of 25 ASD compared with 55 TD adults performing a verbal learning task, with the greatest increases in prefrontal WM and anterior limb of the internal capsule(23). They are also consistent with findings from numerous MRI(67, 68) and DTI(69, 70) studies reporting volumetric and organizational WM abnormalities in ASD, and with postmortem findings of fewer long axons, more short local axons, and thinner myelin(71, 72), which together suggest that compromised integrity of axons or oligodendrocytes may be the anatomical basis for reported long-range underconnectivity and local overconnectivity in functional MRI studies(34-45).

CNS WM consumes approximately one-third the energy of gray matter(1-5) due to the greater energy efficiency of axon action potentials and especially WM synapses(73), with most WM energy devoted to maintaining resting potentials and various housekeeping tasks(73, 74). Hyperperfusion in ASD could derive from pathology in any one or a combination of these

maintenance processes in neuronal axons, the most abundant cellular tissue in WM and its largest component by volume.

Oligodendrocytes, which comprise approximately 5% of all cells and 10-15% of all human glial cells in the brain(75, 76), ensheath WM axons with myelin to speed saltatory conduction(77). Their pathological functioning could alter myelination and, secondarily, WM metabolism and perfusion. Myelination is particularly important for finely calibrating conduction speeds and coordinating signals over long axons, which fMRI studies have suggested is a prominent disturbance in ASD(34-45). Most new myelin in adulthood is formed through an activity-dependent, plastic remodeling of the number, length, and thickness of preexisting myelin sheaths(37, 78-85). Approximately 20% of new myelin in adulthood also derives from the neuronal activity-dependent differentiation of oligodendrocyte precursor cells (OPCs) into new oligodendrocytes(85-87). Thus primary abnormalities in oligodendrocytes could produce altered WM metabolism and blood flow or, alternatively, abnormalities secondary to disturbances in axonal activity, whether from molecular or genetic defects in ASD or altered experiences associated with the illness, that in turn could trigger ongoing, activity-dependent myelin remodeling and its attendant increased metabolic demands.

Astrocytes, the most abundant glial cell type in the CNS, constitute nearly half the volume of WM and contribute significantly to WM metabolism and blood flow(88). They play an essential supporting role in OPC proliferation and differentiation, production of myelin(89), and formation of the blood-brain barrier. They take up potassium and glutamate released into the interstitial fluid to sustain and modulate high-frequency neuronal firing. Though not electrically excitable, they form a large network of astrocyte signaling through gap junctions that propagates Ca^{+2} and ATP waves over long-distances(90, 91). These properties of astrocytes are increasingly

believed to play an important role in learning, memory, and intelligence(92), and genetic mutations affecting astrocyte functioning even produce ASD-like phenotypes of maturational delay, intellectual disability, and seizures(89). Altered astrocyte metabolism could account for our perfusion findings.

Microglia, the least abundant glial cell type, are the primary responders in a CNS cellular immune response. Their relative scarcity makes their metabolism itself an unlikely cause of hyperperfusion in ASD, though the inflammatory responses that they generate could increase perfusion. Excessive microglial cell number and activation have been reported in previous PET and postmortem studies of ASD(93-95), and the reactive oxygen species and proinflammatory cytokines they generate could produce the impaired mitochondrial functioning suggested in prior studies(96), including one study of our participants(46).

Hyperperfusion was also present in the basal ganglia and amygdala. Though predominantly gray matter structures, they do contain axons, myelin, and glia(97, 98), and therefore a disturbance affecting only one of these cell components could produce hyperperfusion in both white and gray matter.

Interactions with Age

We detected a significantly steeper inverse correlation of rCBF with age in the ASD group than in TD controls throughout much of cortical gray matter, but most significantly in the ACC, DLPFC, amygdala, and several other cortical gray matter regions, with rCBF generally higher in children and either similar or lower in adults with ASD compared with controls(Fig.2b). Thus the hyperperfusion detected in ASD across all ages in WM and subcortical gray was also present in cortical gray matter and amygdala, but primarily in ASD children. Prior ^{15}O PET studies have reported declining cerebral metabolic rates(1-5) and blood

flow(1-3, 5) with age in cortical gray matter in healthy individuals; age correlates generally have not been reported in ASD. We detected an age-related decline of rCBF in healthy individuals only in occipital cortex. The decline in other cortical regions was in ASD participants, and in the direction toward values in healthy controls with advancing age, suggesting either that rCBF normalizes with age in cortical gray or that values close to normal in those regions may be a marker for ASD illness that persists into adulthood. By extension, higher rCBF values in children could also represent some kind of adaptive response to the presence of illness. Myriad cellular aging processes could account for the age-related decline in cortical rCBF in ASD, including: fewer neurons(99), dendritic arbors, or spines; reduced activity of the synaptic sodium/potassium pump and resting membrane potential(100); or less oxygen consumption and energy production from neuronal mitochondria in older compared with younger ASD participants(101).

Interactions with Sex

We detected a significant sex-by-diagnosis effect on rCBF in limbic regions, including subgenual ACC, ventral striatum, and amygdala, as well as parietal WM(Fig.2). In each instance, rCBF was greater in TD females than TD males, but this sex difference reversed in ASD, driven by particularly high values in ASD males, higher than in either TD males or females(Fig.2b). These findings suggest that, for reasons unknown, the perfusion abnormalities and cellular processes underlying them in ASD are disproportionately greater in males in limbic gray matter regions, perhaps contributing to the well-known male predominance in prevalence of ASD and to the more severe problems with externalizing and prosocial behaviors commonly found in ASD males(102, 103).

Interactions with IQ

We detected a significant IQ-by-diagnosis interaction effect on rCBF values in frontal WM and subcortical gray matter that derived from a significant decline in rCBF with increasing IQ in the TD group, a correlation that was absent in ASD participants(Fig.2a&b). The hyperperfusion present in most members of the ASD group, though attenuated in younger ASD participants, destroyed the normal association of IQ with rCBF in these regions(Fig.3). The inverse correlation of resting rCBF with IQ in the TD controls is consistent with the neural efficiency hypothesis of intelligence, which posits that those with higher intelligence process information more efficiently, using less energy to accomplish any given task(104). Presumably this greater efficiency is present even in the "resting" brain that is not explicitly engaged in performing any task. The cellular and molecular determinants of greater efficiency are unknown, but could include improved synaptic or network connectivity(105), myelination(105), or maintenance of resting potentials and other housekeeping functions(106, 107). These need not be the same determinants as those that increase perfusion in ASD, but if they are the same, then disturbances in myelin remodeling or axon housekeeping functions are potential culprits in ASD, as both would require increased metabolism to support intellectual functioning at its highest potential.

Metabolite Correlations

rCBF throughout frontal WM in the ASD group correlated inversely with NAA metabolite levels. We reported elsewhere significantly lower NAA concentrations in the ASD group compared with controls(47). Thus, greater rCBF accompanied lower, and increasingly abnormal, NAA levels. As findings from prior studies indicate that reduced NAA concentrations represent a reduced density or functioning of axonal mitochondria(49, 50), then reduced frontal

WM mitochondria could suggest that increased frontal WM rCBF and metabolism represents a compensatory process in ensheathing glia to maintain the energy state of WM axons.

The possibility of compensation is bolstered by evidence that glia support the formidable metabolic housekeeping demands of myelinated axons, which are challenged by sparse mitochondria and slow passive diffusion of nutrients across nodes of Ranvier(108). Myelinating oligodendrocytes couple with associated axons to support neuronal metabolism under stress(109), in part through release of exosomes containing trophic substances(73, 74, 109, 110), and in part through shuttling of lactate and pyruvate to axons to serve as substrates for aerobic ATP production(111). Axonal firing stimulates further oligodendrocyte production of lactate and pyruvate through release of glutamate, which activates oligodendrocyte NMDA receptors to stimulate uptake of glucose and glycolysis, thereby maintaining energy supplies to axons(89, 112, 113). Finally, the myelin sheath has been proposed as an ectopic site of glucose combustion and ATP generation for use by myelinated axons(74, 114-116), though direct experimental and mathematical modeling support for ATP generation in myelin sheaths is lacking(117).

The positive correlations of rCBF with measures of social impairment we observed suggest that this putative compensatory response is either unsuccessful or incomplete, because fully successful compensation would produce an inverse correlation. In the presence of unsuccessful or incomplete compensation, however, greater reductions of NAA and axonal metabolism would produce more severe symptoms and a proportionately greater compensatory response in glial cell metabolism – i.e., it would produce the observed positive associations of social impairment with rCBF. Alternatively, sustained increases in myelin synthesis by oligodendrocytes in ASD WM could deplete the associated axons of NAA, because more myelin synthesis would require transportation of more NAA from neurons to oligodendrocytes for

cleavage and use of its acetate moiety(118, 119). Increased myelin synthesis therefore could account for both reduced NAA in axons but increased rCBF in metabolic support of myelin synthesis. Human postmortem and imaging studies, however, generally have not provided evidence for excessive, ongoing myelination in ASD.

Limitations Though our sample comprised ASD participants with a wide range of intellectual and social functioning, mean IQs were by design comparable to TD participants to limit the potential confounding effects of IQ differences on our findings. This sample selection, however, limits the generalizability of our findings to persons who are more severely affected with ASD, at least with respect to language and cognitive functioning. In addition, a larger sample size would improve statistical power and the stability of interaction effects. Longitudinal imaging studies are needed to support developmentally based interpretations of our findings(10).

Conclusion

Extensive resting frontal WM hyperperfusion in ASD suggests increased metabolic demands of either axons or glia or both. Positive correlations of rCBF with measures of social impairment in the same WM regions suggest that either increased perfusion partially generates those symptoms or is a proportionate response to their presence. The altered associations of rCBF with IQ moreover suggests impaired neural efficiency in frontal WM. The combination of reduced NAA levels with proportionally greater rCBF values in frontal WM suggests that glial cells are attempting unsuccessfully or incompletely to compensate for reduced axonal metabolism in ASD. The most parsimonious explanation for all these findings is the presence of axonal pathology, including reduced NAA and altered mitochondrial metabolism, that disrupts one or more components of the housekeeping processes supporting axonal functioning, thereby reducing the efficiency of information processing. These disruptions trigger compensatory

responses from supporting glial cells to support axon metabolism and proportionately increase rCBF to affected WM. The compensatory response is only partial, however, and in the ASD group disrupts the normal association of greater efficiency of neural processing with increasing IQ observed in the TD group. These findings, if confirmed, suggest cellular and molecular targets for studies of axonal pathology and development of novel therapeutics to bolster glial compensatory responses in ASD.

ACKNOWLEDGMENTS The research was made possible by the provision of data by New York State Psychiatric Institute and Columbia University. We are grateful to Dr. Molly Algermissen for her technical assistance. This study was supported by NIMH grant R01 MH089582 and funding from Children's Hospital Los Angeles and the University of Southern California.

DISCLOSURES The authors report no biomedical financial interests or potential conflicts of interest.

ACCEPTED MANUSCRIPT

REFERENCES

1. Marchal G, Rioux P, Petit-Taboue MC, Sette G, Travere JM, Le Poec C, et al. (1992): Regional cerebral oxygen consumption, blood flow, and blood volume in healthy human aging. *Arch Neurol*. 49:1013-1020.
2. Lenzi GL, Frackowiak RS, Jones T, Heather JD, Lammertsma AA, Rhodes CG, et al. (1981): CMRO2 and CBF by the oxygen-15 inhalation technique. Results in normal volunteers and cerebrovascular patients. *Eur Neurol*. 20:285-290.
3. Pantano P, Baron JC, Lebrun-Grandie P, Duquesnoy N, Bousser MG, Comar D (1984): Regional cerebral blood flow and oxygen consumption in human aging. *Stroke*. 15:635-641.
4. Yamaguchi T, Kanno I, Uemura K, Shishido F, Inugami A, Ogawa T, et al. (1986): Reduction in regional cerebral metabolic rate of oxygen during human aging. *Stroke*. 17:1220-1228.
5. Leenders KL, Perani D, Lammertsma AA, Heather JD, Buckingham P, Healy MJ, et al. (1990): Cerebral blood flow, blood volume and oxygen utilization. Normal values and effect of age. *Brain*. 113 (Pt 1):27-47.
6. Floyd TF, Ratcliffe SJ, Wang J, Resch B, Detre JA (2003): Precision of the CASL-perfusion MRI technique for the measurement of cerebral blood flow in whole brain and vascular territories. *J Magn Reson Imaging*. 18:649-655.
7. Detre JA, Wang J (2002): Technical aspects and utility of fMRI using BOLD and ASL. *Clin Neurophysiol*. 113:621-634.
8. Detre JA, Zhang W, Roberts DA, Silva AC, Williams DS, Grandis DJ, et al. (1994): Tissue specific perfusion imaging using arterial spin labeling. *NMR Biomed*. 7:75-82.
9. Wong EC, Buxton RB, Frank LR (1999): Quantitative perfusion imaging using arterial spin labeling. *Neuroimaging Clin N Am*. 9:333-342.
10. Horga G, Kaur T, Peterson BS (2014): Annual research review: Current limitations and future directions in MRI studies of child- and adult-onset developmental psychopathologies. *J Child Psychol Psychiatry*. 55:659-680.
11. Jann K, Hernandez LM, Beck-Pancer D, McCarron R, Smith RX, Dapretto M, et al. (2015): Altered resting perfusion and functional connectivity of default mode network in youth with autism spectrum disorder. *Brain and behavior*. 5:e00358.
12. Haznedar MM, Buchsbaum MS, Metzger M, Solimando A, Spiegel-Cohen J, Hollander E (1997): Anterior cingulate gyrus volume and glucose metabolism in autistic disorder. *Am J Psychiatry*. 154:1047-1050.
13. Haznedar MM, Buchsbaum MS, Wei TC, Hof PR, Cartwright C, Bienstock CA, et al. (2000): Limbic circuitry in patients with autism spectrum disorders studied with positron emission tomography and magnetic resonance imaging. *Am J Psychiatry*. 157:1994-2001.

14. Zilbovicius M, Boddaert N, Belin P, Poline JB, Remy P, Mangin JF, et al. (2000): Temporal lobe dysfunction in childhood autism: a PET study. Positron emission tomography. *Am J Psychiatry*. 157:1988-1993.

15. Boddaert N, Chabane N, Barthelemy C, Bourgeois M, Poline JB, Brunelle F, et al. (2002): [Bitemporal lobe dysfonction in infantile autism: positron emission tomography study]. *J Radiol*. 83:1829-1833.

16. Dilber C, Caliskan M, Sonmezoglu K, Nisli S, Mukaddes NM, Tatli B, et al. (2013): Positron emission tomography findings in children with infantile spasms and autism. *Journal of clinical neuroscience : official journal of the Neurosurgical Society of Australasia*. 20:373-376.

17. Zurcher NR, Bhanot A, McDougle CJ, Hooker JM (2015): A systematic review of molecular imaging (PET and SPECT) in autism spectrum disorder: current state and future research opportunities. *Neurosci Biobehav Rev*. 52:56-73.

18. Hazlett EA, Buchsbaum MS, Hsieh P, Haznedar MM, Platholi J, LiCalzi EM, et al. (2004): Regional glucose metabolism within cortical Brodmann areas in healthy individuals and autistic patients. *Neuropsychobiology*. 49:115-125.

19. Rumsey JM, Duara R, Grady C, Rapoport JL, Margolin RA, Rapoport SI, et al. (1985): Brain metabolism in autism. Resting cerebral glucose utilization rates as measured with positron emission tomography. *Archives of General Psychiatry*. 42:448-455.

20. Pagani M, Manouilenko I, Stone-Elander S, Odh R, Salmaso D, Hatherly R, et al. (2012): Brief Report: alterations in cerebral blood flow as assessed by PET/CT in adults with autism spectrum disorder with normal IQ. *J Autism Dev Disord*. 42:313-318.

21. Haznedar MM, Buchsbaum MS, Hazlett EA, LiCalzi EM, Cartwright C, Hollander E (2006): Volumetric analysis and three-dimensional glucose metabolic mapping of the striatum and thalamus in patients with autism spectrum disorders. *Am J Psychiatry*. 163:1252-1263.

22. Siegel BV, Jr., Asarnow R, Tanguay P, Call JD, Abel L, Ho A, et al. (1992): Regional cerebral glucose metabolism and attention in adults with a history of childhood autism. *The Journal of neuropsychiatry and clinical neurosciences*. 4:406-414.

23. Mitelman SA, Buchsbaum MS, Young DS, Haznedar MM, Hollander E, Shihabuddin L, et al. (2017): Increased white matter metabolic rates in autism spectrum disorder and schizophrenia. *Brain imaging and behavior*.

24. Carina Gillberg I, Bjure J, Uvebrant P, Vestergren E, Gillberg C (1993): SPECT (Single Photon Emission Computed Tomography) in 31 children and adolescents with autism and autistic-like conditions. *Eur Child Adolesc Psychiatry*. 2:50-59.

25. Mountz JM, Tolbert LC, Lill DW, Katholi CR, Liu HG (1995): Functional deficits in autistic disorder: characterization by technetium-99m-HMPAO and SPECT. *J Nucl Med*. 36:1156-1162.

26. Hashimoto T, Sasaki M, Fukumizu M, Hanaoka S, Sugai K, Matsuda H (2000): Single-photon emission computed tomography of the brain in autism: effect of the developmental level. *Pediatr Neurol*. 23:416-420.

27. Ohnishi T, Matsuda H, Hashimoto T, Kunihiro T, Nishikawa M, Uema T, et al. (2000): Abnormal regional cerebral blood flow in childhood autism. *Brain*. 123 (Pt 9):1838-1844.

28. Starkstein SE, Vazquez S, Vrancic D, Nanclares V, Manes F, Piven J, et al. (2000): SPECT findings in mentally retarded autistic individuals. *The Journal of neuropsychiatry and clinical neurosciences*. 12:370-375.

29. Kaya M, Karasalihoglu S, Ustun F, Gultekin A, Cermik TF, Fazlioglu Y, et al. (2002): The relationship between 99mTc-HMPAO brain SPECT and the scores of real life rating scale in autistic children. *Brain Dev*. 24:77-81.

30. Burroni L, Orsi A, Monti L, Hayek Y, Rocchi R, Vattimo AG (2008): Regional cerebral blood flow in childhood autism: a SPET study with SPM evaluation. *Nucl Med Commun*. 29:150-156.

31. Degirmenci B, Miral S, Kaya GC, Iyilikci L, Arslan G, Baykara A, et al. (2008): Technetium-99m HMPAO brain SPECT in autistic children and their families. *Psychiatry Res*. 162:236-243.

32. Wilcox J, Tsuang MT, Ledger E, Algeo J, Schnurr T (2002): Brain perfusion in autism varies with age. *Neuropsychobiology*. 46:13-16.

33. Gupta SK, Ratnam BV (2009): Cerebral perfusion abnormalities in children with autism and mental retardation: a segmental quantitative SPECT study. *Indian Pediatr*. 46:161-164.

34. Just MA, Keller TA, Malave VL, Kana RK, Varma S (2012): Autism as a neural systems disorder: a theory of frontal-posterior underconnectivity. *Neurosci Biobehav Rev*. 36:1292-1313.

35. Brock J, Brown CC, Boucher J, Rippon G (2002): The temporal binding deficit hypothesis of autism. *Dev Psychopathol*. 14:209-224.

36. Denisova K, Zhao G, Wang Z, Goh S, Huo Y, Peterson BS (2017): Cortical interactions during the resolution of information processing demands in autism spectrum disorders. *Brain and behavior*. 7:e00596.

37. Just MA, Cherkassky VL, Keller TA, Minshew NJ (2004): Cortical activation and synchronization during sentence comprehension in high-functioning autism: evidence of underconnectivity. *Brain*. 127:1811-1821.

38. Belmonte MK, Allen G, Beckel-Mitchener A, Boulanger LM, Carper RA, Webb SJ (2004): Autism and abnormal development of brain connectivity. *J Neurosci*. 24:9228-9231.

39. Ecker C, Ronan L, Feng Y, Daly E, Murphy C, Ginestet CE, et al. (2013): Intrinsic gray-matter connectivity of the brain in adults with autism spectrum disorder. *Proc Natl Acad Sci U S A*. 110:13222-13227.

40. Khan S, Gramfort A, Shetty NR, Kitzbichler MG, Ganesan S, Moran JM, et al. (2013): Local and long-range functional connectivity is reduced in concert in autism spectrum disorders. *Proc Natl Acad Sci U S A*. 110:3107-3112.

41. Cherkassky VL, Kana RK, Keller TA, Just MA (2006): Functional connectivity in a baseline resting-state network in autism. *Neuroreport*. 17:1687-1690.

42. Monk CS, Peltier SJ, Wiggins JL, Weng SJ, Carrasco M, Risi S, et al. (2009): Abnormalities of intrinsic functional connectivity in autism spectrum disorders. *Neuroimage*. 47:764-772.

43. Damarla SR, Keller TA, Kana RK, Cherkassky VL, Williams DL, Minshew NJ, et al. (2010): Cortical underconnectivity coupled with preserved visuospatial cognition in autism: Evidence from an fMRI study of an embedded figures task. *Autism research : official journal of the International Society for Autism Research*. 3:273-279.

44. Dinstein I, Pierce K, Eyler L, Solso S, Malach R, Behrmann M, et al. (2011): Disrupted neural synchronization in toddlers with autism. *Neuron*. 70:1218-1225.

45. Lee PS, Yerys BE, Della Rosa A, Foss-Feig J, Barnes KA, James JD, et al. (2009): Functional connectivity of the inferior frontal cortex changes with age in children with autism spectrum disorders: a fcMRI study of response inhibition. *Cereb Cortex*. 19:1787-1794.

46. Goh S, Dong Z, Zhang Y, DiMauro S, Peterson BS (2014): Mitochondrial dysfunction as a neurobiological subtype of autism spectrum disorder: evidence from brain imaging. *JAMA psychiatry*. 71:665-671.

47. O'Neill J, Bansal R, Goh S, Rodi M, Sawardekar S, Peterson BS Parsing the heterogeneity of brain metabolic disturbances in Autism Spectrum Disorder. *Submitted.*

48. Madhavarao CN, Chinopoulos C, Chandrasekaran K, Namboodiri MAA (2003): Characterization of the N-acetylaspartate biosynthetic enzyme from rat brain. *Journal of Neurochemistry*. 86:824-835.

49. Rae CD (2014): A guide to the metabolic pathways and function of metabolites observed in human brain 1H magnetic resonance spectra. *Neurochem Res*. 39:1-36.

50. Clark JB (1998): N-Acetyl Aspartate: A Marker for Neuronal Loss or Mitochondrial Dysfunction. *Developmental Neuroscience*. 20:271-276.

51. O'Neill J, Eberling JL, Schuff N, Jagust W, Reed B, Soto G, et al. (2000): Method to correlate 1H MRSI and 18FDG-PET. *Magnetic Resonance in Medicine*. 43:244-250.

52. American Psychiatric Association (2000): *Diagnostic and Statistical Manual of Mental Disorders, 4th Edition, Text Revision (DSM-IV-TR)*. Washington.

53. Rutter M, Caspi A, Moffitt TE (2003): Using sex differences in psychopathology to study causal mechanisms: unifying issues and research strategies. 44:1092-1115.

54. Baron-Cohen S, Wheelwright S, Skinner R, Martin J, Clubley E (2001): The autism-spectrum quotient (AQ): evidence from Asperger syndrome/high-functioning autism, males and females, scientists and mathematicians. *J Autism Dev Disord*. 31:5-17.

55. Lord C, Risi S, Lambrecht L, Cook EH, Jr., Leventhal BL, DiLavore PC, et al. (2000): The autism diagnostic observation schedule-generic: a standard measure of social and communication deficits associated with the spectrum of autism. *J Autism Dev Disord*. 30:205-223.

56. Bastiaansen JA, Meffert H, Hein S, Huizinga P, Ketelaars C, Pijnenborg M, et al. (2011): Diagnosing autism spectrum disorders in adults: the use of Autism Diagnostic Observation Schedule (ADOS) module 4. *J Autism Dev Disord*. 41:1256-1266.

57. Gotham K, Risi S, Pickles A, Lord C (2007): The Autism Diagnostic Observation Schedule: revised algorithms for improved diagnostic validity. *J Autism Dev Disord*. 37:613-627.

58. Lord C, Rutter M, Le Couteur A (1994): Autism Diagnostic Interview-Revised: a revised version of a diagnostic interview for caregivers of individuals with possible pervasive developmental disorders. *J Autism Dev Disord*. 24:659-685.

59. Huerta M, Bishop SL, Duncan A, Hus V, Lord C (2012): Application of DSM-5 criteria for autism spectrum disorder to three samples of children with DSM-IV diagnoses of pervasive developmental disorders. *Am J Psychiatry*. 169:1056-1064.

60. Kaufman J, Birmaher B, Brent D, Rao U, Flynn C, Moreci P, et al. (1997): Schedule for Affective Disorders and Schizophrenia for School-Age Children-Present and Lifetime Version (K-SADS-PL): initial reliability and validity data. *J Am Acad Child Adolesc Psychiatry*. 36:980-988.

61. First MB (1997): *Structured clinical interview for the DSM-IV axis I disorders: SCID-I/P, version 2.0*. New York: Biometrics Research Dept: New York State Psychiatric Institute.

62. Wechsler D (1991): Wechsler Intelligence Scale for Children-Third Edition (WISC-III). San Antonio, TX: Psychological Corporation.

63. Wechsler D (1997): *Wechsler Adult Intelligence Scale*. 3rd ed. San Antonio, TX: The Psychological Corporation.

64. Wechsler D (1999): *WASI Manual. Wechsler Abbreviated Scale of Intelligence*. The Psychological Corporation.

65. Oldfield RC (1971): The assessment and analysis of handedness: the Edinburgh inventory. *Neuropsychologia*. 9:97-113.

66. Hollingshead AB (1975): *Four-factor index of social status*. New Haven, CT: Yale University Press.

67. Courchesne E (2004): Brain development in autism: early overgrowth followed by premature arrest of growth. *Mental Retardation & Developmental Disabilities Research Rev*. 10:106-111.

68. Herbert MR, Ziegler DA, Makris N, Filipek PA, Kemper TL, Normandin JJ, et al. (2004): Localization of white matter volume increase in autism and developmental language disorder. *Ann Neurol*. 55:530-540.

69. Travers BG, Adluru N, Ennis C, Tromp do PM, Destiche D, Doran S, et al. (2012): Diffusion tensor imaging in autism spectrum disorder: a review. *Autism research : official journal of the International Society for Autism Research*. 5:289-313.

70. Ameis SH, Catani M (2015): Altered white matter connectivity as a neural substrate for social impairment in Autism Spectrum Disorder. *Cortex*. 62:158-181.

71. Courchesne E, Pierce K, Schumann CM, Redcay E, Buckwalter JA, Kennedy DP, et al. (2007): Mapping early brain development in autism. *Neuron*. 56:399-413.

72. Zikopoulos B, Barbas H (2010): Changes in prefrontal axons may disrupt the network in autism. *J Neurosci*. 30:14595-14609.

73. Harris JJ, Attwell D (2012): The energetics of CNS white matter. *J Neurosci*. 32:356-371.

74. Beirowski B (2013): Concepts for regulation of axon integrity by enwrapping glia. *Frontiers in cellular neuroscience*. 7:256.

75. Staugaitis SM, Trapp BD (2009): NG2-positive glia in the human central nervous system. *Neuron Glia Biol*. 5:35-44.

76. Dawson MR, Polito A, Levine JM, Reynolds R (2003): NG2-expressing glial progenitor cells: an abundant and widespread population of cycling cells in the adult rat CNS. *Mol Cell Neurosci*. 24:476-488.

77. Redmond SA, Mei F, Eshed-Eisenbach Y, Osso LA, Leshkowitz D, Shen YA, et al. (2016): Somatodendritic Expression of JAM2 Inhibits Oligodendrocyte Myelination. *Neuron*. 91:824-836.

78. Fields RD (2015): A new mechanism of nervous system plasticity: activity-dependent myelination. *Nat Rev Neurosci*. 16:756-767.

79. Yeung MS, Zdunek S, Bergmann O, Bernard S, Salehpour M, Alkass K, et al. (2014): Dynamics of oligodendrocyte generation and myelination in the human brain. *Cell*. 159:766-774.

80. Gibson EM, Purger D, Mount CW, Goldstein AK, Lin GL, Wood LS, et al. (2014): Neuronal activity promotes oligodendrogenesis and adaptive myelination in the mammalian brain. *Science*. 344:1252304.

81. Young KM, Psachoulia K, Tripathi RB, Dunn SJ, Cossell L, Attwell D, et al. (2013): Oligodendrocyte dynamics in the healthy adult CNS: evidence for myelin remodeling. *Neuron*. 77:873-885.

82. Stevens B, Porta S, Haak LL, Gallo V, Fields RD (2002): Adenosine: a neuron-glial transmitter promoting myelination in the CNS in response to action potentials. *Neuron*. 36:855-868.

83. Orkand RK, Nicholls JG, Kuffler SW (1966): Effect of nerve impulses on the membrane potential of glial cells in the central nervous system of amphibia. *J Neurophysiol*. 29:788-806.

84. Micu I, Plemel JR, Lachance C, Proft J, Jansen AJ, Cummins K, et al. (2016): The molecular physiology of the axo-myelinic synapse. *Exp Neurol*. 276:41-50.

85. Almeida RG, Lyons DA (2017): On Myelinated Axon Plasticity and Neuronal Circuit Formation and Function. *J Neurosci*. 37:10023-10034.

86. Rivers LE, Young KM, Rizzi M, Jamen F, Psachoulia K, Wade A, et al. (2008): PDGFRA/NG2 glia generate myelinating oligodendrocytes and piriform projection neurons in adult mice. *Nat Neurosci*. 11:1392-1401.

87. Sampaio-Baptista C, Johansen-Berg H (2017): White Matter Plasticity in the Adult Brain. *Neuron*. 96:1239-1251.

88. Walhovd KB, Johansen-Berg H, Karadottir RT (2014): Unraveling the secrets of white matter--bridging the gap between cellular, animal and human imaging studies. *Neuroscience*. 276:2-13.

89. Lundgaard I, Osorio MJ, Kress BT, Sanggaard S, Nedergaard M (2014): White matter astrocytes in health and disease. *Neuroscience*. 276:161-173.

90. Haas B, Schipke CG, Peters O, Sohl G, Willecke K, Kettenmann H (2006): Activity-dependent ATP-waves in the mouse neocortex are independent from astrocytic calcium waves. *Cereb Cortex*. 16:237-246.

91. Orthmann-Murphy JL, Freidin M, Fischer E, Scherer SS, Abrams CK (2007): Two distinct heterotypic channels mediate gap junction coupling between astrocyte and oligodendrocyte connexins. *J Neurosci*. 27:13949-13957.

92. Han X, Chen M, Wang F, Windrem M, Wang S, Shanz S, et al. (2013): Forebrain engraftment by human glial progenitor cells enhances synaptic plasticity and learning in adult mice. *Cell Stem Cell*. 12:342-353.

93. Suzuki K, Sugihara G, Ouchi Y, Nakamura K, Futatsubashi M, Takebayashi K, et al. (2013): Microglial activation in young adults with autism spectrum disorder. *JAMA psychiatry*. 70:49-58.

94. Morgan JT, Chana G, Pardo CA, Achim C, Semendeferi K, Buckwalter J, et al. (2010): Microglial activation and increased microglial density observed in the dorsolateral prefrontal cortex in autism. *Biol Psychiatry*. 68:368-376.

95. Tetreault NA, Hakeem AY, Jiang S, Williams BA, Allman E, Wold BJ, et al. (2012): Microglia in the cerebral cortex in autism. *J Autism Dev Disord*. 42:2569-2584.

96. Masi A, Quintana DS, Glozier N, Lloyd AR, Hickie IB, Guastella AJ (2015): Cytokine aberrations in autism spectrum disorder: a systematic review and meta-analysis. *Mol Psychiatry*. 20:440-446.

97. Rafols JA, Cheng HW, McNeill TH (1989): Golgi study of the mouse striatum: age-related dendritic changes in different neuronal populations. *J Comp Neurol*. 279:212-227.

98. Lebel C, Walker L, Leemans A, Phillips L, Beaulieu C (2008): Microstructural maturation of the human brain from childhood to adulthood. *Neuroimage*. 40:1044-1055.

99. Terry RD, DeTeresa R, Hansen LA (1987): Neocortical cell counts in normal human adult aging. *Ann Neurol*. 21:530-539.

100. Ando S, Tanaka Y (1990): Synaptic membrane aging in the central nervous system. *Gerontology*. 36 Suppl 1:10-14.

101. Grimm A, Eckert A (2017): Brain aging and neurodegeneration: from a mitochondrial point of view. *Journal of Neurochemistry*. 143:418-431.

102. Werling DM, Geschwind DH (2013): Sex differences in autism spectrum disorders. *Current Opinion in Neurology*. 26:146-153.

103. Halladay AK, Bishop S, Constantino JN, Daniels AM, Koenig K, Palmer K, et al. (2015): Sex and gender differences in autism spectrum disorder: summarizing evidence gaps and identifying emerging areas of priority. *Molecular autism*. 6:36.

104. Haier RJ, Siegel B, Tang C, Abel L, Buchsbaum MS (1992): Intelligence and changes in regional cerebral glucose metabolic rate following learning. *Intelligence*. 16:415-426.

105. Malpas CB, Genc S, Saling MM, Velakoulis D, Desmond PM, O'Brien TJ (2016): MRI correlates of general intelligence in neurotypical adults. *Journal of clinical neuroscience : official journal of the Neurosurgical Society of Australasia*. 24:128-134.

106. Hallermann S, de Kock CP, Stuart GJ, Kole MH (2012): State and location dependence of action potential metabolic cost in cortical pyramidal neurons. *Nat Neurosci*. 15:1007-1014.

107. Sengupta B, Stemmler M, Laughlin SB, Niven JE (2010): Action potential energy efficiency varies among neuron types in vertebrates and invertebrates. *PLoS Comput Biol*. 6:e1000840.

108. Edgar JM, McCulloch MC, Thomson CE, Griffiths IR (2008): Distribution of mitochondria along small-diameter myelinated central nervous system axons. *J Neurosci Res*. 86:2250-2257.

109. Fruhbeis C, Frohlich D, Kuo WP, Amphornrat J, Thilemann S, Saab AS, et al. (2013): Neurotransmitter-triggered transfer of exosomes mediates oligodendrocyte-neuron communication. *PLoS Biol*. 11:e1001604.

110. Kramer-Albers EM, Bretz N, Tenzer S, Winterstein C, Mobius W, Berger H, et al. (2007): Oligodendrocytes secrete exosomes containing major myelin and stress-protective proteins: Trophic support for axons? *Proteomics Clin Appl*. 1:1446-1461.

111. Funfschilling U, Supplie LM, Mahad D, Boretius S, Saab AS, Edgar J, et al. (2012): Glycolytic oligodendrocytes maintain myelin and long-term axonal integrity. *Nature*. 485:517-521.

112. Saab AS, Tzvetavona ID, Trevisiol A, Baltan S, Dibaj P, Kusch K, et al. (2016): Oligodendroglial NMDA Receptors Regulate Glucose Import and Axonal Energy Metabolism. *Neuron*. 91:119-132.

113. Belanger M, Allaman I, Magistretti PJ (2011): Brain energy metabolism: focus on astrocyte-neuron metabolic cooperation. *Cell metabolism*. 14:724-738.

114. Ravera S, Panfoli I, Calzia D, Aluigi MG, Bianchini P, Diaspro A, et al. (2009): Evidence for aerobic ATP synthesis in isolated myelin vesicles. *Int J Biochem Cell Biol*. 41:1581-1591.

115. Ravera S, Bartolucci M, Calzia D, Aluigi MG, Ramoino P, Morelli A, et al. (2013): Tricarboxylic acid cycle-sustained oxidative phosphorylation in isolated myelin vesicles. *Biochimie*. 95:1991-1998.

116. Morelli A, Ravera S, Panfoli I (2011): Hypothesis of an energetic function for myelin. *Cell Biochem Biophys*. 61:179-187.

117. Harris JJ, Attwell D (2013): Is myelin a mitochondrion? *J Cereb Blood Flow Metab*. 33:33-36.

118. Moffett JR, Ross B, Arun P, Madhavarao CN, Namboodiri AM (2007): N-Acetylaspartate in the CNS: from neurodiagnostics to neurobiology. *Prog Neurobiol*. 81:89-131.

119. Francis JS, Strande L, Markov V, Leone P (2012): Aspartoacylase supports oxidative energy metabolism during myelination. *J Cereb Blood Flow Metab*. 32:1725-1736.

ACCEPTED MANUSCRIPT

FIGURE LEGENDS

Figure 1. Group Comparisons and Symptom Correlations The right sides of the images correspond to the right side of the brain. All analyses control for the effects of age and sex, and the significance levels in all maps are FDR-corrected for the number of statistical comparisons.

First Row Shown is the T1-weighted anatomical template to which rCBF values for all participants were mapped at transaxial slice levels positioned parallel to the Anterior Commissure-Posterior Commissure (AC-PC) line, and corresponding to the positioning of the statistical maps shown in the other rows. The z-values represent slice level (in millimeters) in the Talairach coordinate system.

Second Row This shows the statistically significant differences in rCBF values between the ASD group and TD controls while covarying for age and sex, displayed at a threshold of $P<0.05$ after correction for multiple comparisons. Voxels in red indicate significantly increased rCBF, and blue voxels reduced rCBF, in ASD relative to controls. Perfusion values at rest in the ASD group were higher bilaterally throughout white matter of all the frontal lobe, internal capsule, and dorsal parietal lobe, and in gray matter of the basal ganglia, thalamus, and amygdala.

Third & Fourth Rows Red and blue voxels represent, respectively, significant positive or inverse correlations of ADOS total scores and SRS social affect scores with rCBF values in the ASD group, after FDR correction for multiple comparisons.

Abbreviations Am: amygdala; BS: brainstem; CC: corpus callosum; Cd: caudate; CR: corona radiata; CS: centrum semovale; H: hippocampus; IC: internal capsule; IF: inferior frontal gyrus; IT: inferior temporal gyrus; L: lenticular nucleus; MB: midbrain; MT: middle temporal gyrus; OFC: orbitofrontal cortex; OR optic radiations; PCC: posterior cingulate cortex; ST: superior temporal gyrus; Th: thalamus; VS: ventral striatum

Figure 2 Modifying Effects of Age, Sex, and FSIQ the significance levels in all maps are FDR-corrected for the number of statistical comparisons

Left Panel In the first two columns are maps showing the significance of age correlations with resting rCBF at each voxel in the ASD and TD groups separately, while covarying for sex. Red and blue voxels represent, respectively, significant positive or inverse correlations of age with rCBF values. The third column shows effects of the interaction of age with diagnosis on rCBF at each voxel, or the voxels where the correlations of age with rCBF differ significantly across the ASD and TD groups, while covarying for sex and including the main effects of age and diagnosis in a hierarchically well formulated statistical model.

Middle Panel In the first two columns are maps showing the significance of sex difference in rCBF at each voxel in the ASD and TD groups separately, while covarying for age. Red and blue voxels represent significantly higher rCBF values in males or females, respectively. The third column shows effects of the interaction of sex with diagnosis on rCBF at each voxel, or the voxels where sex differences in rCBF differ significantly across the ASD and TD groups, while covarying for age and including the main effects of sex and diagnosis in a hierarchically well formulated statistical model.

Right Panel In the first two columns are maps showing the significance of correlations of FSIQ (full scale IQ) with resting rCBF at each voxel in the ASD and TD groups separately, while covarying for age and sex. Red and blue voxels represent, respectively, significant positive or inverse correlations of FSIQ with rCBF values. The third column shows effects of the interaction of FSIQ with diagnosis on rCBF at each voxel, or the voxels where the correlations of FSIQ with rCBF differ significantly across the ASD and TD groups, while covarying for age and sex and

including the main effects of FSIQ and diagnosis in a hierarchically well formulated statistical model.

Abbreviations Am: amygdala; Cd: caudate; CR: corona radiata; CS: centrum semovale; dACC: dorsal anterior cingulate cortex; DLPFC: dorsolateral prefrontal cortex; Hy: hypothalamus; IC: internal capsule; IF: inferior frontal gyrus; Ins: insula; IT: inferior temporal gyrus; LG: lingual gyrus; MO: middle occipital gyrus; OFC: orbitofrontal cortex; OR optic radiations; pgACC: pregenual anterior cingulate cortex; PCC: posterior cingulate cortex; sgACC: subgenual anterior cingulate cortex; ST: superior temporal gyrus; VS: ventral striatum

Figure 3. Data Displays for Age, Sex, and FSIQ Effects These are shown for representative regions indicated from a slice taken from Figure 2, shown above each plot in the statistical map. The line leading from the regional label to the image indicates the voxels with the images that were sampled to generate the data shown in the scatterplots. The scatterplots illustrate the age-related decline in rCBF in most cortical regions for ASD and the inverse correlation of rCBF with full scale IQ (FSIQ) in the TD but not ASD group. Bar graphs for sex effects demonstrate in ASD participants the reversal of female>male sex differences present in the TD group. Error bars represent standard error.

Figure 4. Correlations of rCBF with NAA Metabolite Levels and Lactate Top 3 Rows show the voxel-wise correlations of NAA level with rCBF in the ASD (N=36, 29 males, 7 females, mean age 25.6 years) and TD (N=63, 48 males, 15 females, mean age 22.3 years) groups combined (top row) and separately, while covarying for age and sex. Significance levels are FDR-corrected for the number of statistical comparisons. Primarily inverse correlations (blue voxels) are present in the ASD group in frontal white matter of the centrum semiovale (CS) and corona radiata (CR), internal capsule (IC), and external capsule (EC), and in the midcingulate

cortex (MCC) and posterior cingulate cortex (PCC). In the TD group, inverse correlations are seen in similar locations, but are smaller in spatial extent and weaker in statistical significance; positive correlations (red voxels) in the TD group are scattered throughout cortical gray matter (insula: Ins; posterior cingulate cortex: PCC) and inverse correlations are present in frontal white matter (CS, CR). Bottom Row The 6 ASD participants with detectable lactate compared with the 30 without detectable lactate had significantly lower rCBF values (blue voxels) in the dorsal prefrontal cortex (DPFC), pregenual anterior cingulate cortex (pgACC), posterior cingulate cortex (PCC), genu of the corpus callosum (gCC), and posterior white matter of the centrum semiovale (CS) and parieto-occipital (PO) region.

ACCEPTED MANUSCRIPT

Table 1. Participant Characteristics

	ASD	TD	Test Stat	df	P-value
N	44	66			
Mean Age	24.9±15.6	22.0±11.2	T=1.1	108	0.26
Age Range	5.9–60.7	6.9–59.0			
Sex	32m/12f	50m/16f	$\times^2$=0.13	1	0.72
SES	48.8±10.5	53.5±11.1	T=1.90	85	0.06
Handedness	38R,6L	62R,4L	$\times^2$=2.8	1	0.11
Ethnic/Racial Minority	9	18	$\times^2$=0.77	1	0.38
Framewise Motion (mm)	0.17±0.06	0.16±0.06	T=0.88	109	0.37
RMS Motion (mm)	0.09±0.03	0.09±0.04	T=0.89	109	0.37
FSIQ	112.3±18.3	116.7±10.6	T=1.42	60.8	0.16
ADOS Total[a]	10.8±4.1	–			
ADOS Social Affect	9.1±3.8	–			
ADOS Restrict & Repet Beh	1.7±1.6	–			
SRS Total[b]	83.0±27.2	20.8±18.3	T=12.1	61.8	4×10^{-14}
SRS Awareness	10.6±3.3	5.1±3.2	T=7.8	85	1×10^{-11}
SRS Cognition	15.4±4.8	3.1±3.6	T=13.3	66.7	2×10^{-20}
SRS Communication	28.4±9.0	6.2±7.2	T=12.8	85	1×10^{-21}
SRS Motivation	13.7±5.3	3.5±3.3	T=10.4	58.8	7×10^{-15}
SRS Mannerisms	15.6±6.9	3.0±3.8	T=10.1	53.9	4×10^{-14}

[a]ADOS scores were available for 41 ASD participants
[b]SRS scores were available for 38 ASD and 49 TD participants
ADOS=Autism Diagnostic Observation Schedule; Restrict & Repet Beh=Restricted and Repetitive Behaviors
SRS=Social Responsiveness Scale; Awareness=Social Awareness; Cognition=Social Cognition; Communication=Social Communication; Motivation=Social Motivation; Mannerisms=Restricted Interests and Repetitive Behaviors
SES=socioeconomic status measured with the Hollingshead; this was available in 31 ASD and 56 TD participants
FSIQ was available in 43 ASD and 65 TD participants
RMS=Root Mean Square motion estimate during the ASL scan

ACCEPTED MANUSCRIPT

ACCEPTED MANUSCRIPT

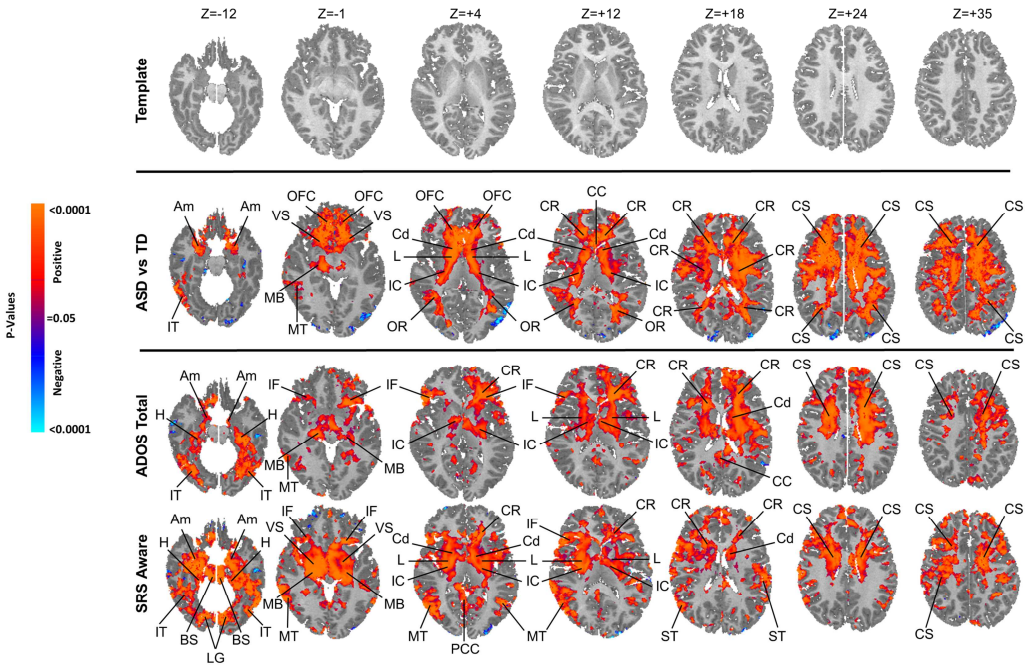

ACCEPTED MANUSCRIPT

ACCEPTED MANUSCRIPT

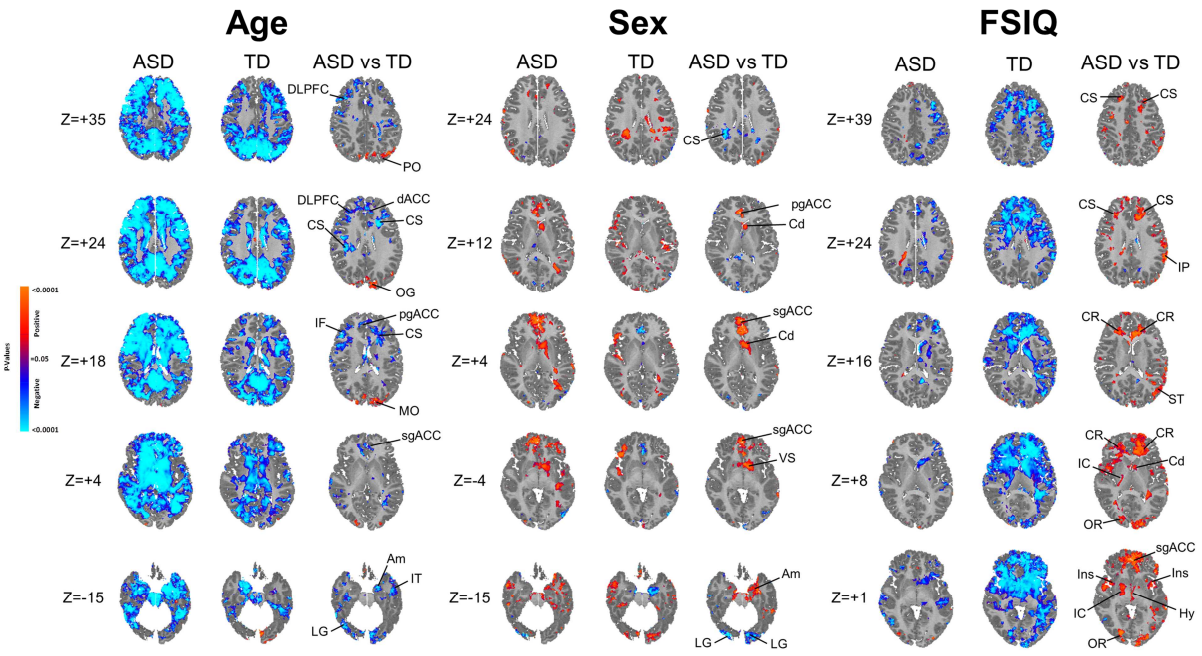

AGE: ASD vs TD

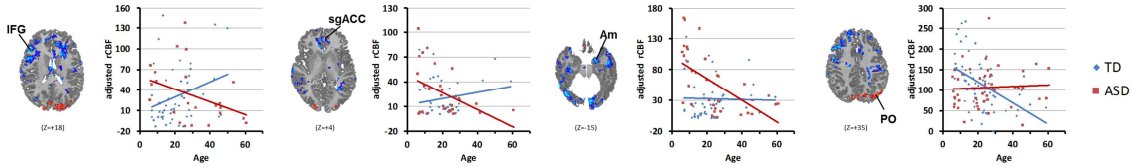

FSIQ: ASD vs TD

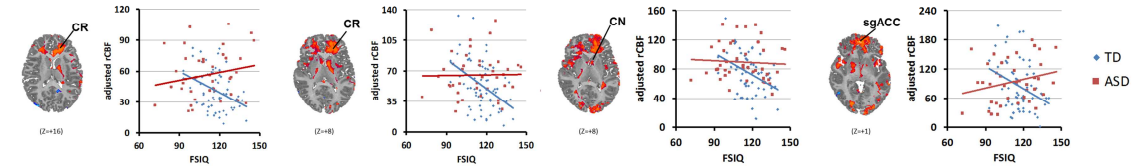

SEX: ASD vs TD

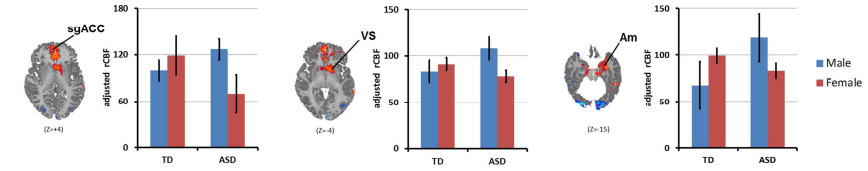

ACCEPTED MANUSCRIPT

ACCEPTED MANUSCRIPT

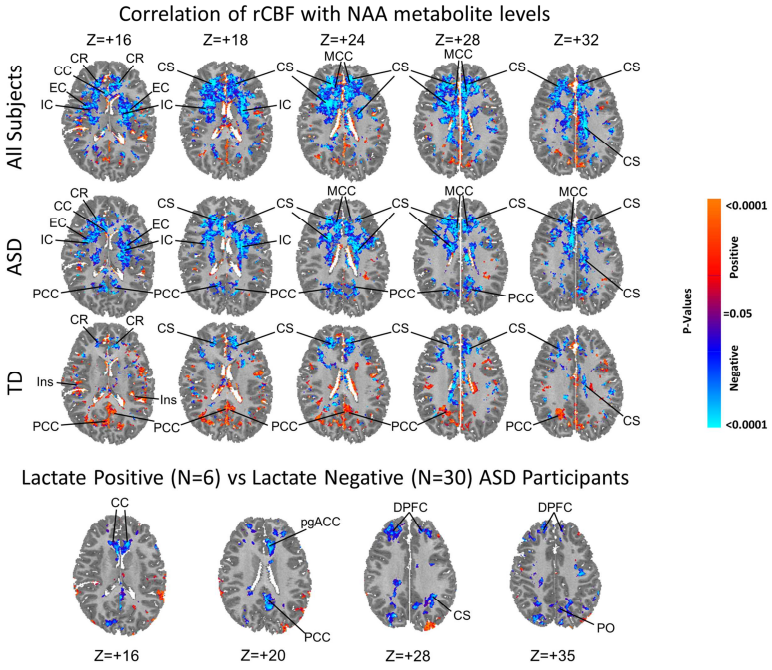

ACCEPTED MANUSCRIPT

ACCEPTED MANUSCRIPT

Hyperperfusion of Frontal White and Subcortical Gray Matter in Autism Spectrum Disorder

Supplemental Information

Table of Contents

ACCEPTED MANUSCRIPT

ACCEPTED MANUSCRIPT

SECTION 7: PRIMARY ANALYSES SEPARATELY IN YOUTH AND ADULTS

ACCEPTED MANUSCRIPT

ACCEPTED MANUSCRIPT

SUPPLEMENTAL TEXT

ACCEPTED MANUSCRIPT

ACCEPTED MANUSCRIPT

Section 1: MRI Scanning Procedures and Pulse Sequences

Images were acquired on a GE Signa 3T (Tesla) HDx system with an 8-channel, receive-only head coil.

ASL We optimized our Pulsed Arterial Spin Labeling (PASL) perfusion sequence for parallel imaging at 3T using a PICORE (Proximal Inversion with Control for Off-Resonance Effects) QUIPSS II (Quantitative Imaging of Perfusion using a Single Subtraction) pulse sequence (1). We placed a 9-cm tagging slab 16-mm below the proximal edge of the imaging volume. We acquired the control images by applying off-resonance adiabatic hyperbolic secant RF pulse with the same frequency offset as that for the labeled images without the slice-selective gradient, so as to control for off-resonance effects of the inversion pulses used for acquiring the labeled images. We used a single-shot, gradient-echo, echo planar imaging (EPI) sequence for image acquisition, with time to QUIPSS saturation TI_1=600 ms and inversion time of the first slice TI_2 =1300 ms. Acquisition parameters included FOV 24 cm, 64x64 matrix, TE(echo time)/TR (repetition time)=24/2300ms, flip angle 90°, slice thickness 6 mm, inter-slice spacing 0.5 mm, providing a nominal spatial resolution of 3.75x3.75x6.5 mm. We acquired 18 slices from inferior to superior in sequential order. Each ASL scan with 151 acquisitions plus 5 dummy images required 5 min 59 sec.

A separate M0 scan using gradient-echo EPI with TR of 15sec was acquired at the same resolution and slice position as the ASL data. The M_{0wm} from white matter is measured and then used in the off-line computation of rCBF (1).

ASL Localizer We also acquired a T1-weighted, localizer image with high in-plane resolution in the same slice locations as the ASL data for coregistering each participant's ASL data to its T1-weighted anatomical MR image. The localizer image was acquired using a 2D, fast spin echo pulse sequence with echo train length=9, TR = 2150ms, TE = 9.94ms, TI = 840ms, flip angle = 90^o, in-plane resolution = 0.94 x 0.94 mm^2, slice thickness = 6.5mm. Total acquisition time = 1 min, 46 sec.

MRS data were acquired in 6 axial-oblique slabs (2-mm gap) parallel to the anterior commissure-posterior commissure (AC-PC): one slab below, one slab containing, and 4 slabs above the AC-PC. We used a water-suppressed MPCSI sequence with TR/TE=2800/144 ms, voxels 10x10x10 mm^3, and suppressed lipid signal from the scalp using eight saturation bands. Scan time, including shimming, was 20 min.

MRS Localizer A "localizer" MRI with voxels 0.98x0.98x10 mm^3 was acquired in register with MPCSI and was used to coregister and normalize MPCSI data into the common coordinate space of a template brain. Whole-brain T1-weighted (T1) MRI was obtained using 3D spoiled gradient recall with 0.98x0.98x1.0 mm^3 voxels. The T1 was used to prescribe MPCSI and to segment the brain into gray and white matter.

Additional Sequences included Anatomical MRI, Diffusion Tensor Imaging, Task-Based functional MRI, and Resting-State functional MRI

Total Scan Time was approximately 75 minutes, with additional time included for participant breaks to rest and move about, and reacquire sequences that had evidence of motion artifact.

Section 2: Image Processing Methods

ACCEPTED MANUSCRIPT

ASL We aligned the PASL brain images and the M_{0_WM} image to the first PASL image for each participant in native imaging space to correct for head motion. We spatially smoothed the coregistered PASL images using a Gaussian kernel of 6mm FWHM (Full Width at Half Maximum) to improve signal-to-noise ratio while avoiding loss of spatial precision in locating our effects of interest. We generated a brain mask for each participant based on the mean PASL image. We constructed for each participant a voxel-wise map of rCBF from the PASL time series and M_{0_WM} image using in-house software: (1) We pair-wise subtracted the control images from the labeled images; (2) From the average of the subtracted images, we calculated rCBF at each voxel as $rCBF = \frac{6000*\Delta I}{2\alpha*M_{0\_B}*TI_1*exp(-TI_2/T_{1\_B})}$, where ΔI is the image difference obtained in step 1; α is the tagging efficiency, for which we used the default value of 0.9; $TI_1 = 600$ ms is the time to QUIPSS saturation; $TI_2 = 1300$ ms is the inversion time of the first slice and is slice time corrected for the rest of the slices in the imaging volume; and T_{1B} is the T_1 of blood, for which we used the default value of 1664 ms (2); M_{0_B} is the MR signal from a voxel filled with arterial blood, estimated from the M_{0_WM} map as $M_{0\_B} = rM_{0\_WM}e^{(1/T_{2WM}-1/T_{2B})TE}$ where *r* is the proton density ratio of blood, for which we used a default value of 1.06; and where the default values for T_{2WM} and T_{2B} were 70 ms and 200 ms, respectively (1, 3, 4). We used a 6 degrees-of-freedom rigid-body transformation such that mutual information (5) is increased to coregister the anatomical images to the localizer images for each participant. Subsequently, each participant's anatomical image is used as an intermediary source to coregister the rCBF images to a template brain by applying a similarity (5) followed with a nonlinear transformation based on fluid flow (6). We selected a single individual brain as the template brain, which was morphologically the most representative of the brains for TD participants (7).

We quantified the amount of head motion in the ASL data of each participant using two summary statistics, Root Mean Squared (RMS) (8) and Mean Frame-wise Displacement (FD) metric sums differentiated realignment estimates (9), derived from three translational (x,y,z) and three angular rotational (roll, pitch, yaw). Motion during the ASL scan was minimal and comparable across groups (Table 1).

MRS Following time-domain preprocessing, MPCSI data were transformed into the frequency domain and loaded into a 3DiCSI software package (http://hatch.cpmc.columbia.edu/software.html) that identified brain-internal MPCSI voxels. Spectra were fit for NAA (N-acetylaspartate), Glx, Cr (creatine), Cho (choline) and lipids using Gaussian-Lorentzian curves and least-squares estimation. Areas under the curves estimated metabolite concentrations in each voxel. Data were quality controlled by inspection of each spectrum, rejecting spectra with lipid contamination, insufficient water suppression, unresolved Cr and Cho, or linewidth > 12 Hz. We calculated background noise as the standard deviation of the part of the real spectrum free from metabolite signal, then generated a spectroscopic image for NAA as the ratio of peak area to background noise for each voxel, accounting for variations in receiver and transmitter gain. The brain was extracted from each T1 volume, warped into a cross-participant template, and segmented into gray and white matter. We corrected the spectroscopic images for partial-voluming (variable gray- *vs.* white-matter content across MPCSI voxels) and for the MPCSI point-spread function (dispersion of the MR signal into neighboring voxels) using linear regression to estimate the concentration of that metabolite in gray matter and white matter in each voxel and neighboring voxels. We resampled metabolite levels from the low-resolution MPCSI to the high-resolution T1 during spatial normalization, which

ACCEPTED MANUSCRIPT

required coregistering and nonlinearly warping the MPCSI volume for each participant onto the T1 template brain. We then used the T1 image and high-resolution localizer to coregister each metabolite image to the study template to permit correlation of NAA levels with rCBF measures at each voxel. Processing for the detection of lactate in this sample has been described in detail previously (10).

References

1. Wong EC, Buxton RB, Frank LR (1998): Quantitative imaging of perfusion using a single subtraction (QUIPSS and QUIPSS II). *Magn Reson Med*. 39:702-708.
2. Lu H, Clingman C, Golay X, van Zijl PC (2004): Determining the longitudinal relaxation time (T1) of blood at 3.0 Tesla. *Magn Reson Med*. 52:679-682.
3. Jarnum H, Steffensen EG, Knutsson L, Frund ET, Simonsen CW, Lundbye-Christensen S, et al. (2010): Perfusion MRI of brain tumours: a comparative study of pseudo-continuous arterial spin labelling and dynamic susceptibility contrast imaging. *Neuroradiology*. 52:307-317.
4. Alsop DC, Detre JA (1996): Reduced transit-time sensitivity in noninvasive magnetic resonance imaging of human cerebral blood flow. *J Cereb Blood Flow Metab*. 16:1236-1249.
5. Viola P, Wells, W. M. (1995): Alignment by Maximization of Mutual Information. *IEEE Proc of the 5th Int Conf on Computer Vision*. Boston, MA, pp 16-23.
6. Christensen GE, Joshi SC, Miller MI (1997): Volumetric Transformation of Brain Anatomy. *IEEE Transactions on Medical Imaging*. 16:1369-1383.
7. Peterson BS, Warner V, Bansal R, Zhu H, Hao X, Liu J, et al. (2009): Cortical thinning in persons at increased familial risk for major depression. *Proc Natl Acad Sci U S A*. 106:6273-6278.
8. Jenkinson M, Bannister P, Brady M, Smith S (2002): Improved optimization for the robust and accurate linear registration and motion correction of brain images. *Neuroimage*. 17:825-841.
9. Power JD, Barnes KA, Snyder AZ, Schlaggar BL, Petersen SE (2012): Spurious but systematic correlations in functional connectivity MRI networks arise from subject motion. *NeuroImage*. 59:2142-2154.
10. Goh S, Dong Z, Zhang Y, DiMauro S, Peterson BS (2014): Mitochondrial dysfunction as a neurobiological subtype of autism spectrum disorder: evidence from brain imaging. *JAMA psychiatry*. 71:665-671.

ACCEPTED MANUSCRIPT

Supplemental Materials Section 3:
3a: Main Text Figures Showing All Slices

ACCEPTED MANUSCRIPT

ACCEPTED MANUSCRIPT

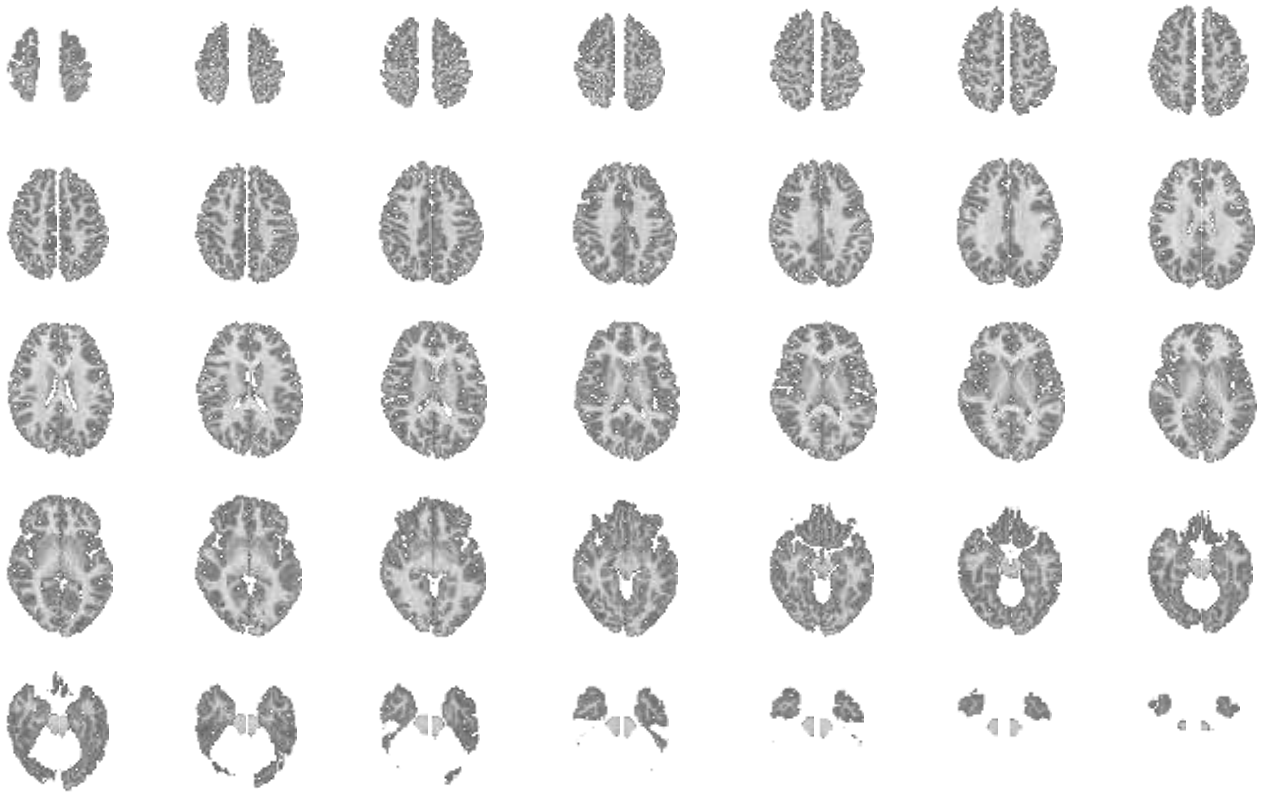

Supplementary Figure S1. T1-Weighted Anatomical Template

Shown are all slices of the T1-weighted anatomical template on which statistical maps were overlaid, with transaxial slice levels positioned parallel to the Anterior Commissure-Posterior Commissure (AC-PC) line. The z-values represent slice level (in millimeters) in the Talairach coordinate system. The right sides of the images correspond to the right side of the brain.

ACCEPTED

ACCEPTED MANUSCRIPT

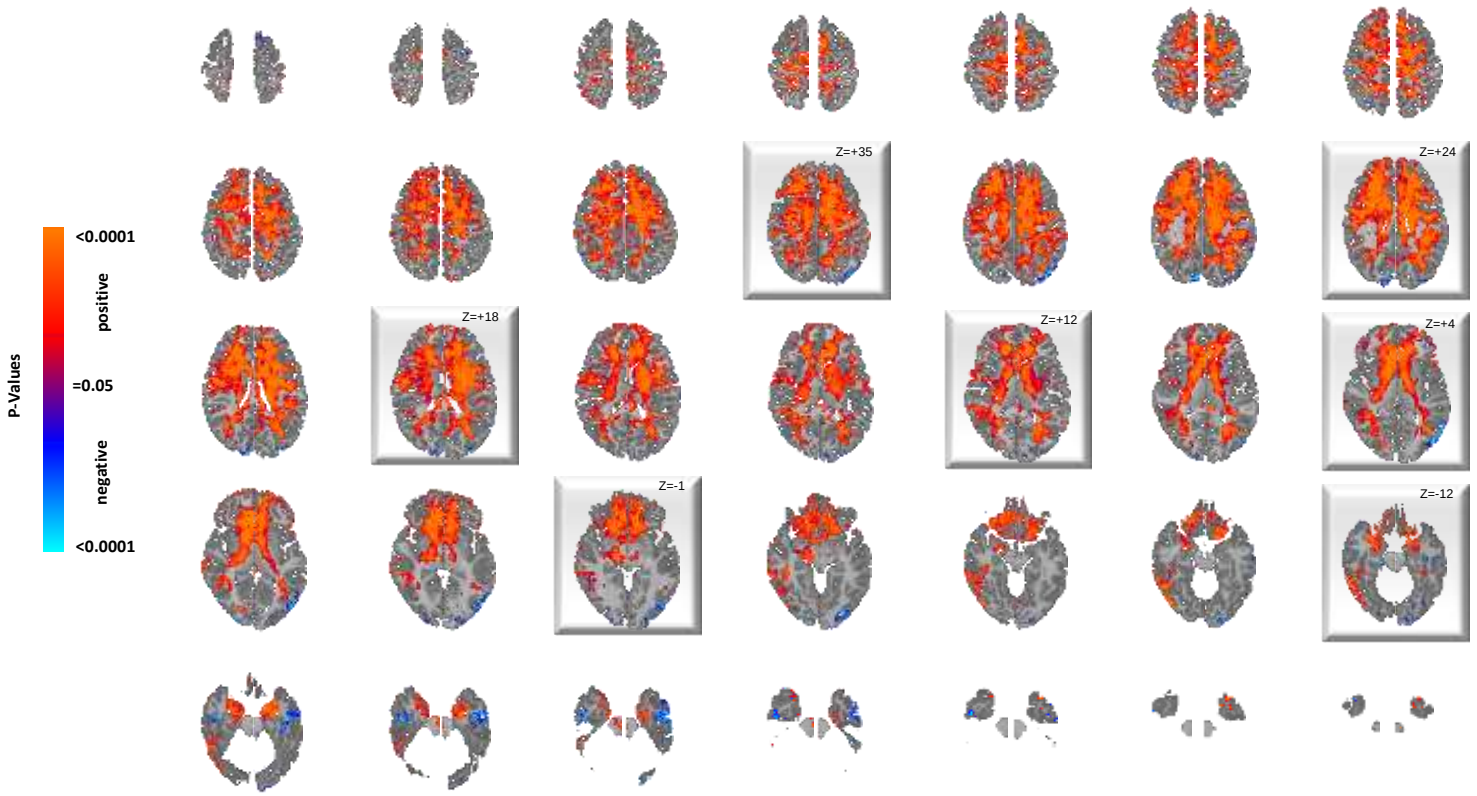

Supplementary Figure S2. Main Effect of Diagnosis for All Slices

This shows the statistically significant differences in rCBF values between the ASD group and TD controls for all slices while covarying for age and sex, displayed at a threshold of P<0.05 after correction for multiple comparisons. Voxels in red indicate significantly increased rCBF, and blue voxels reduced rCBF, in ASD relative to controls. Highlighted slices (with their z-level Talairach coordinates) are those displayed in Figure 1 of the main text.

ACCEPTED MANUSCRIPT

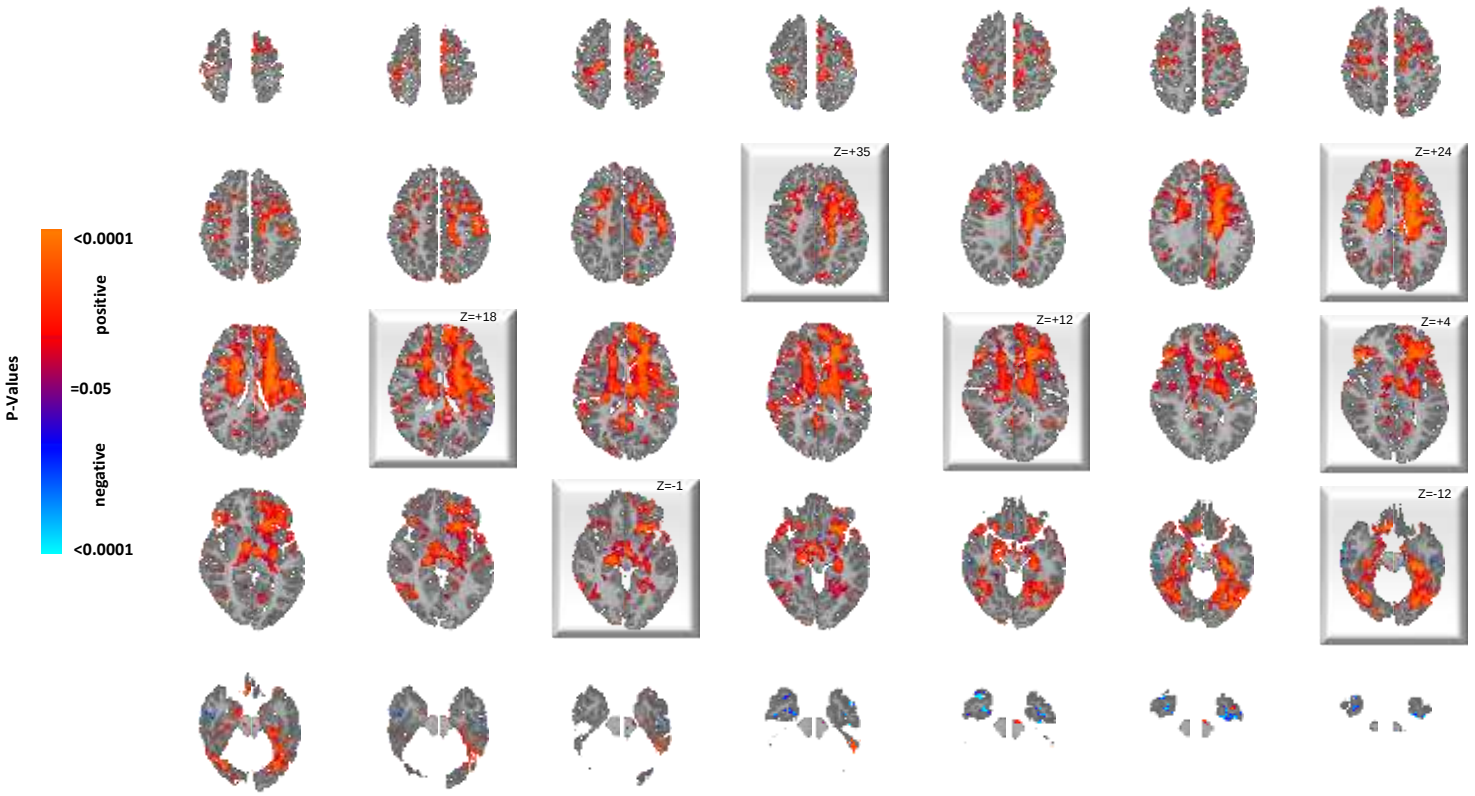

Supplementary Figure S3. Correlation of rCBF with ADOS Total Scores for All Slices

Shown here are all slices for the statistically significant correlations of ADOS Total scores with rCBF values in the ASD group, while covarying for age and sex, displayed at a threshold of P<0.05 after FDR correction for multiple comparisons. Red and blue voxels represent, respectively, significant positive or inverse correlations of ADOS Total scores with rCBF values in the ASD group. Highlighted slices (with their z-level Talairach coordinates) are those displayed in Figure 1 of the main text.

ACCEPTED MANUSCRIPT

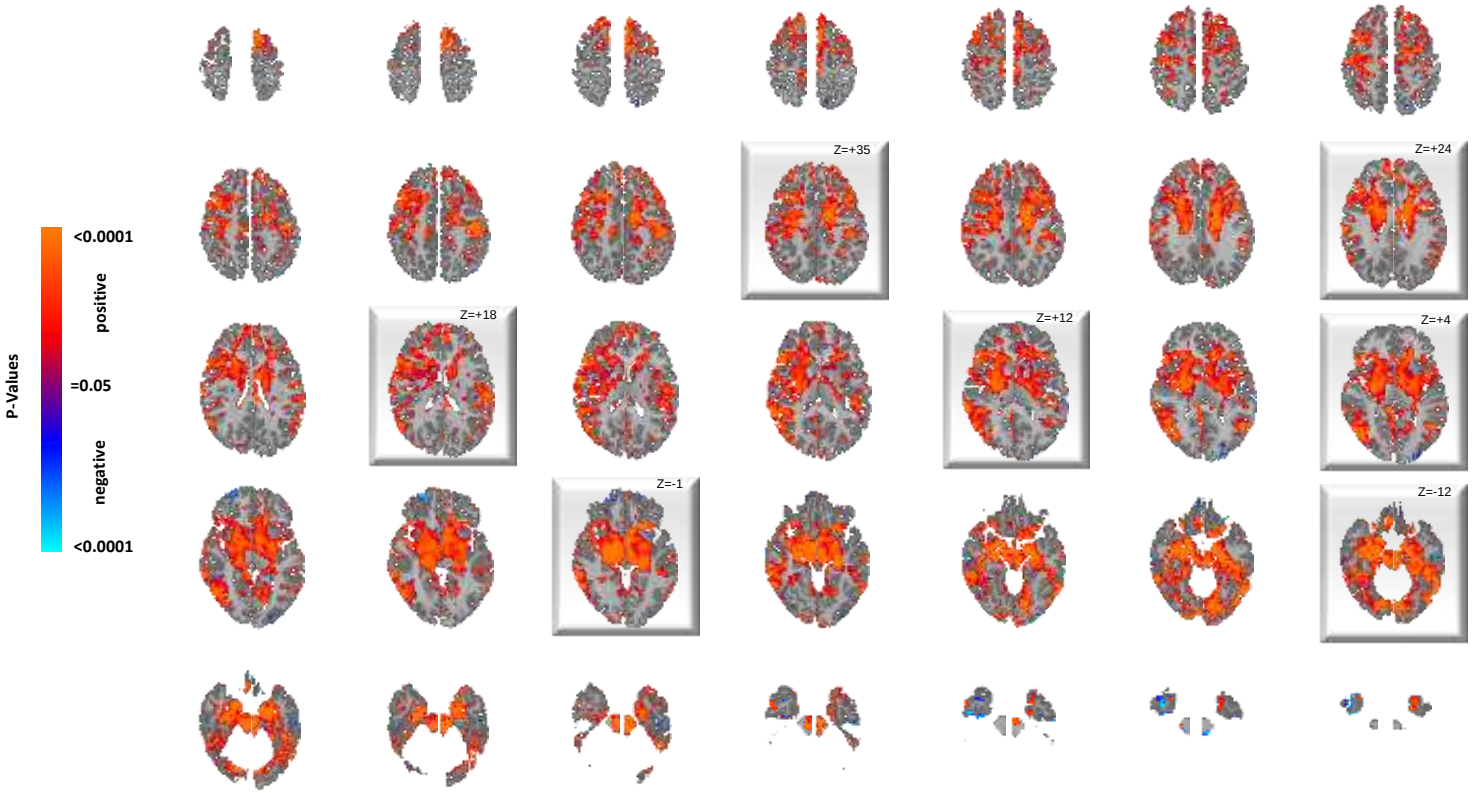

Supplementary Figure S4. Correlation of rCBF with SRS Social Awareness Scores for All Slices

Shown here are all slices for the statistically significant correlations of SRS Awareness scores with rCBF values in the ASD group, while covarying for age and sex, displayed at a threshold of P<0.05 after FDR correction for multiple comparisons. Red and blue voxels represent, respectively, significant positive or inverse correlations of SRS Awareness scores with rCBF values in the ASD group. Highlighted slices (with their z-level Talairach coordinates) are those displayed in Figure 1 of the main text.

ACCEPTED MANUSCRIPT

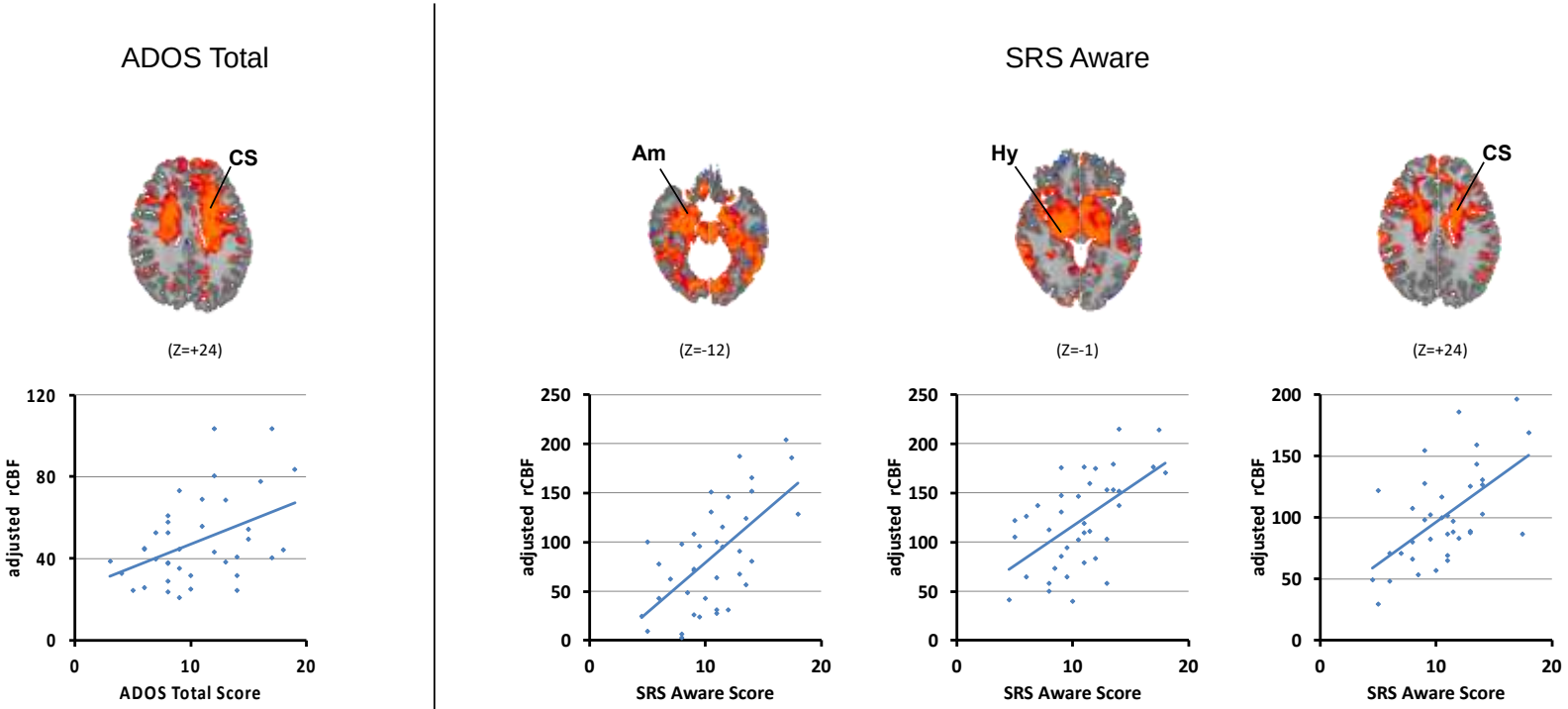

Supplementary Figure S5. Scatterplots for the Correlations of rCBF with ADOS Total and SRS Awareness Scores

These are shown for representative regions indicated above each plot in the statistical map in slices selected from the statistical maps representing the correlation of rCBF with ADOS Total or SRS Awareness scores. The line leading from the regional label to the image indicates the voxels with the images that were sampled to generate the data shown in the scatterplots. The effects of age and sex are partialed out of the rCBF values (hence the negative values for adjusted rCBF values on the y-axis. The scatterplots show that the data are well distributed around the regression lines.

ACCEPTED MANUSCRIPT

Supplemental Materials Section 3b:
Age Effects Showing All Slices

ACCEPTED MANUSCRIPT

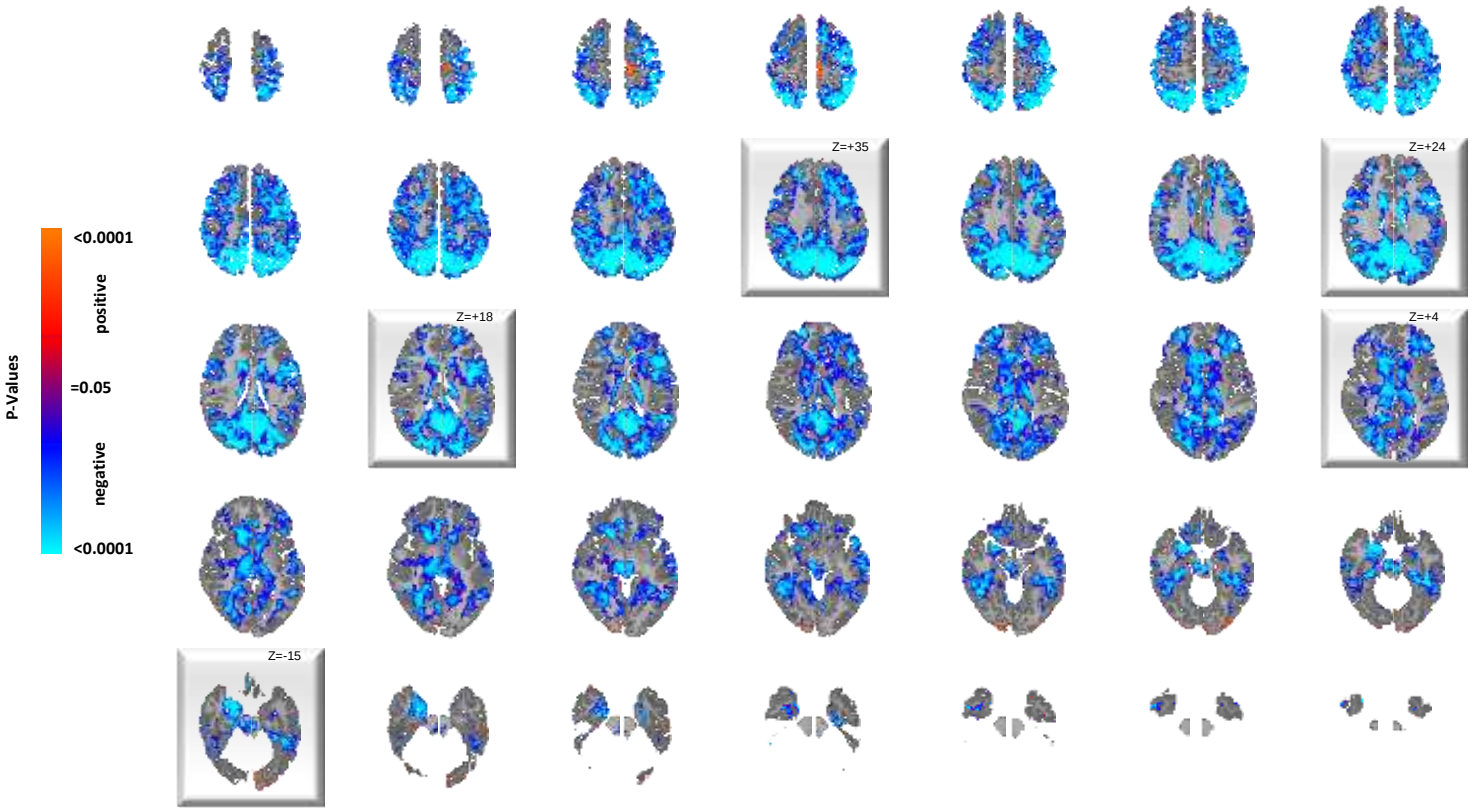

Supplementary Figure S6. Correlates of rCBF with Age in the TD Group Only for All Slices

This map shows the significance of age correlations with resting rCBF at each voxel in the TD group, while covarying for sex, in all slices. Red and blue voxels represent, respectively, significant positive or inverse correlations of age with rCBF values. Highlighted slices (with their z-level Talairach coordinates) are those displayed in Figure 2 of the main text.

ACCEPTED

ACCEPTED MANUSCRIPT

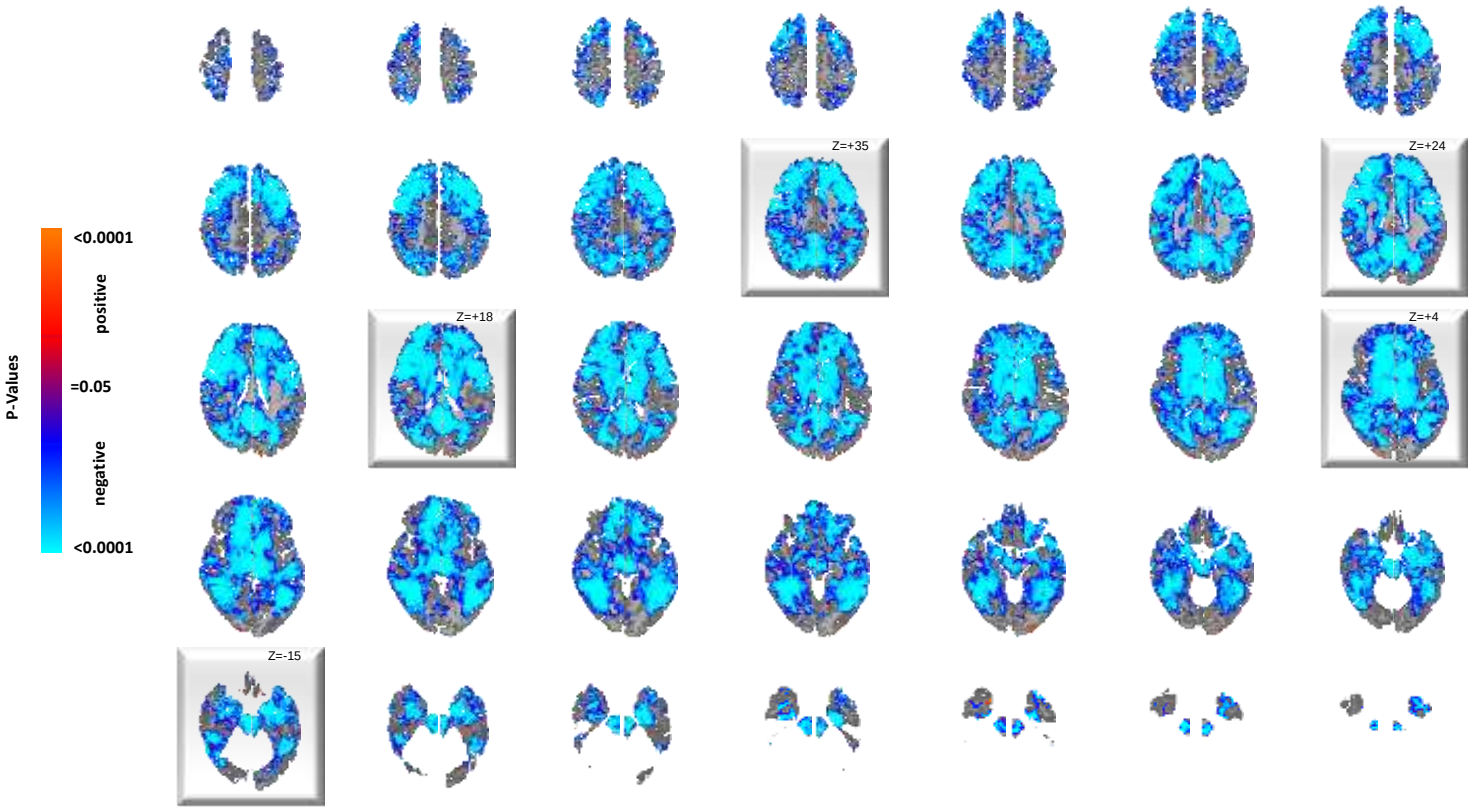

Supplementary Figure S7. Correlates of rCBF with Age in the ASD Group Only for All Slices

This map shows the significance of age correlations with resting rCBF at each voxel in the ASD group, while covarying for sex, in all slices. Red and blue voxels represent, respectively, significant positive or inverse correlations of age with rCBF values. Highlighted slices (with their z-level Talairach coordinates) are those displayed in Figure 2 of the main text.

ACCEPTED MANUSCRIPT

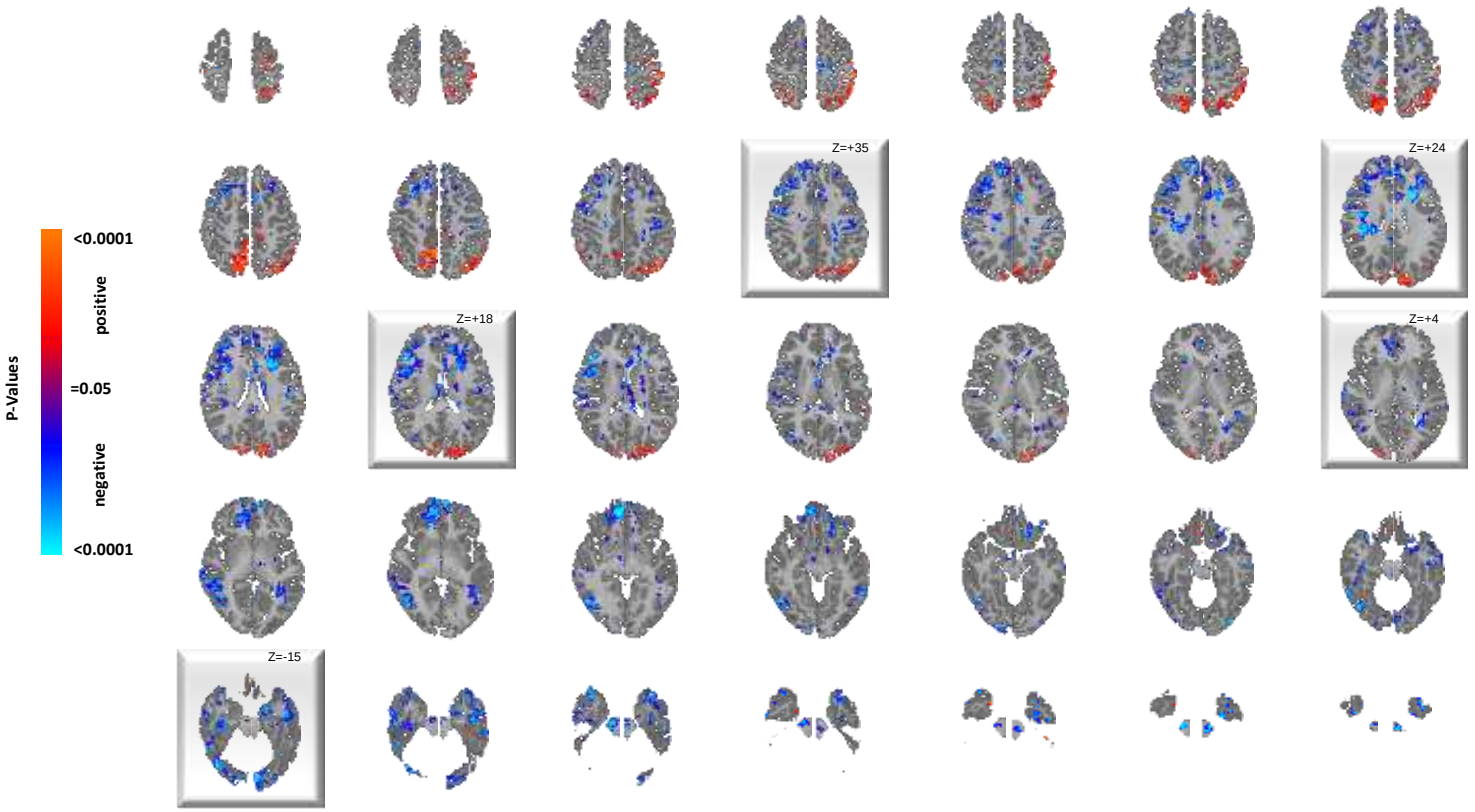

Supplementary Figure S8. The Interaction of Diagnosis with Age in All Slices

This map shows the significant effects of the interaction of age with diagnosis (ASD or TD) on rCBF at each voxel in all slices, while covarying for sex and including the main effects of age and diagnosis in a hierarchically well formulated statistical model. The interaction effect indicates voxels where the correlation of age with rCBF differs significantly across the ASD and TD groups. Red and blue voxels represent the mathematical sign (positive or negative, respectively) of the F-test statistic for the interaction. Highlighted slices (with their z-level Talairach coordinates) are those displayed in Figure 2 of the main text.

ACCEPTED MANUSCRIPT

Supplemental Materials Section 3c:
Sex Effects Showing All Slices

ACCEPTED MANUSCRIPT

ACCEPTED MANUSCRIPT

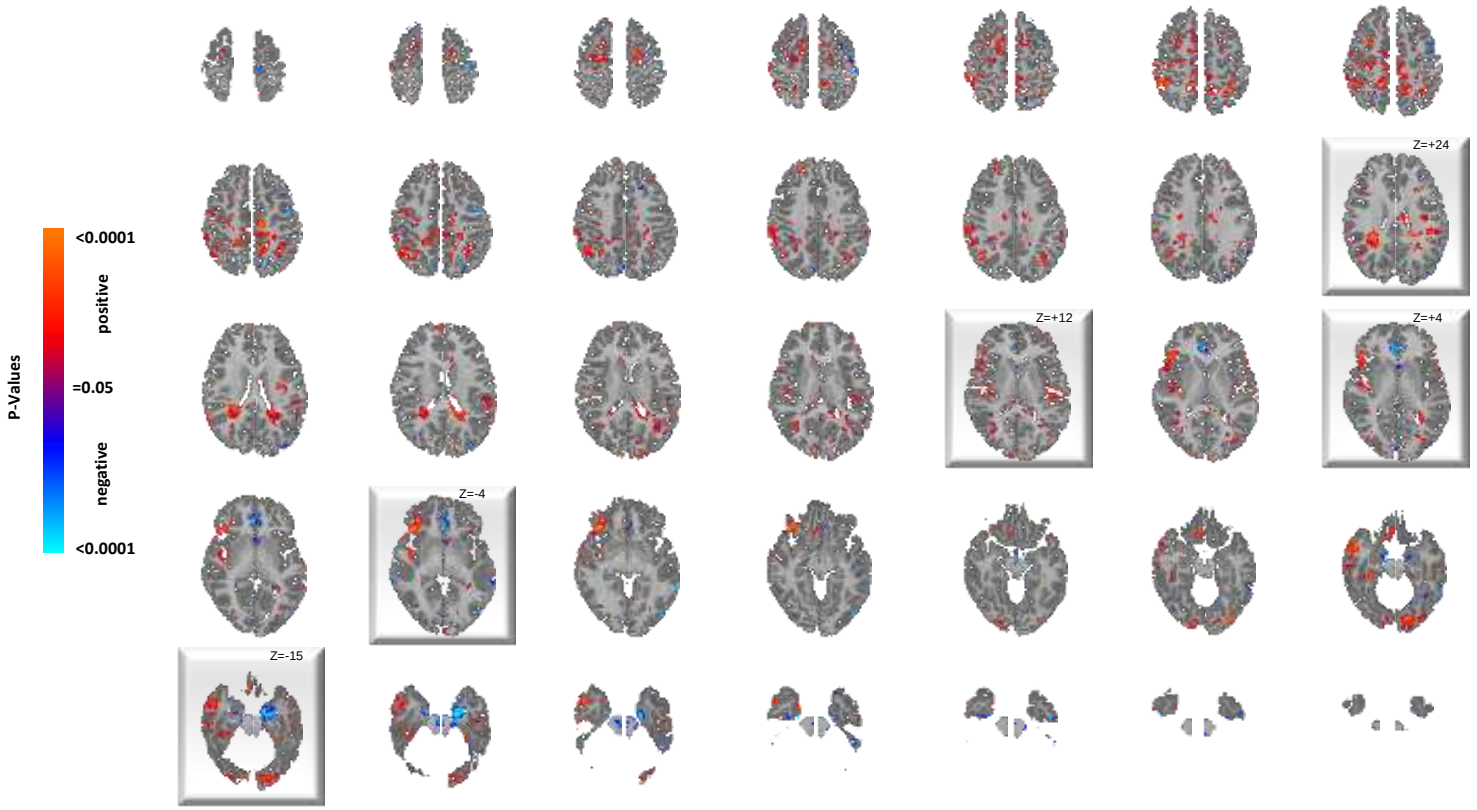

Supplementary Figure S9. Sex Differences in rCBF within the TD Group Only for All Slices

This shows all maps illustrating the significance of sex correlations with resting rCBF at each voxel in the TD group in all slices, while covarying for age. Red and blue voxels represent significantly larger rCBF values in males or females, respectively. Shown here are all slices for which data was collected in the brain. Highlighted slices (with their z-level Talairach coordinates) are those displayed in Figure 2 of the main text.

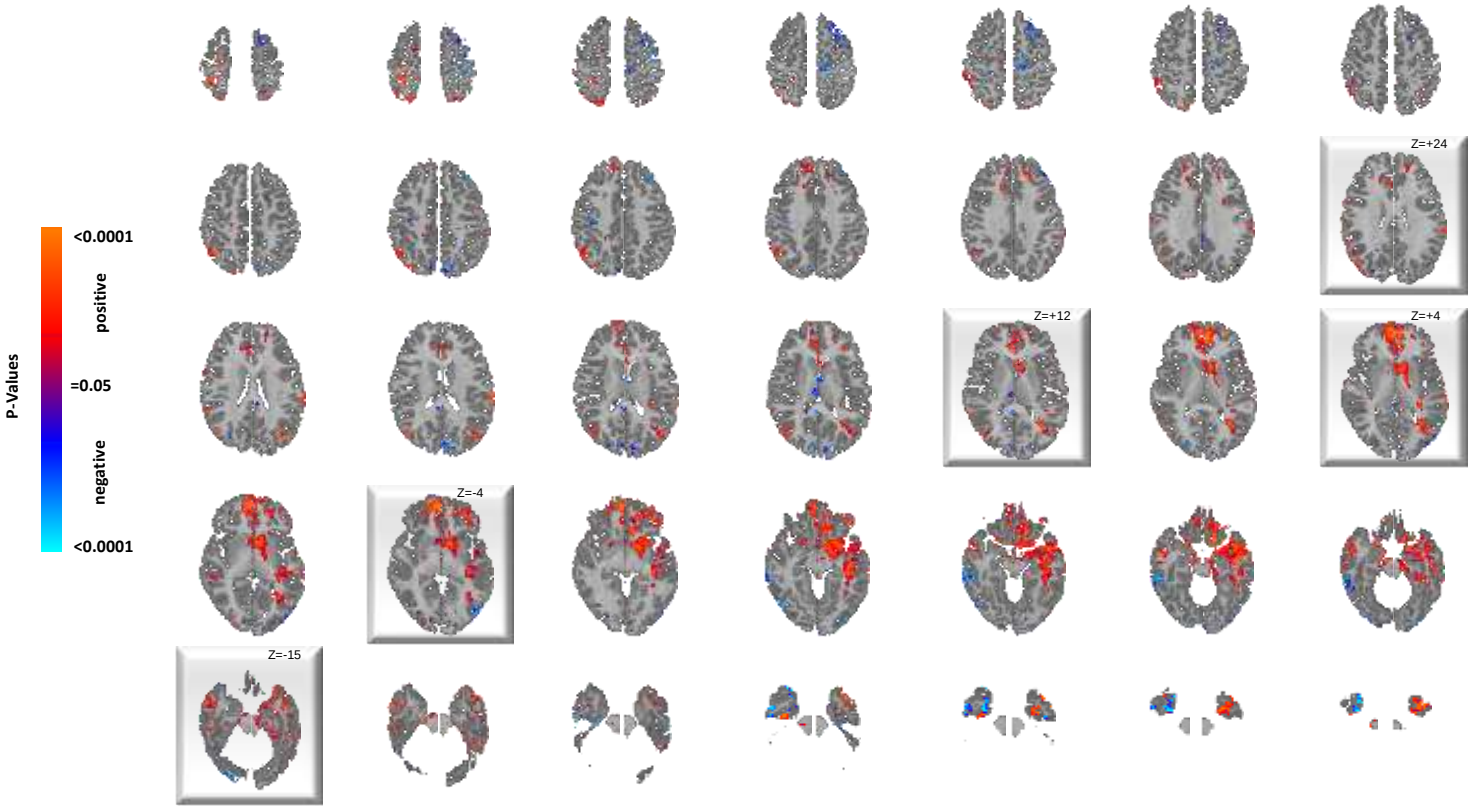

Supplementary Figure S10. Sex Differences in rCBF within the ASD Group Only for All Slices

This shows all maps illustrating the significance of sex correlations with resting rCBF at each voxel in the ASD group in all slices, while covarying for age. Red and blue voxels represent significantly larger rCBF values in males or females, respectively. Shown here are all slices for which data was collected in the brain. Highlighted slices (with their z-level Talairach coordinates) are those displayed in Figure 2 of the main text.

ACCEPTED MANUSCRIPT

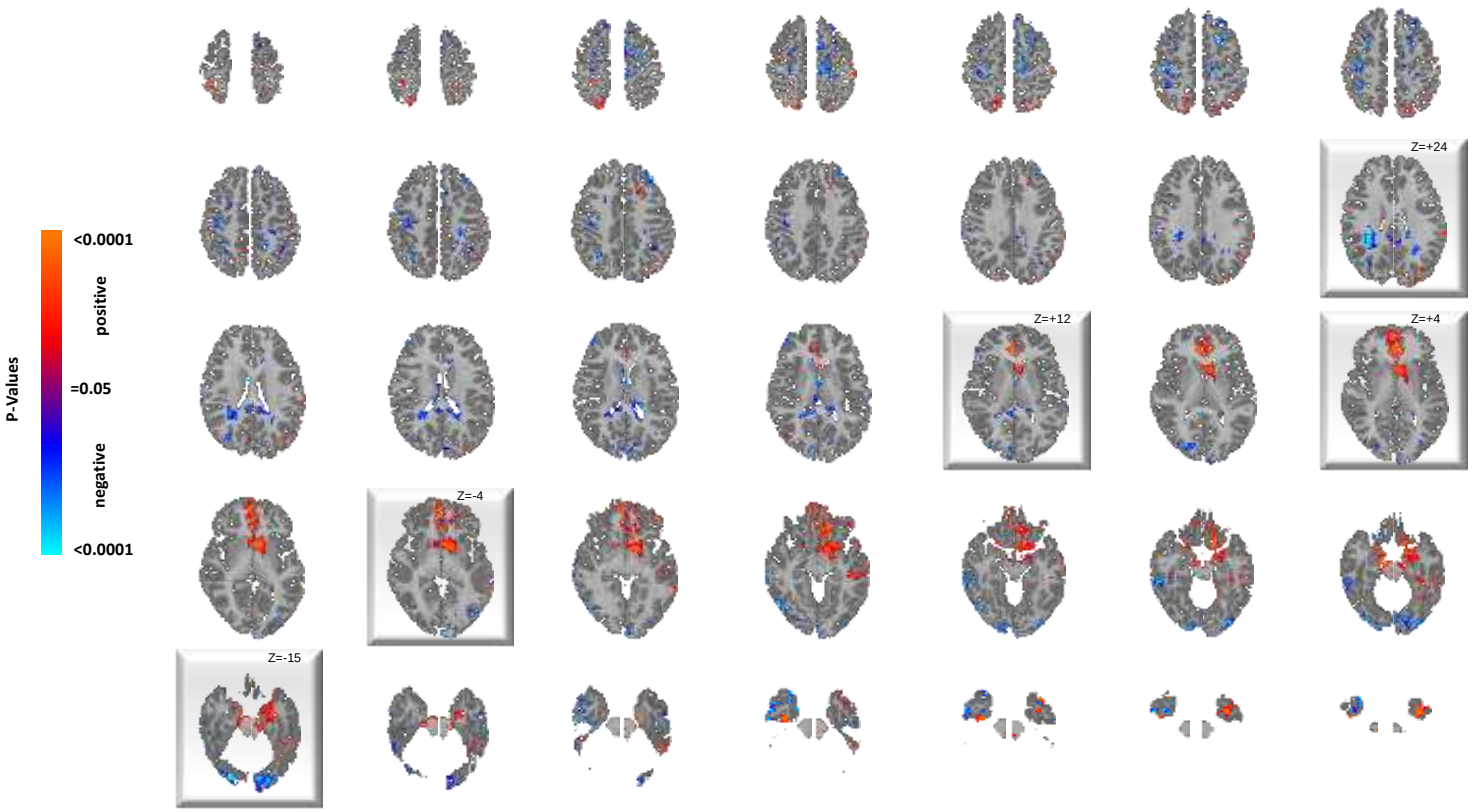

Supplementary Figure S11. The Interaction of Diagnosis with Sex in All Slices

This map shows the significant interaction effects of sex (male or female) with diagnosis (ASD or TD) on rCBF at each voxel in all slices, while covarying for age and including the main effects of sex and diagnosis in a hierarchically well formulated statistical model. The interaction effect indicates voxels where the correlation of age with rCBF differs significantly across the ASD and TD groups. Red and blue voxels represent the mathematical sign (positive or negative, respectively) of the F-test statistic for the interaction. Highlighted slices (with their z-level Talairach coordinates) are those displayed in Figure 2 of the main text.

ACCEPTED MANUSCRIPT

Supplemental Materials Section 3d:
FSIQ Effects Showing All Slices

ACCEPTED MANUSCRIPT

ACCEPTED MANUSCRIPT

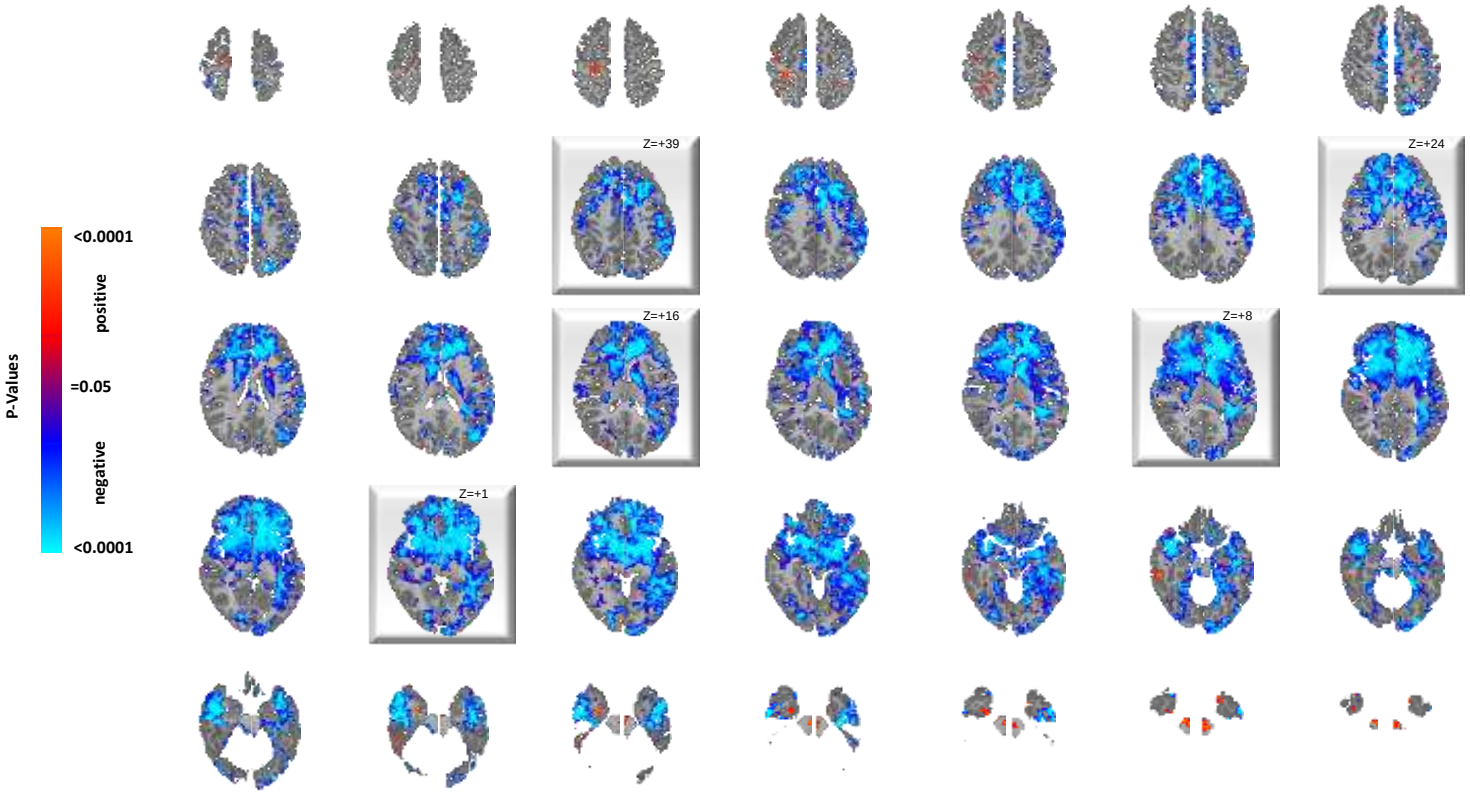

Supplementary Figure S12. Correlates of rCBF with FSIQ in the TD Group Only for All Slices

This shows all maps illustrating the significance of FSIQ correlations with resting rCBF at each voxel in the TD group in all slices, while covarying for age and sex. Red and blue voxels represent, respectively, significant positive or inverse correlations of FSIQ with rCBF values. Highlighted slices (with their z-level Talairach coordinates) are those displayed in Figure 2 of the main text.

ACCEPTED MANUSCRIPT

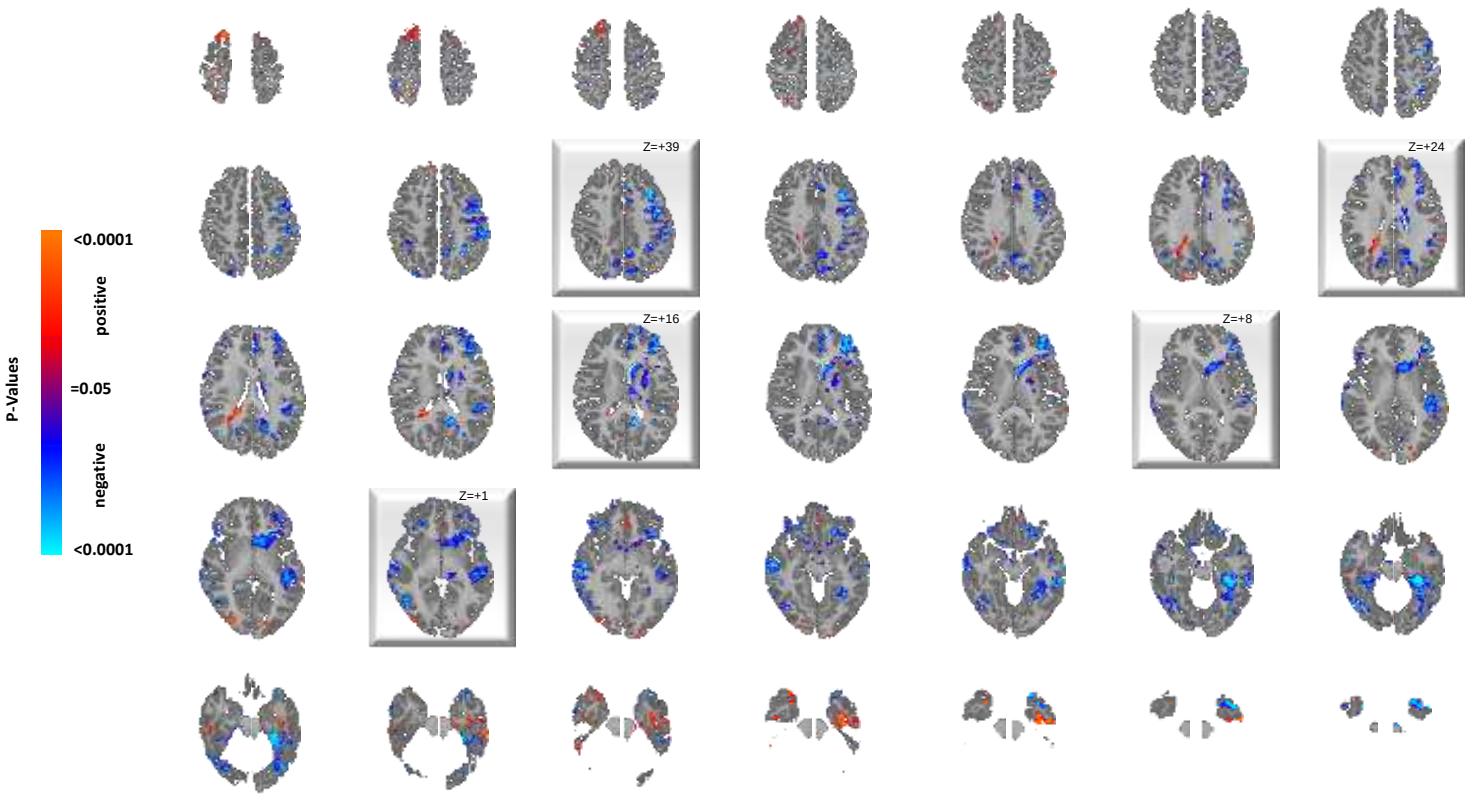

Supplementary Figure S13. Correlates of rCBF with FSIQ in the ASD Group Only for All Slices

This shows all maps illustrating the significance of FSIQ correlations with resting rCBF at each voxel in the ASD group in all slices, while covarying for age and sex. Red and blue voxels represent, respectively, significant positive or inverse correlations of FSIQ with rCBF values. Highlighted slices (with their z-level Talairach coordinates) are those displayed in Figure 2 of the main text.

ACCEPTED MANUSCRIPT

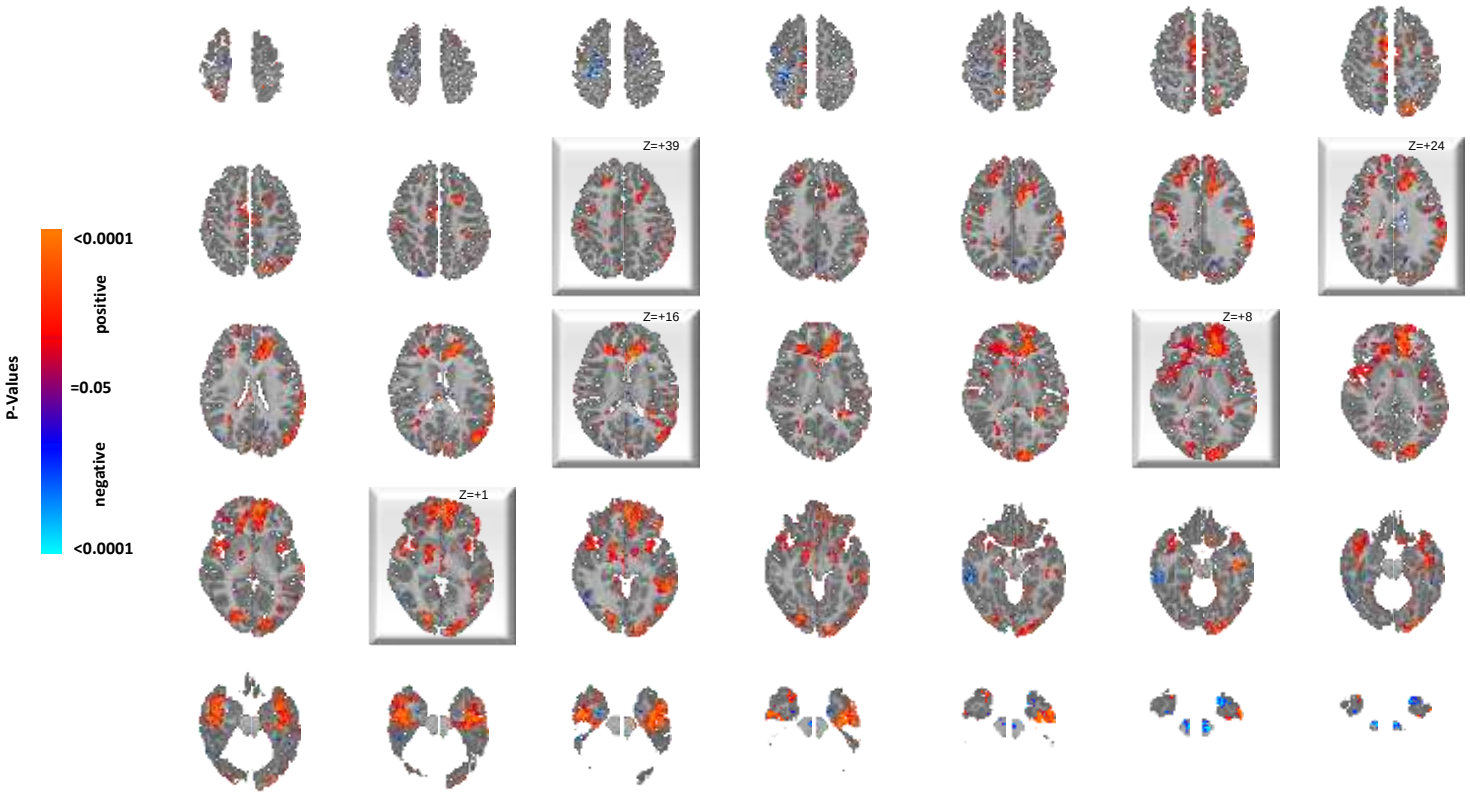

Supplementary Figure S14. The Interaction of Diagnosis with FSIQ in All Slices

This map shows the significant interaction effects of FSIQ with diagnosis (ASD or TD) on rCBF at each voxel in all slices, while covarying for age and sex and including the main effects of FSIQ and diagnosis in a hierarchically well formulated statistical model. The interaction effect indicates voxels where the correlation of FSIQ with rCBF differs significantly across the ASD and TD groups. Red and blue voxels represent the mathematical sign (positive or negative, respectively) of the F-test statistic for the interaction. Highlighted slices (with their z-level Talairach coordinates) are those displayed in Figure 2 of the main text.

ACCEPTED MANUSCRIPT

Supplemental Materials Section 3e:
Correlations of rCBF with NAA Metabolite Concentrations

ACCEPTED MANUSCRIPT

ACCEPTED MANUSCRIPT

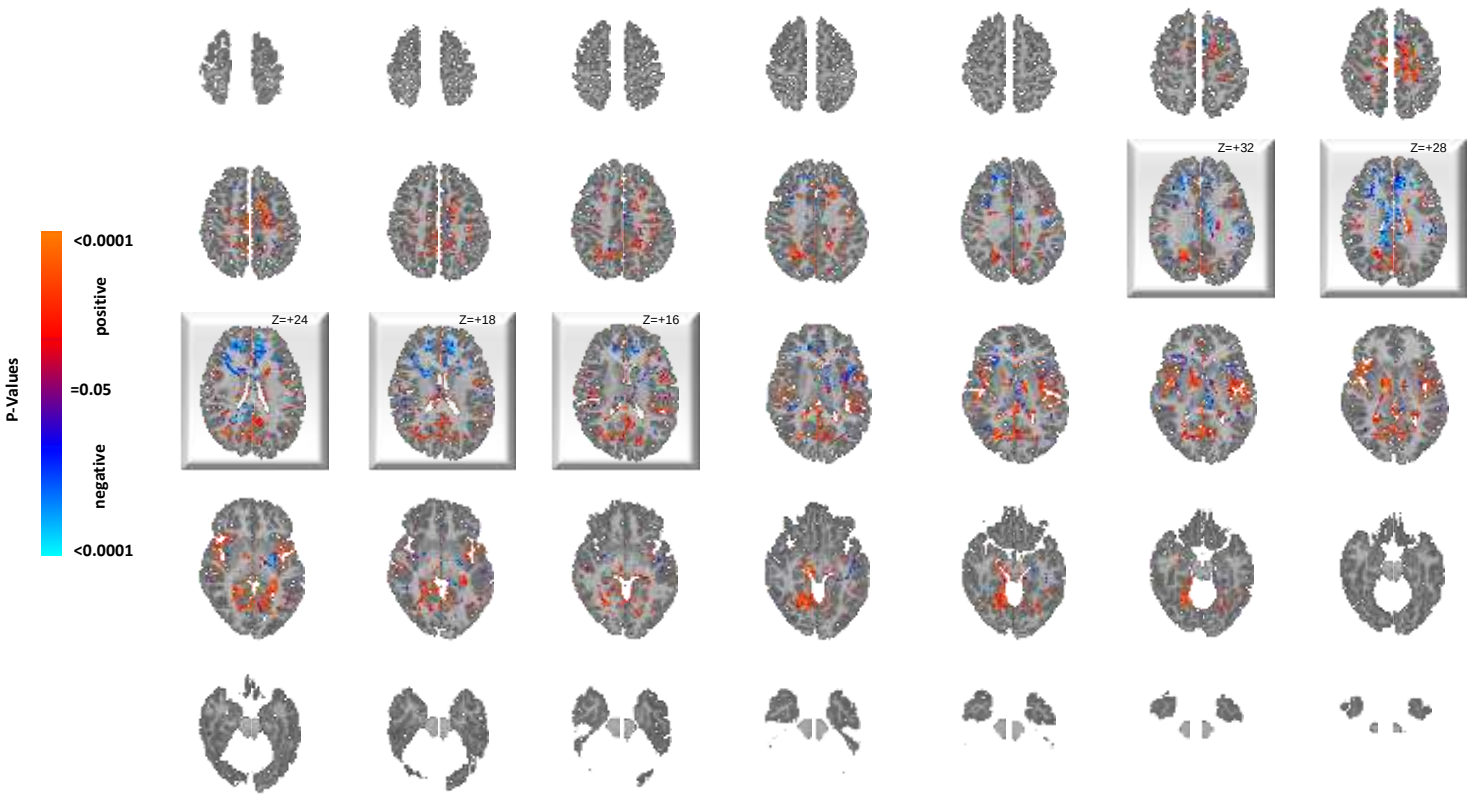

Supplementary Figure S15. Voxelwise Correlation of rCBF with NAA Concentrations in the TD Group Only in All Slices
Shown here are the voxel-wise correlations of NAA concentration with rCBF in the TD group (N=63, 48 males, 15 females, mean age 22.3 years) in all slices, while covarying for age and sex. Significance levels are FDR-corrected for the number of statistical comparisons. Red and blue voxels represent, respectively, significant positive or inverse correlations of NAA levels with rCBF values. Highlighted slices (with their z-level Talairach coordinates) are those displayed in Figure 3 of the main text.

ACCEPTED MANUSCRIPT

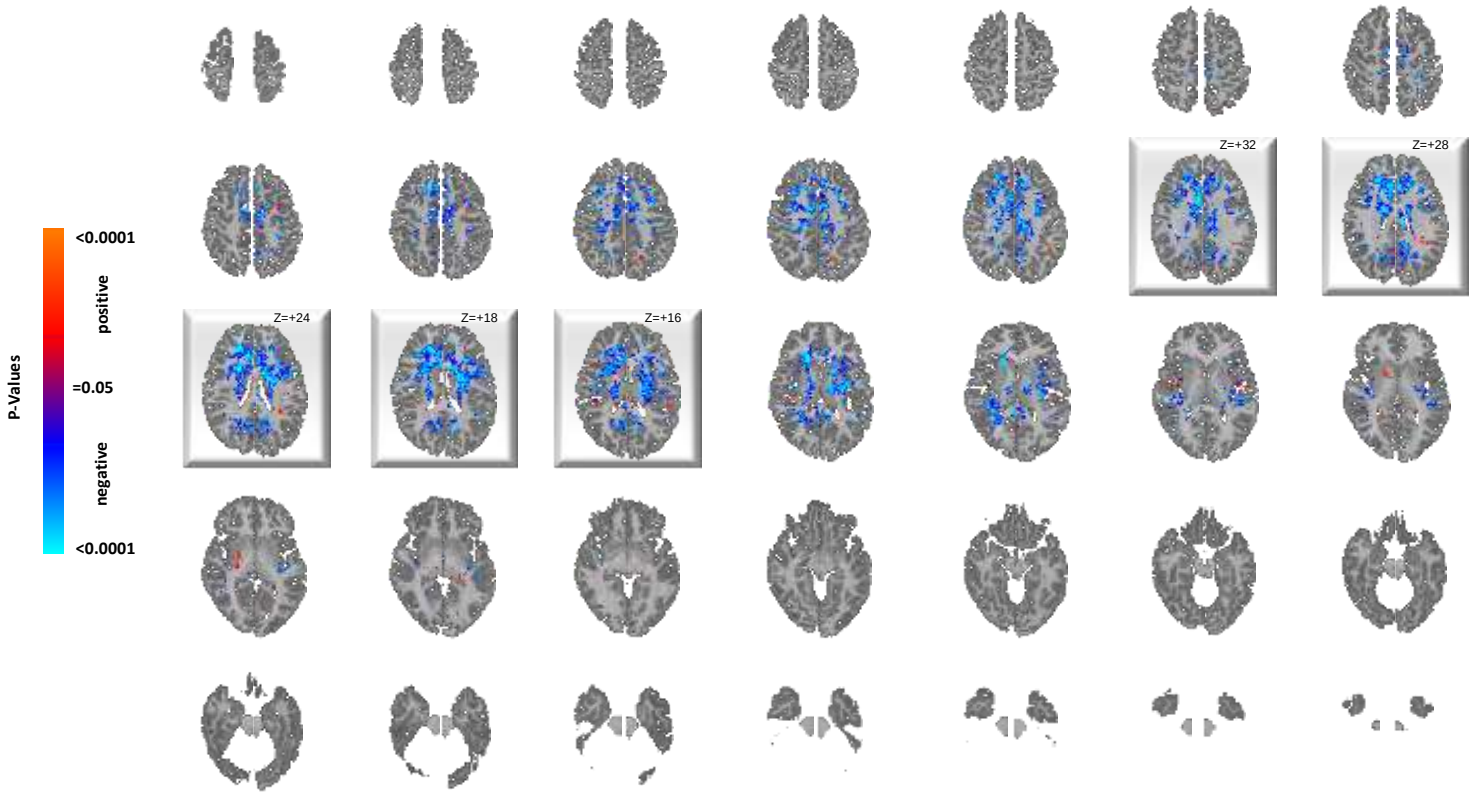

Supplementary Figure S16. Voxelwise Correlation of rCBF with NAA Concentrations in the ASD Group Only in All Slices
Shown here are the voxel-wise correlations of NAA concentration with rCBF in the ASD group (N=36, 29 males, 7 females, mean age 25.6 years) group in all slices, while covarying for age and sex. Significance levels are FDR-corrected for the number of statistical comparisons. Red and blue voxels represent, respectively, significant positive or inverse correlations of NAA levels with rCBF values. Highlighted slices (with their z-level Talairach coordinates) are those displayed in Figure 3 of the main text.

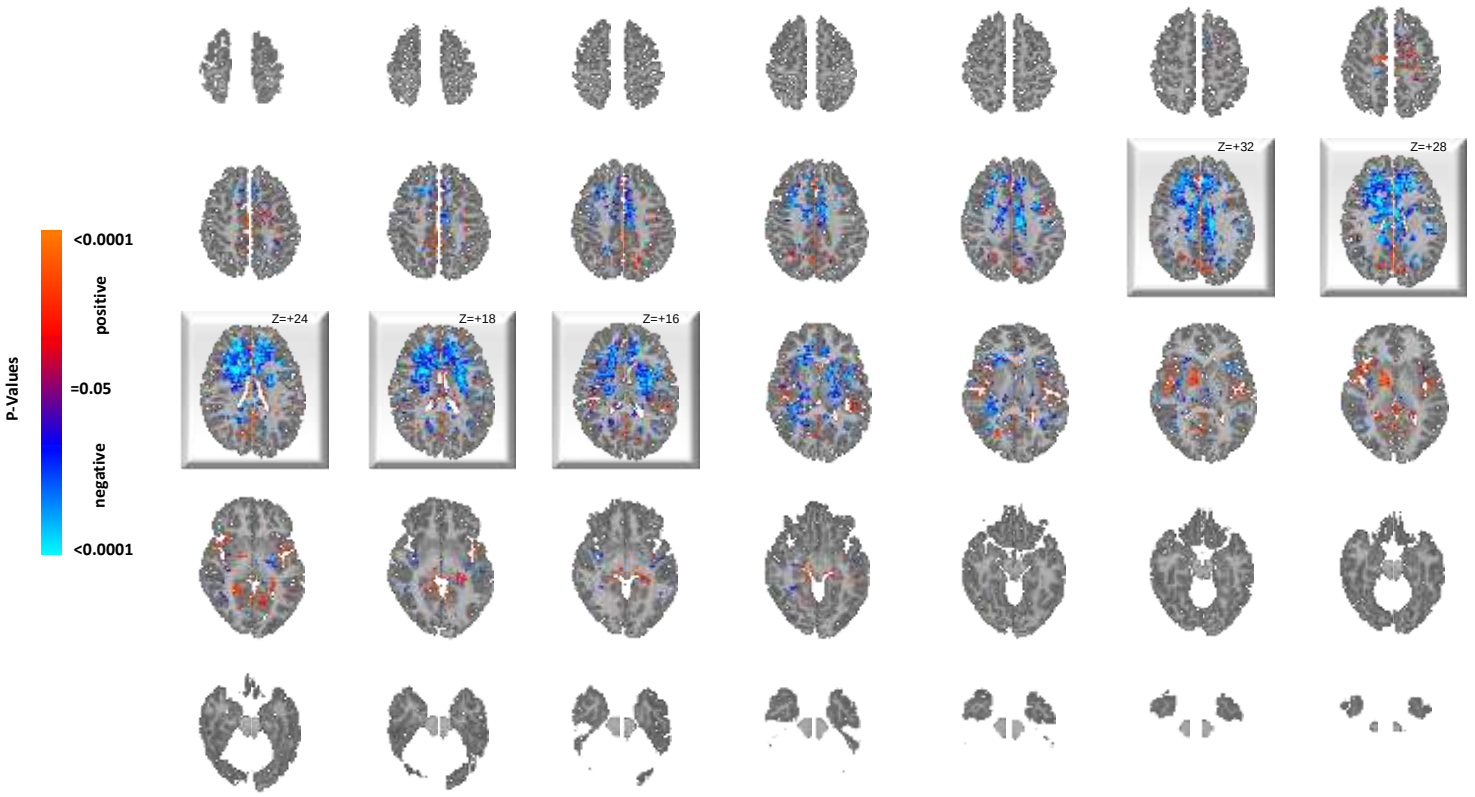

Supplementary Figure S17. Voxelwise Correlation of rCBF with NAA Concentrations in All Participants for All Slices
Shown here are the voxel-wise correlations of NAA concentration with rCBF in the ASD (N=36, 29 males, 7 females, mean age 25.6 years) and TD (N=63, 48 males, 15 females, mean age 22.3 years) groups combined in all slices, while covarying for age and sex. Significance levels are FDR-corrected for the number of statistical comparisons. Red and blue voxels represent, respectively, significant positive or inverse correlations of NAA level with rCBF values in the ASD group compared to the TD group. Highlighted slices (with their z-level Talairach coordinates) are those displayed in Figure 3 of the main text.

ACCEPTED MANUSCRIPT

Supplemental Materials Section 3f:
Correlations of rCBF with Detectable Lactate

ACCEPTED MANUSCRIPT

ACCEPTED MANUSCRIPT

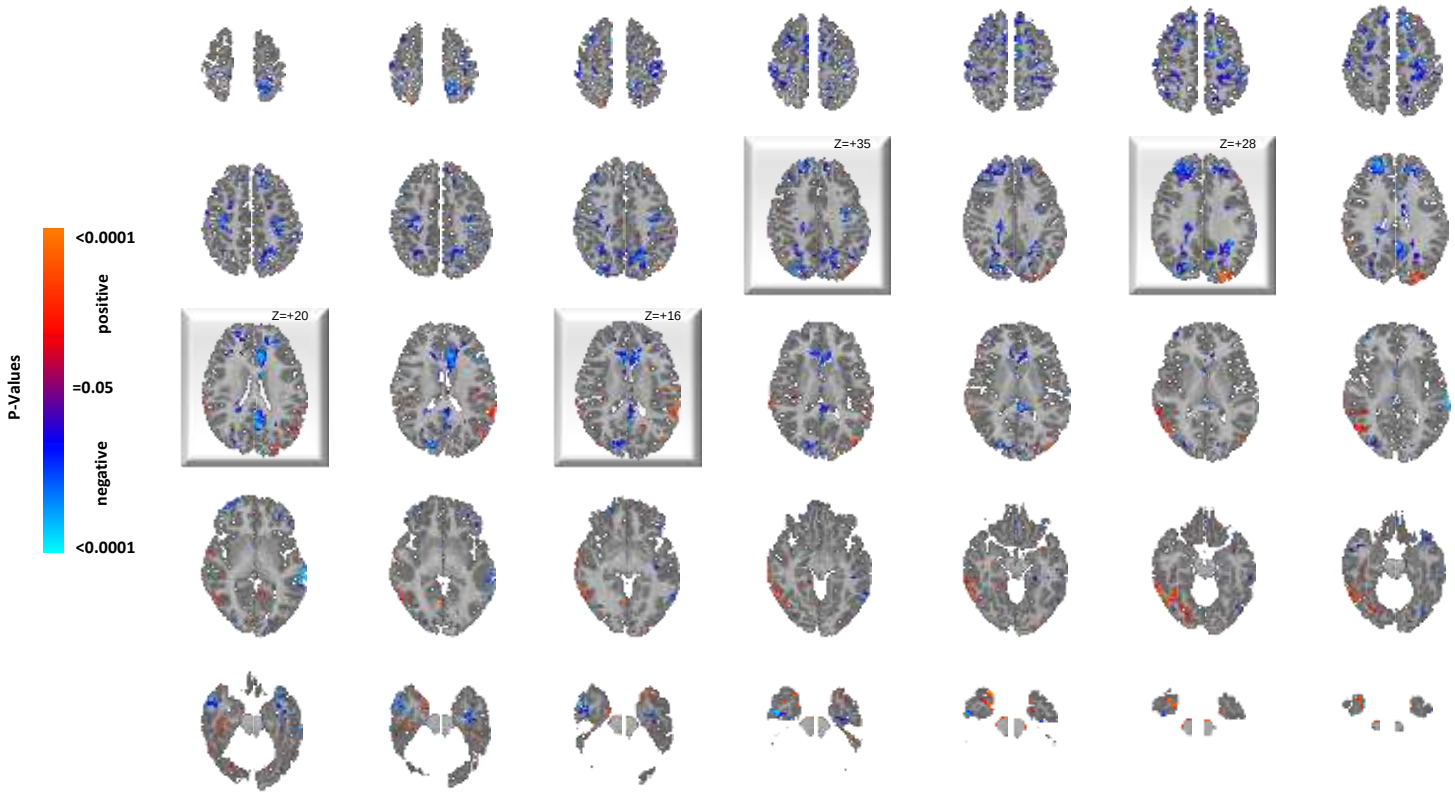

Supplementary Figure S18. rCBF in ASD Participants with or without Detectable Lactate for All Slices

This map shows all slices for the voxel-wise statistical comparison of rCBF in ASD participants who had detectable lactate (N=6, __ males, __ females, mean age __ years) compared with the ASD participants who did not have detectable lactate at any voxel, while covarying for age and sex. Significance levels are FDR-corrected for the number of statistical comparisons. Red and blue voxels represent, respectively, significantly higher or lower rCBF values, respectively, in ASD participants who had detectable lactate. Highlighted slices (with their z-level Talairach coordinates) are those displayed in Figure 3 of the main text.

ACCEPTED MANUSCRIPT

Supplemental Materials Section 4:
Group Average rCBF Maps

ACCEPTED MANUSCRIPT

ACCEPTED MANUSCRIPT

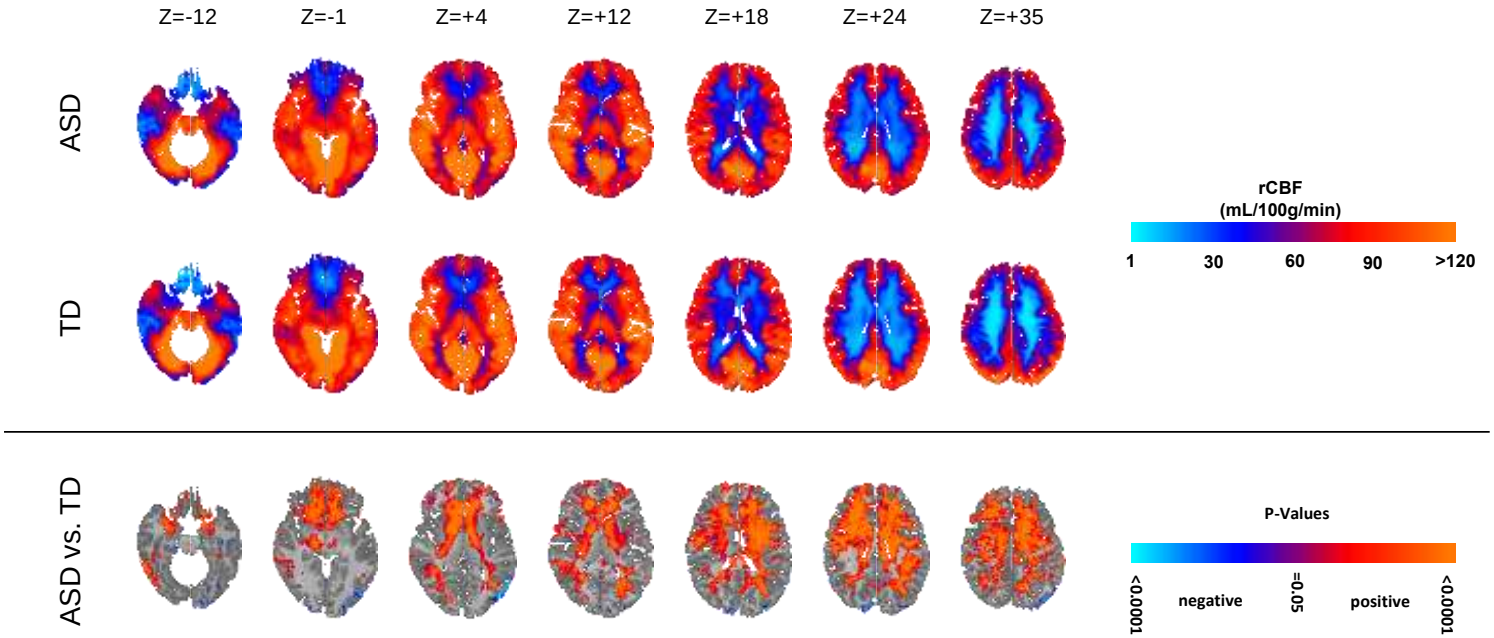

Supplementary Figure S19. Group Average Maps Contributing to Significant Group Differences in rCBF in Representative Slices
Top Row: This is a map showing the group average rCBF at each voxel in the ASD group only, partialing out the effects of age and sex, for the slices shown in Figure 1 of the main text.
Middle Row: This is a map showing the group average rCBF at each voxel in the TD group only, partialing out the effects of age and sex, for the slices shown in Figure 1 of the main text.
Bottom Row: These are the statistically significant group differences (ASD vs TD) in rCBF while covarying for age and sex, displayed at a threshold of P<0.05 after correction for multiple comparisons, for the slices shown in Figure 1 of the main text.

ACCEPTED

ACCEPTED MANUSCRIPT

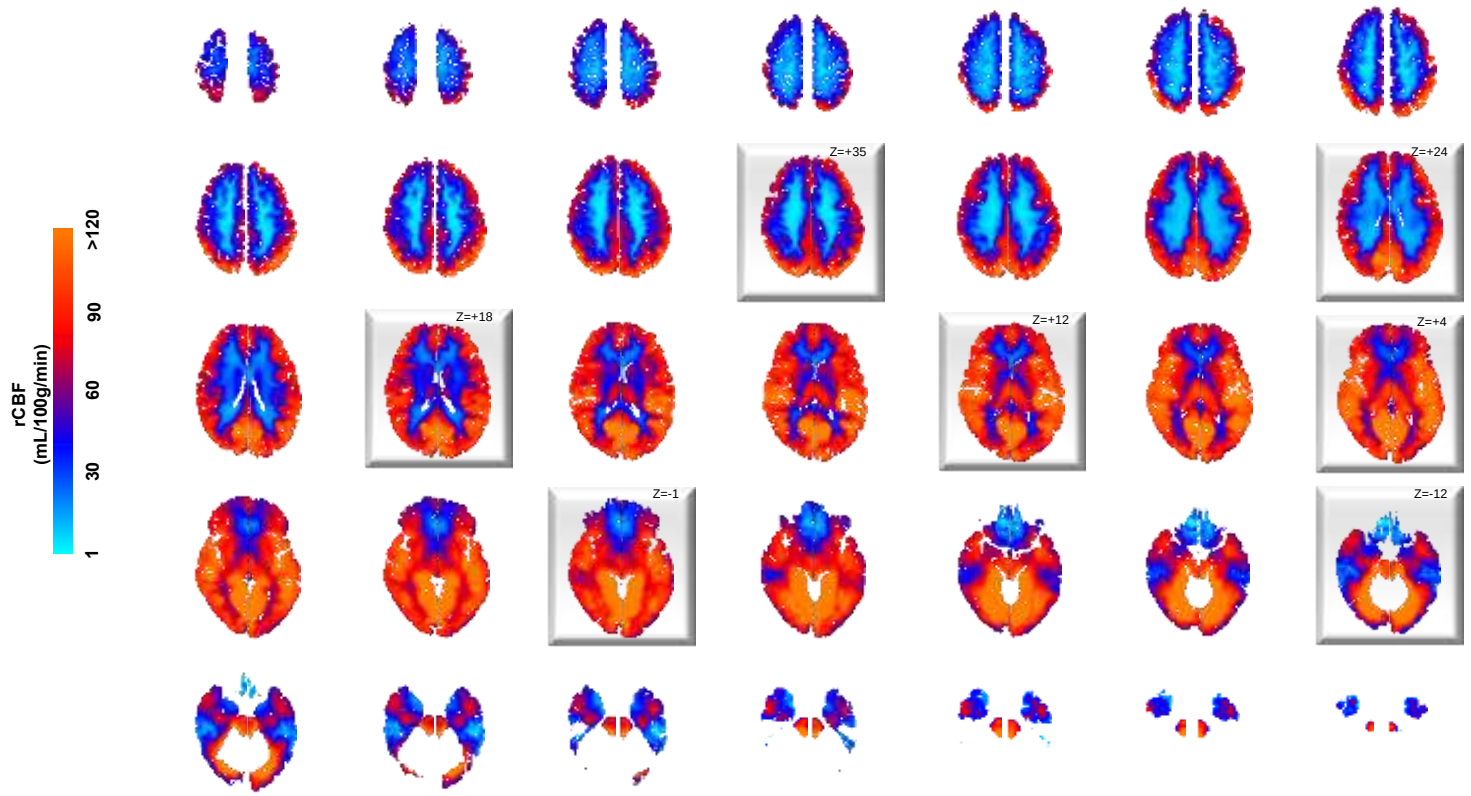

Supplementary Figure S20. Average Perfusion in the TD Group in All Slices

This is a map showing the group average rCBF at each voxel in all slices in the TD group only, partialing out the effects of age and sex.

ACCEPTED MANUSCRIPT

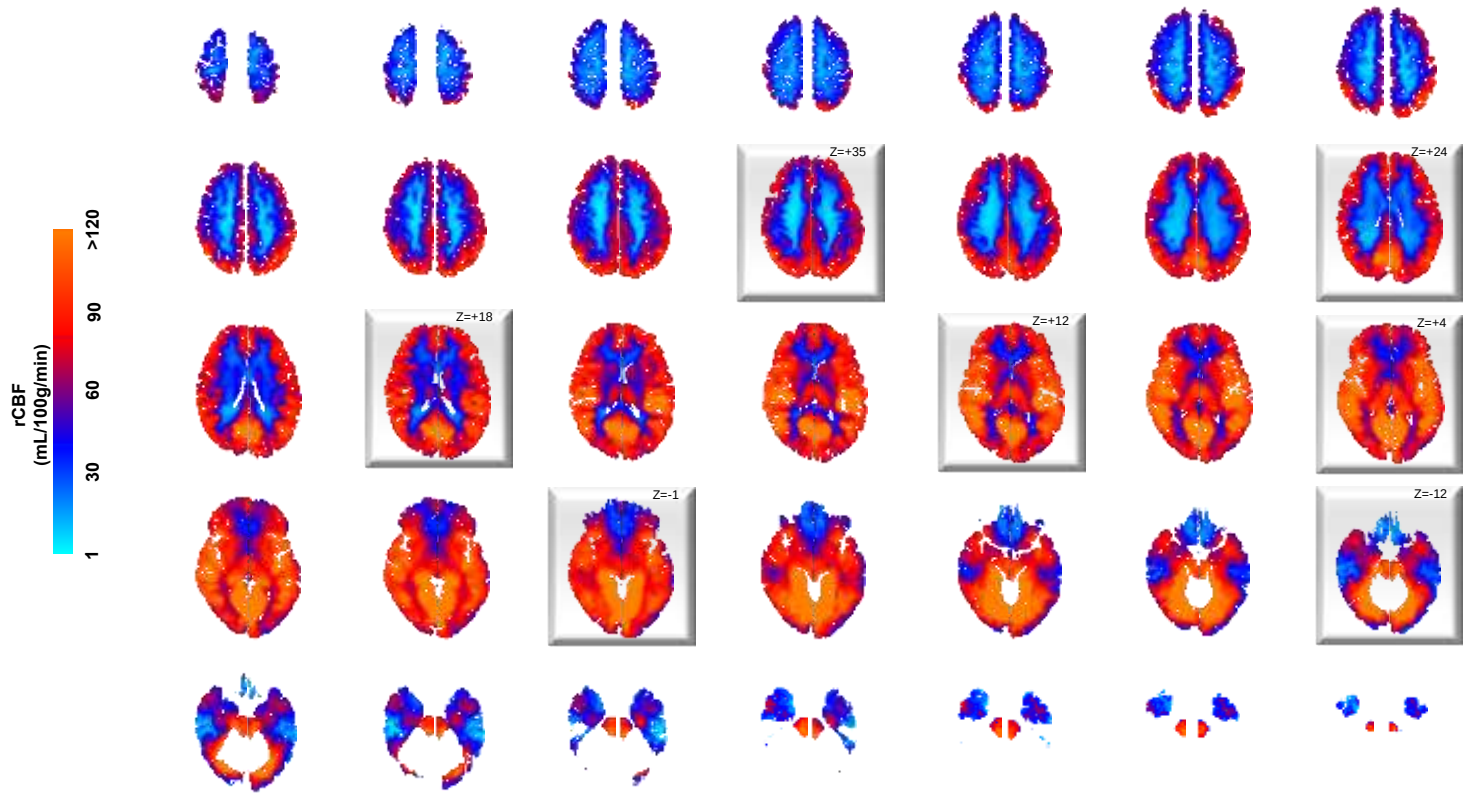

Supplementary Figure S21. Average Perfusion in the ASD Group in All Slices

This is a map showing the group average rCBF at each voxel in all slices in the ASD group only, partialing out the effects of age and sex.

ACCEPTED MANUSCRIPT

Supplemental Materials Section 5a:
rCBF Correlations with Scores in Other ADOS Symptom Domains

ACCEPTED MANUSCRIPT

ACCEPTED MANUSCRIPT

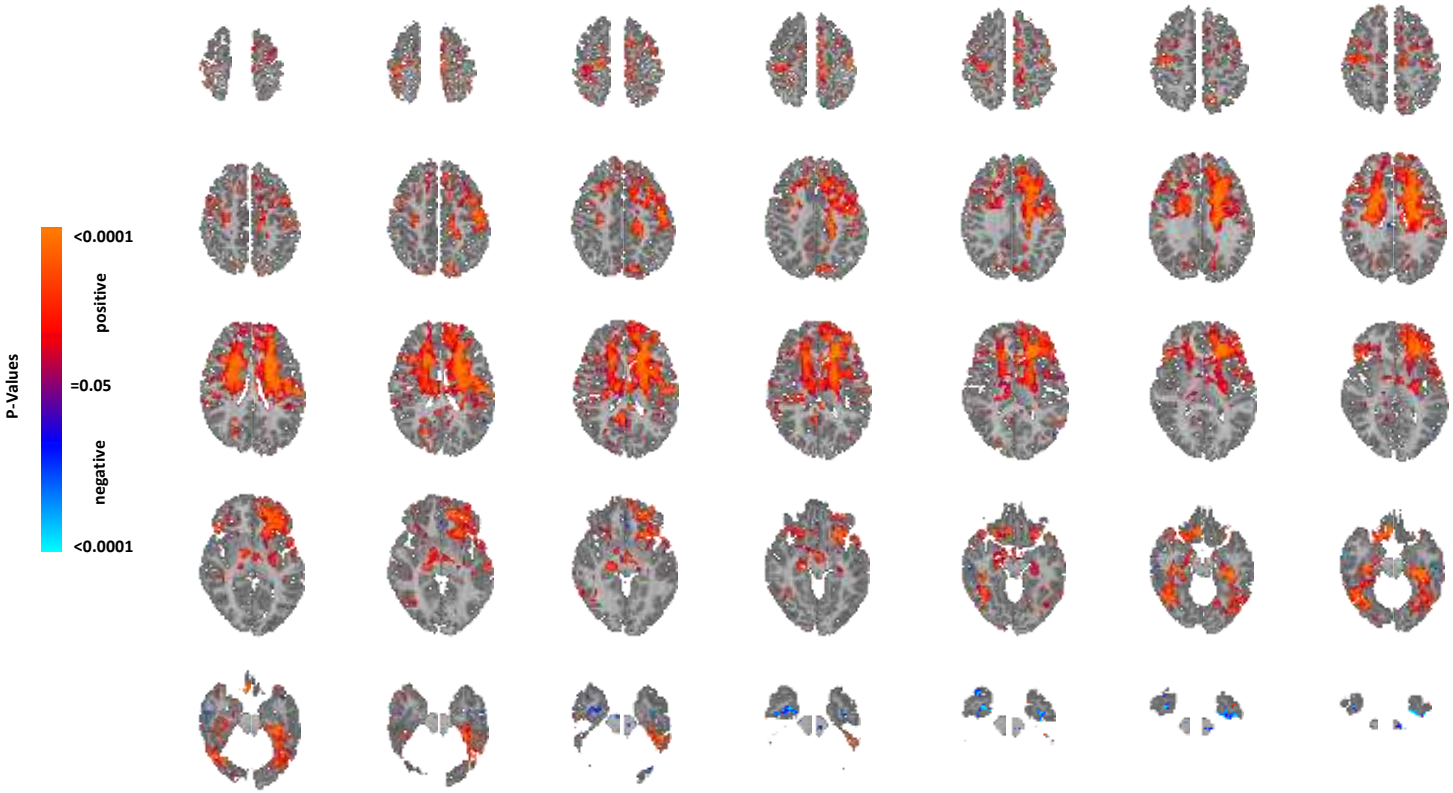

Supplementary Figure S22. Correlation of rCBF with ADOS Social Affect Scores for All Slices

This shows the statistically significant correlations of ADOS Social Affect scores with rCBF values in the ASD group for all slices while covarying for age and sex, displayed at a threshold of P<0.05 after FDR correction for multiple comparisons. Red and blue voxels represent, respectively, significant positive or inverse correlations of ADOS Social Affect scores with rCBF values in the ASD group.

ACCEPTED MANUSCRIPT

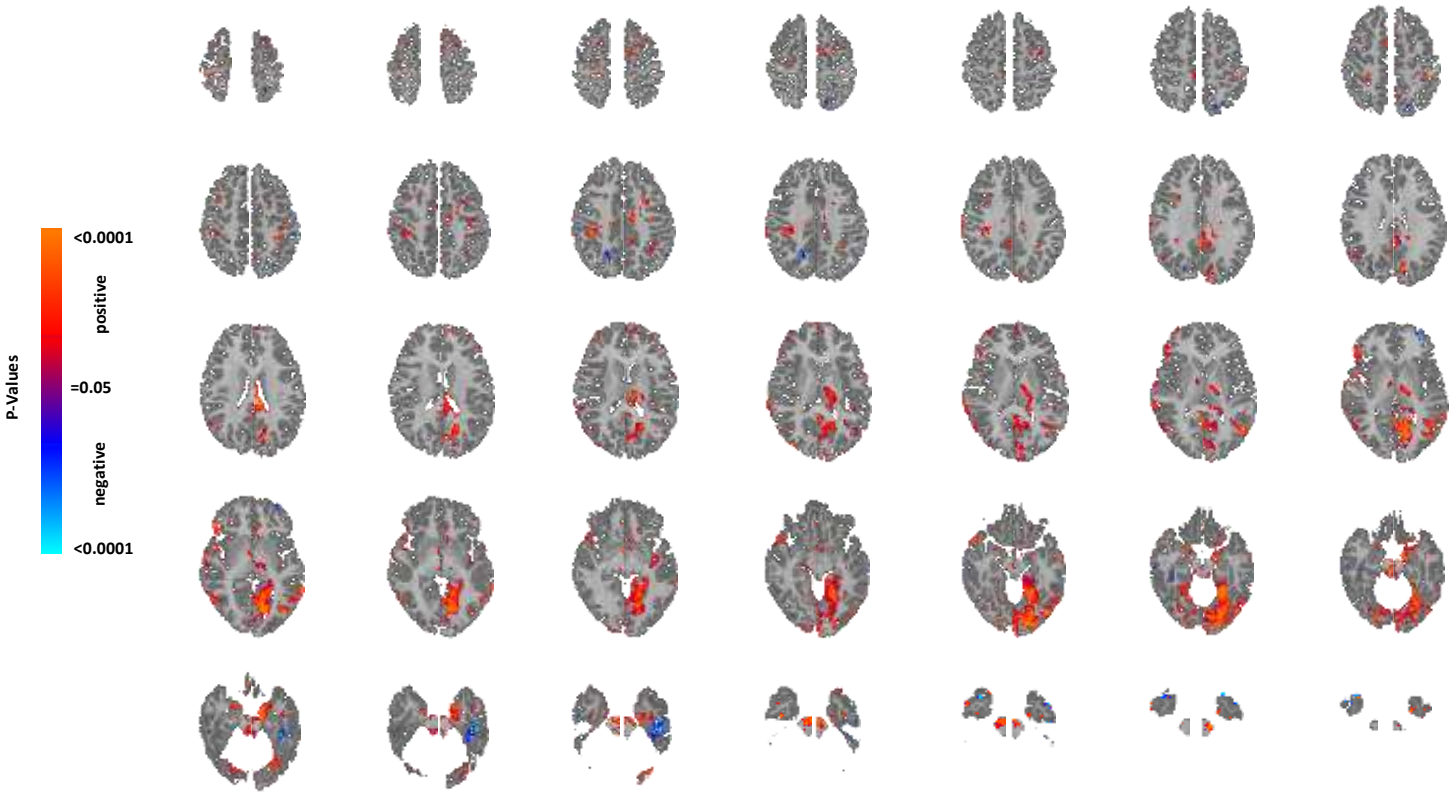

Supplementary Figure S23. Correlation of rCBF with ADOS Restrictive and Repetitive Behaviors Scores for All Slices
This shows the statistically significant correlations of ADOS Restrictive and Repetitive Behaviors scores with rCBF values in the ASD group for all slices while covarying for age and sex, displayed at a threshold of P<0.05 after FDR correction for multiple comparisons. Red and blue voxels represent, respectively, significant positive or inverse correlations of ADOS Restrictive and Repetitive Behaviors scores with rCBF values in the ASD group.

ACCEPTED MANUSCRIPT

Supplemental Materials Section 5b:
SRS Symptom Domains

ACCEPTED MANUSCRIPT

ACCEPTED MANUSCRIPT

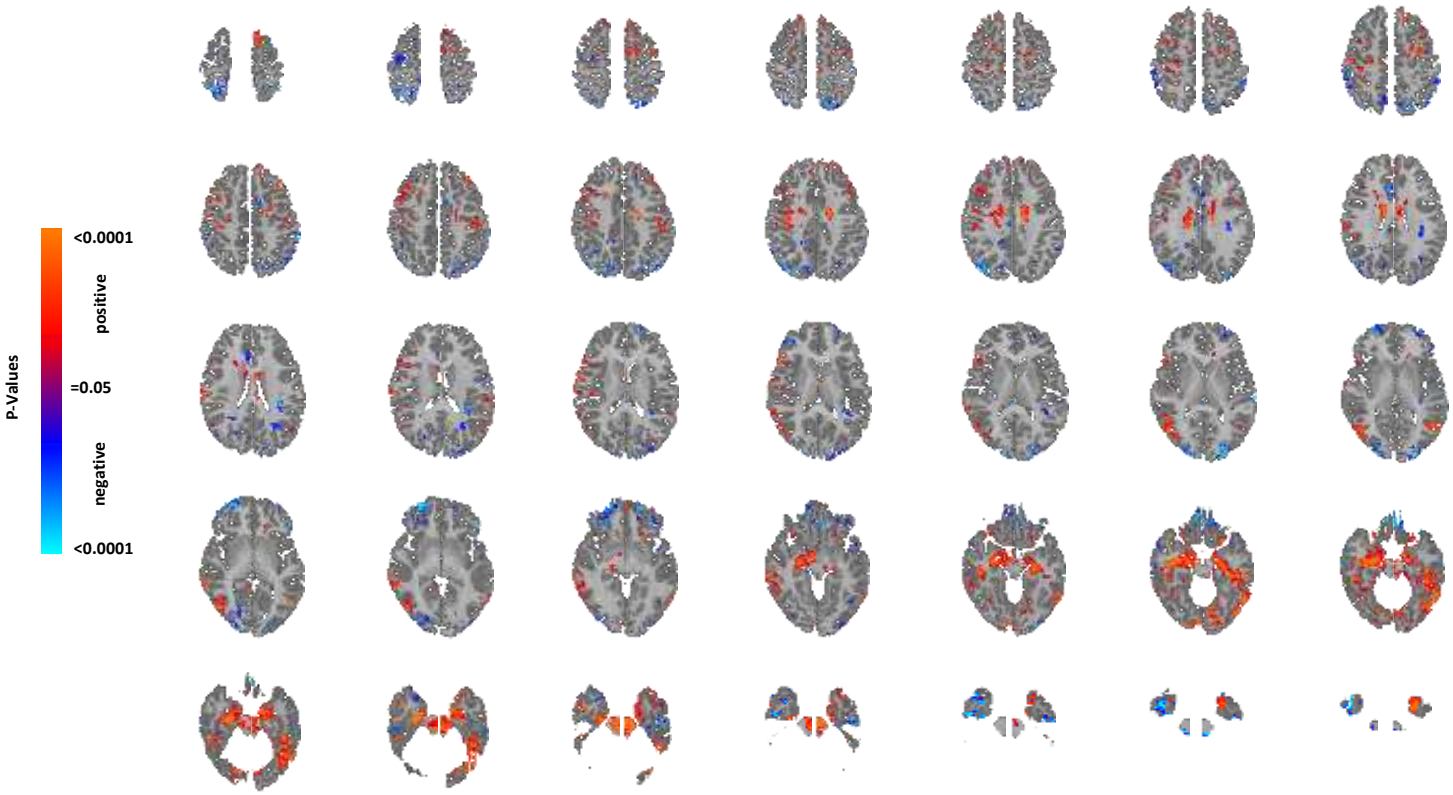

Supplementary Figure S24. Correlation of rCBF with SRS Total Scores for All Slices

This shows the statistically significant correlations of SRS Total scores with rCBF values in the ASD group for all slices while covarying for age and sex, displayed at a threshold of P<0.05 after FDR correction for multiple comparisons. Red and blue voxels represent, respectively, significant positive or inverse correlations of SRS Total scores with rCBF values in the ASD group.

ACCEPTED MANUSCRIPT

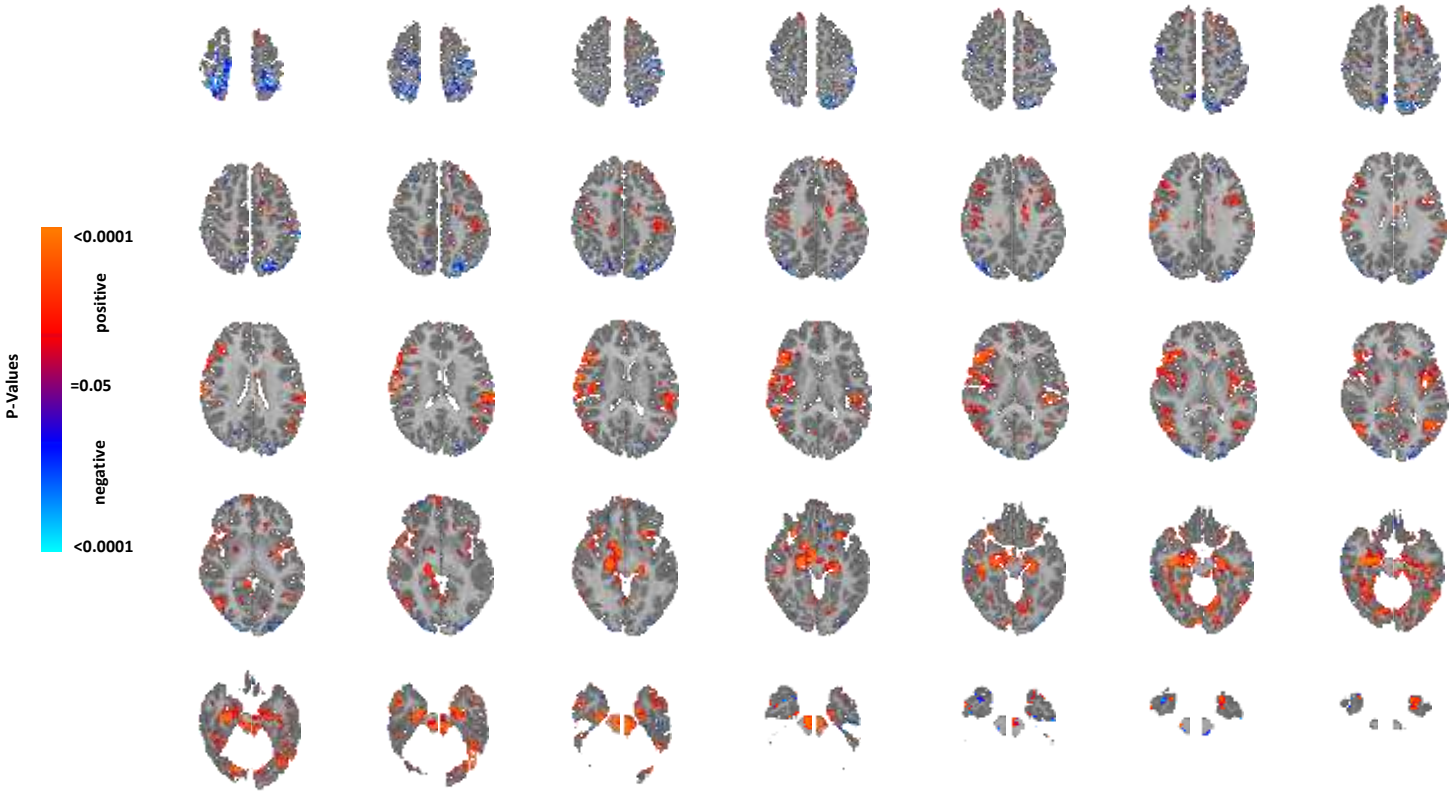

Supplementary Figure S25. Correlation of rCBF with SRS Motivation Scores for All Slices

This shows the statistically significant correlations of SRS Motivation scores with rCBF values in the ASD group for all slices while covarying for age and sex, displayed at a threshold of P<0.05 after FDR correction for multiple comparisons. Red and blue voxels represent, respectively, significant positive or inverse correlations of SRS Motivation scores with rCBF values in the ASD group.

ACCEPTED MANUSCRIPT

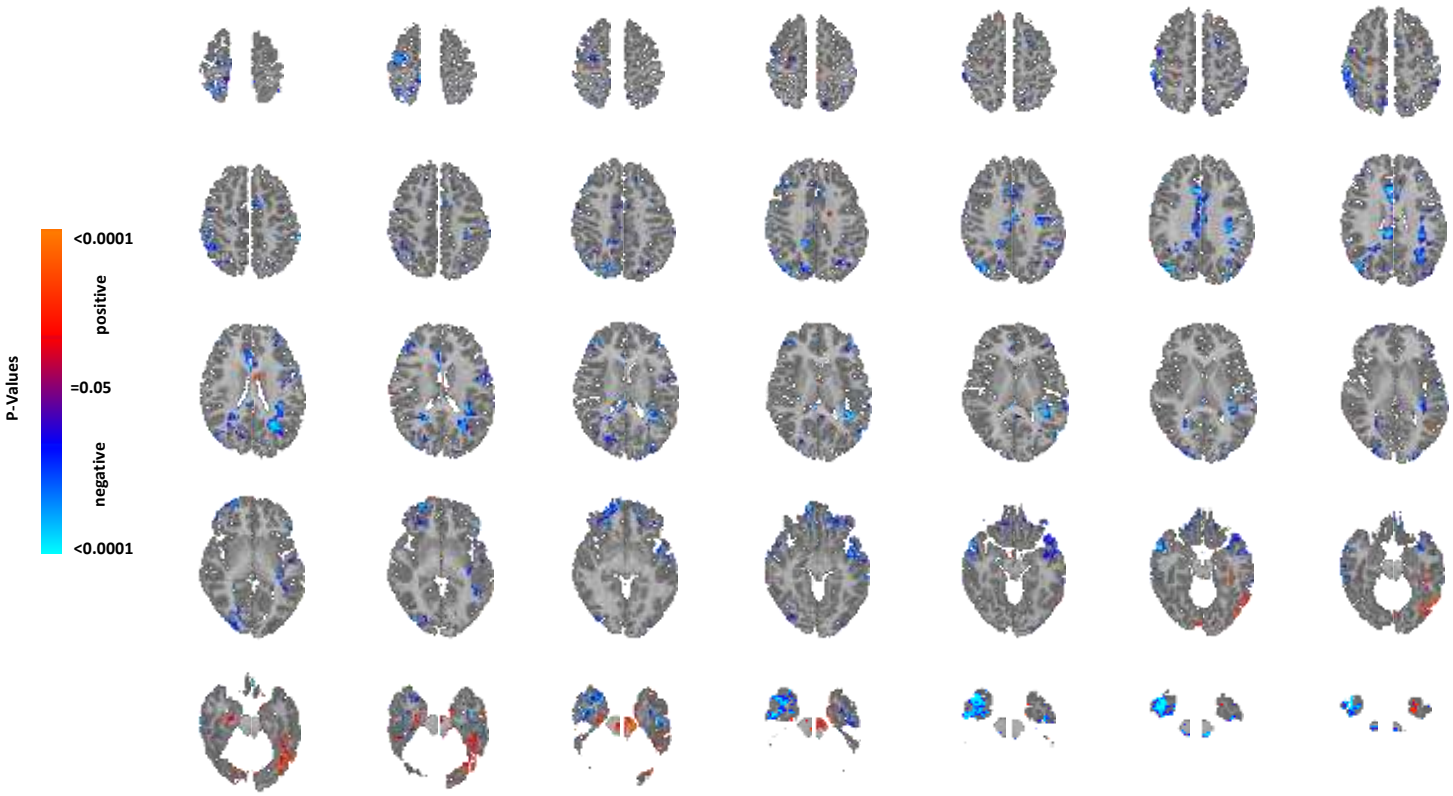

Supplementary Figure S26. Correlation of rCBF with SRS Mannerism Scores for All Slices

This shows the statistically significant correlations of SRS Mannerism scores with rCBF values in the ASD group for all slices while covarying for age and sex, displayed at a threshold of P<0.05 after FDR correction for multiple comparisons. Red and blue voxels represent, respectively, significant positive or inverse correlations of SRS Mannerism scores with rCBF values in the ASD group.

ACCEPTED

ACCEPTED MANUSCRIPT

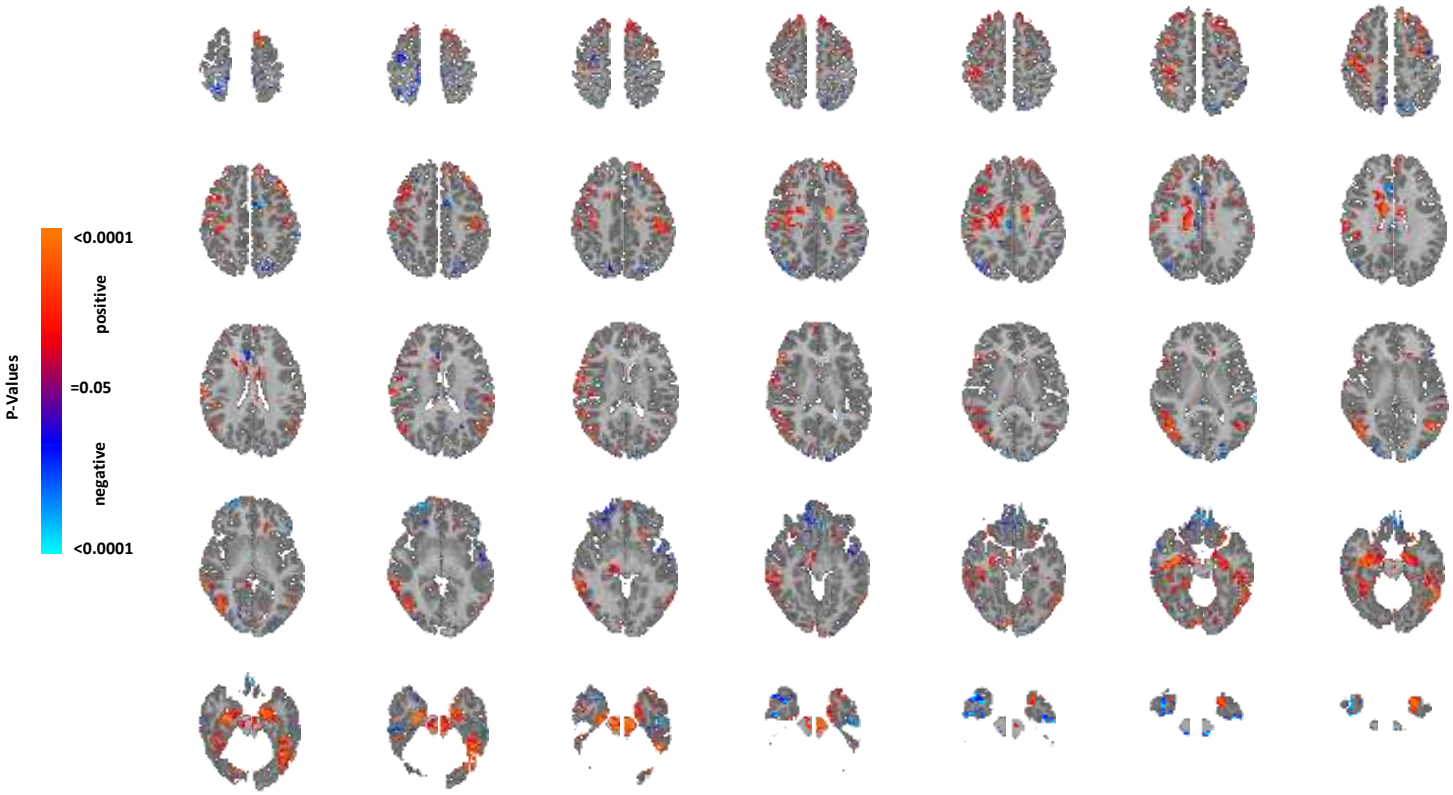

Supplementary Figure S27. Correlation of rCBF with SRS Communication Scores for All Slices

This shows the statistically significant correlations of SRS Communication scores with rCBF values in the ASD group for all slices while covarying for age and sex, displayed at a threshold of P<0.05 after FDR correction for multiple comparisons. Red and blue voxels represent, respectively, significant positive or inverse correlations of SRS Communication scores with rCBF values in the ASD group.

ACCEPTED MANUSCRIPT

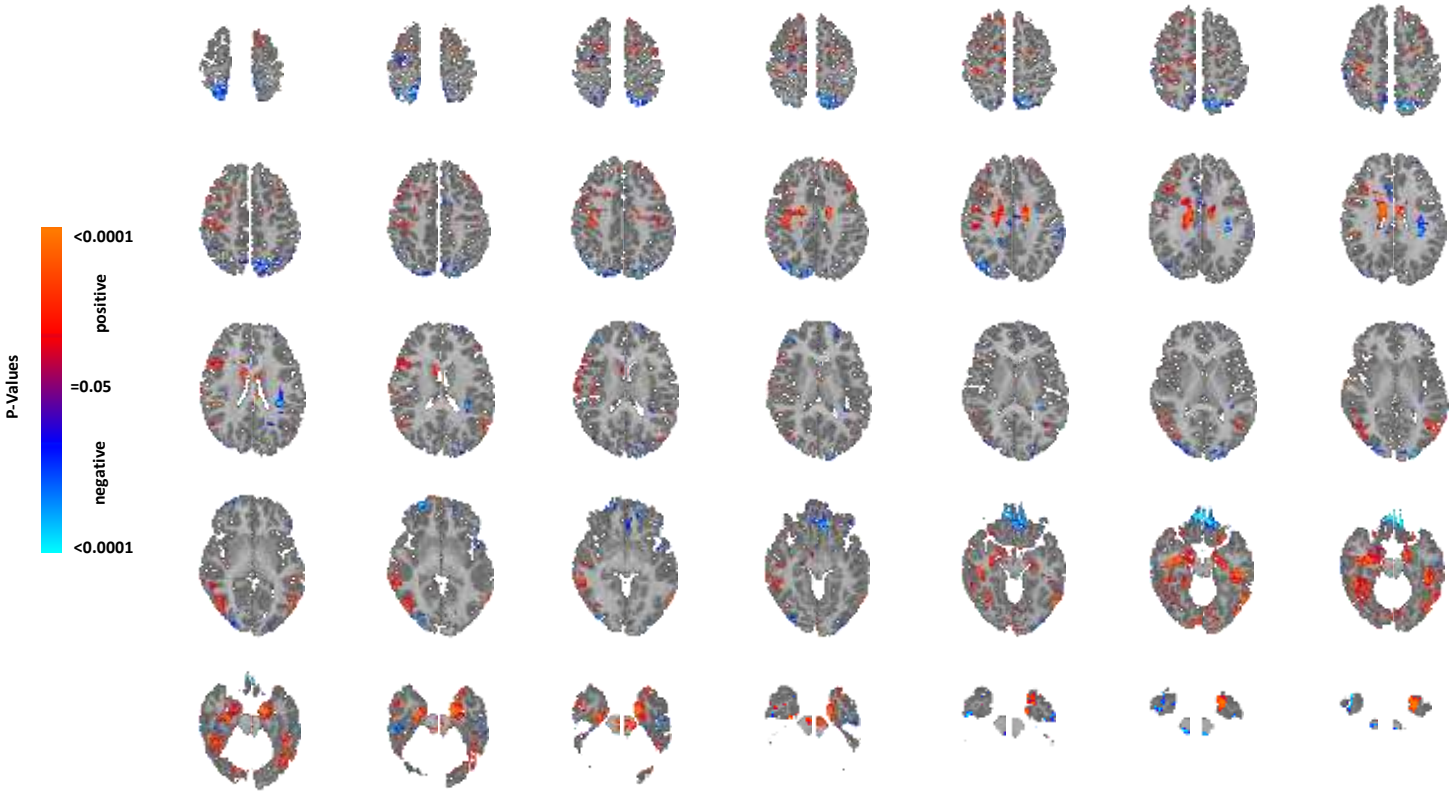

Supplementary Figure S28. Correlation of rCBF with SRS Cognition Scores for All Slices

This shows the statistically significant correlations of SRS Cognition scores with rCBF values in the ASD group for all slices while covarying for age and sex, displayed at a threshold of P<0.05 after FDR correction for multiple comparisons. Red and blue voxels represent, respectively, significant positive or inverse correlations of SRS Cognition scores with rCBF values in the ASD group.

ACCEPTED MANUSCRIPT

Supplemental Materials Section 6:
Main Text Figures with Additional Covariates

ACCEPTED MANUSCRIPT

ACCEPTED MANUSCRIPT

Supplemental Materials Section 6a:
FSIQ Added to Base Model

ACCEPTED MANUSCRIPT

ACCEPTED MANUSCRIPT

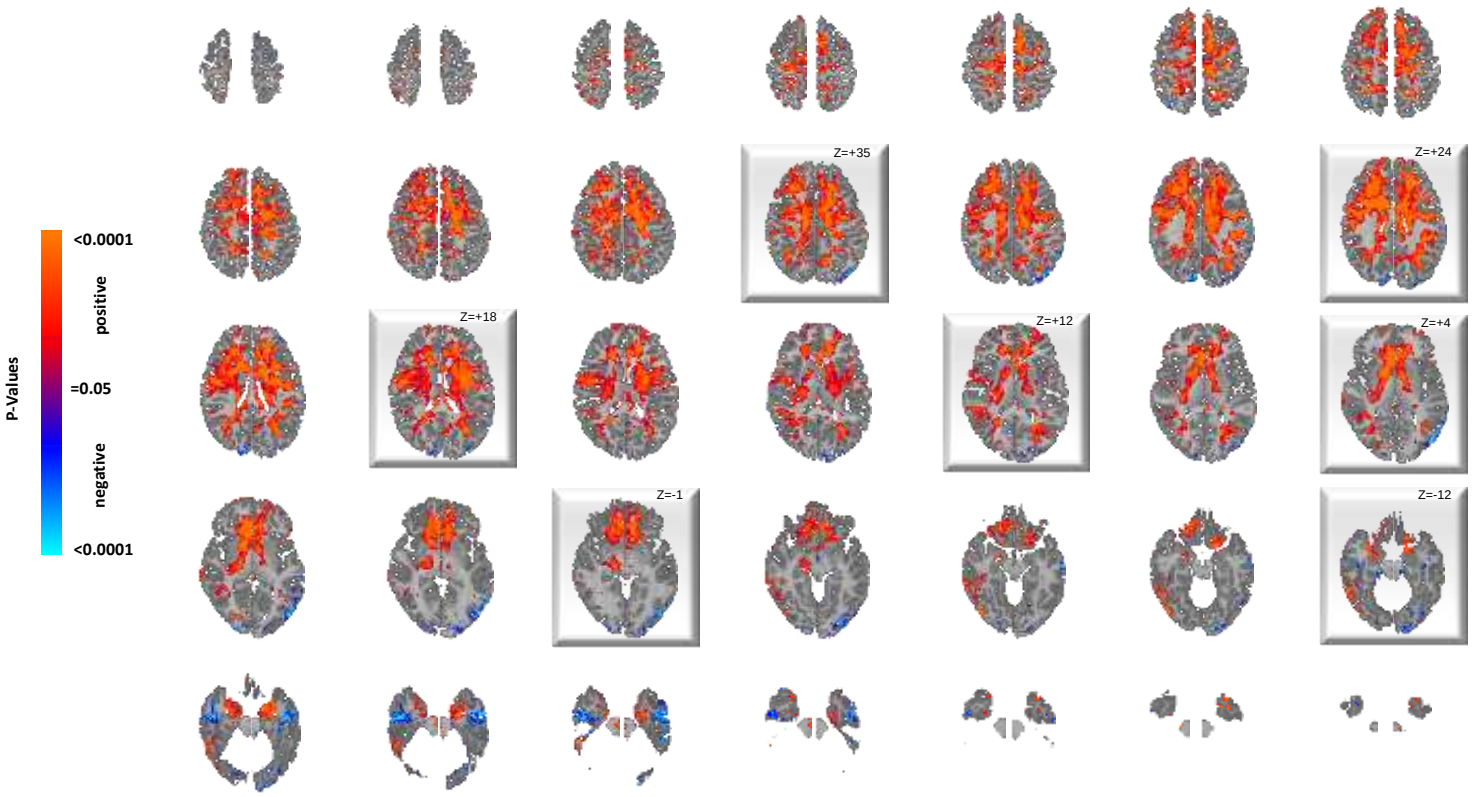

Supplementary Figure S29. Effects of Diagnosis on rCBF while Covarying for FSIQ

This shows the statistically significant differences in rCBF values between the ASD group and TD controls for all slices while covarying for age, sex, and FSIQ, displayed at a threshold of P<0.05 after correction for multiple comparisons. Voxels in red indicate significantly increased rCBF, and blue voxels reduced rCBF, in ASD relative to controls. Highlighted slices (with their z-level Talairach coordinates) are those displayed in Figure 1 of the main text.

ACCEPTED MANUSCRIPT

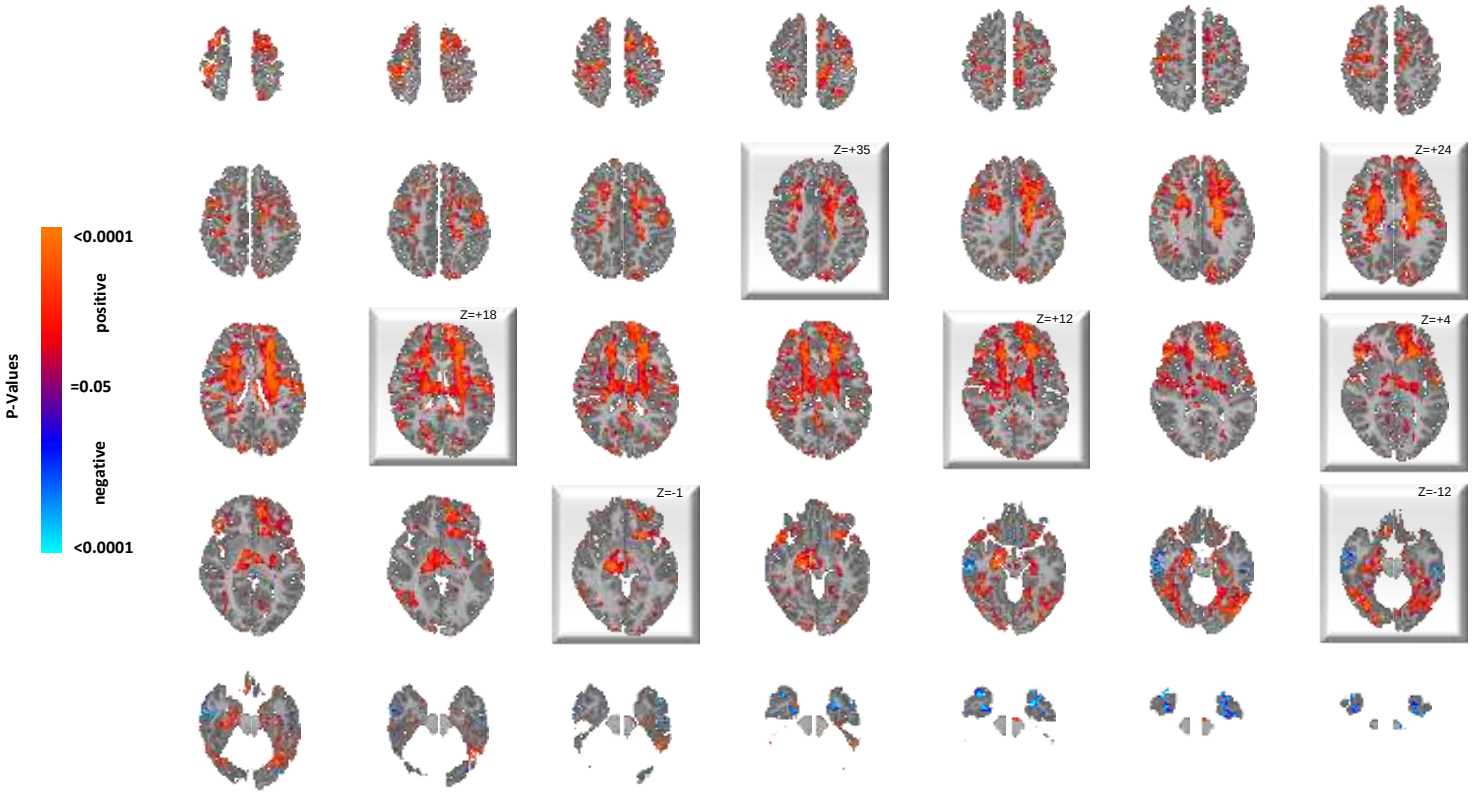

Supplementary Figure S30. Correlation of rCBF with ADOS Total Scores while Covarying for FSIQ

Shown here are all slices for the statistically significant correlations of ADOS Total scores with rCBF values in the ASD group, while covarying for age, sex, and FSIQ, displayed at a threshold of P<0.05 after FDR correction for multiple comparisons. Red and blue voxels represent, respectively, significant positive or inverse correlations of ADOS Total scores with rCBF values in the ASD group. Highlighted slices (with their z-level Talairach coordinates) are those displayed in Figure 1 of the main text.

ACCEPTED MANUSCRIPT

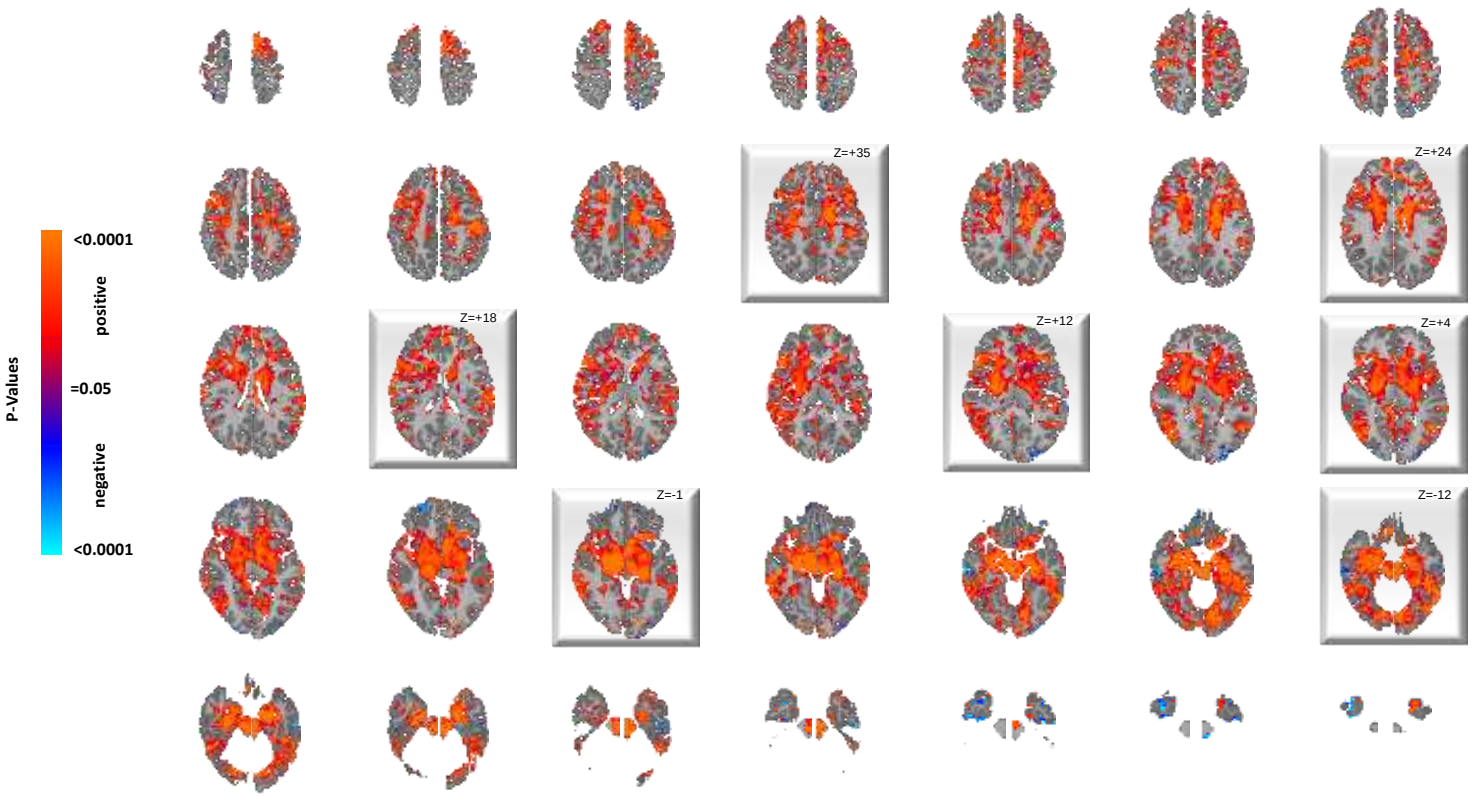

Supplementary Figure S31. Correlation of rCBF with SRS Awareness Scores while Covarying for FSIQ

Shown here are all slices for the statistically significant correlations of SRS Awareness scores with rCBF values in the ASD group, while covarying for age, sex, and FSIQ displayed at a threshold of P<0.05 after FDR correction for multiple comparisons. Red and blue voxels represent, respectively, significant positive or inverse correlations of SRS Awareness scores with rCBF values in the ASD group. Highlighted slices (with their z-level Talairach coordinates) are those displayed in Figure 1 of the main text.

ACCEPTED MANUSCRIPT

Supplemental Materials Section 6b:
Psychotropic Medication Effects Added to Base Model

ACCEPTED MANUSCRIPT

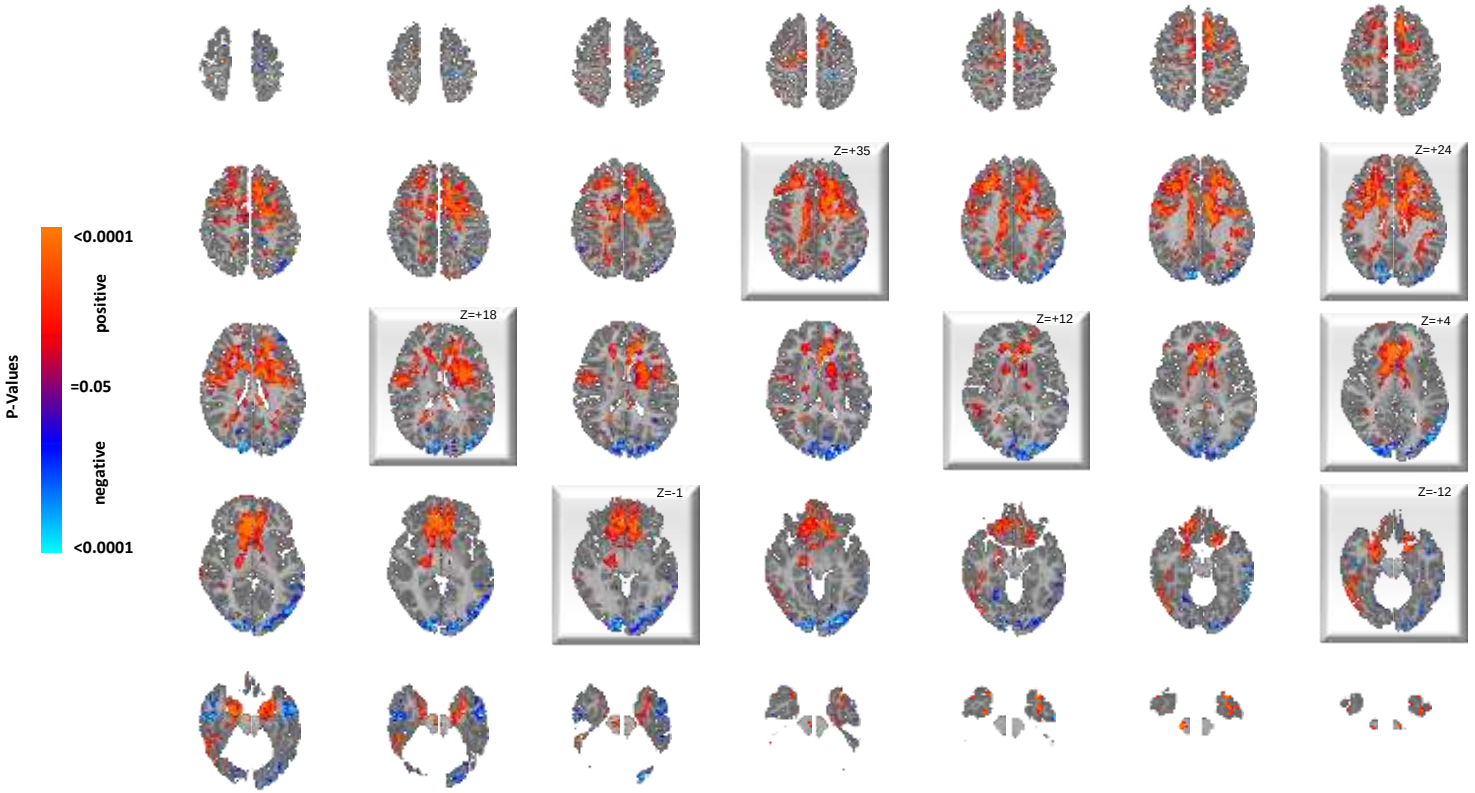

Supplementary Figure S32. Effects of Diagnosis on rCBF while Excluding ASD Participants Taking Any Psychotropic Medication
This map shows in all slices the statistically significant differences in rCBF values between a subset of the ASD group (N=29, 22 males, 7 females, mean age 23.7 years) who were not taking any psychotropic medications at the time of the MRI scan and all TD controls (N=65, 49 males, 16 females, mean age 21.6 years) while covarying for age and sex, displayed at a threshold of P<0.05 after correction for multiple comparisons. Voxels in red indicate significantly increased rCBF, and blue voxels reduced rCBF, in ASD relative to controls. Highlighted slices (with their z-level Talairach coordinates) are those displayed in Figure 1 of the main text.

ACCEPTED MANUSCRIPT

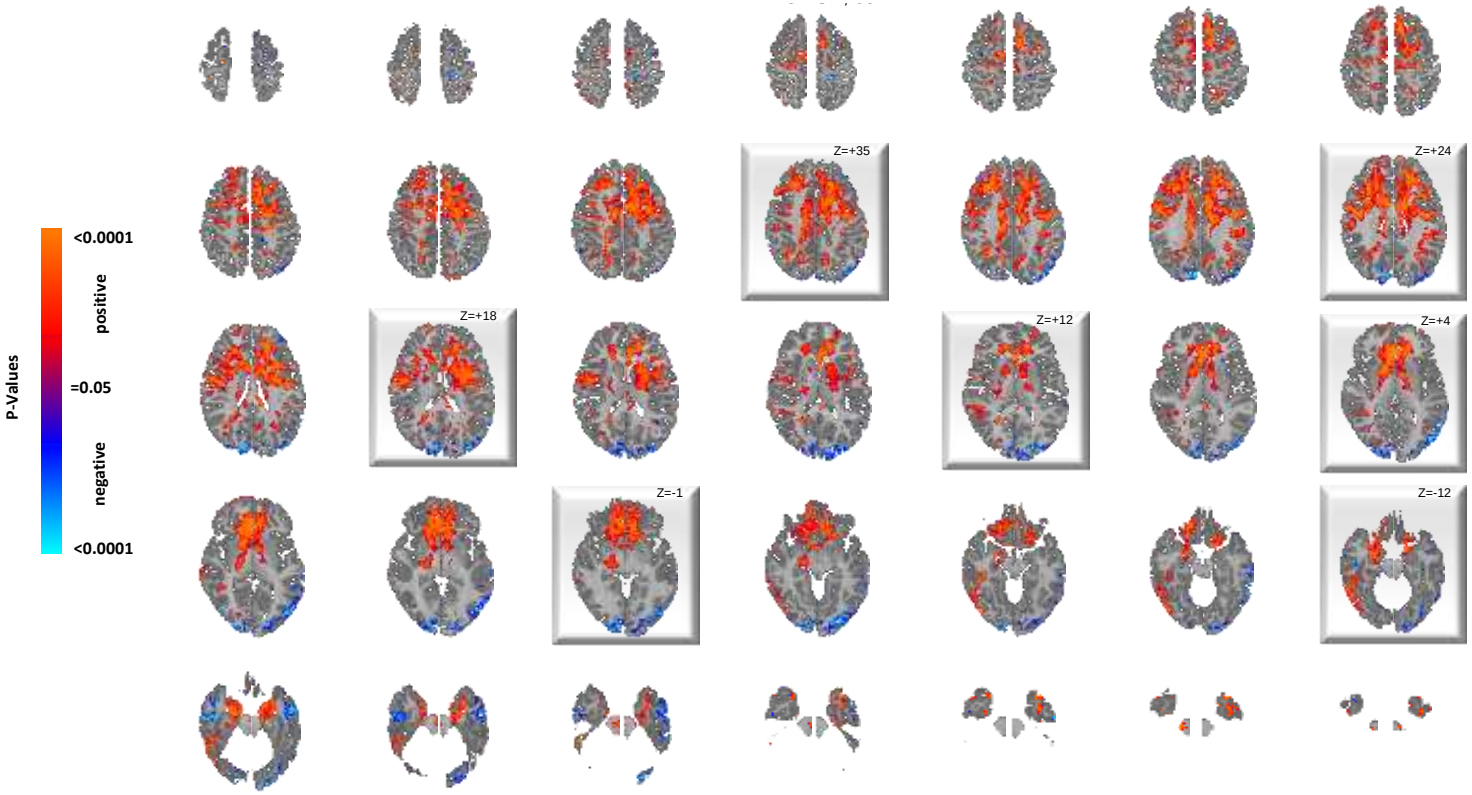

Supplementary Figure S33. Effects of Diagnosis on rCBF while Covarying for the Use of Any Psychotropic Medication at the Time of MRI Scan

This map shows in all slices the statistically significant differences in rCBF values between the ASD group (N=43, 31 males, 12 females, mean age 25.3 years) and TD controls (N=65, 49 males, 16 females, mean age 21.6 years) while covarying for age, sex, and the use of any psychotropic medication at the time of MRI scan, displayed at a threshold of P<0.05 after correction for multiple comparisons. Voxels in red indicate significantly increased rCBF, and blue voxels reduced rCBF, in ASD relative to controls. Highlighted slices (with their z-level Talairach coordinates) are those displayed in Figure 1 of the main text.

ACCEPTED MANUSCRIPT

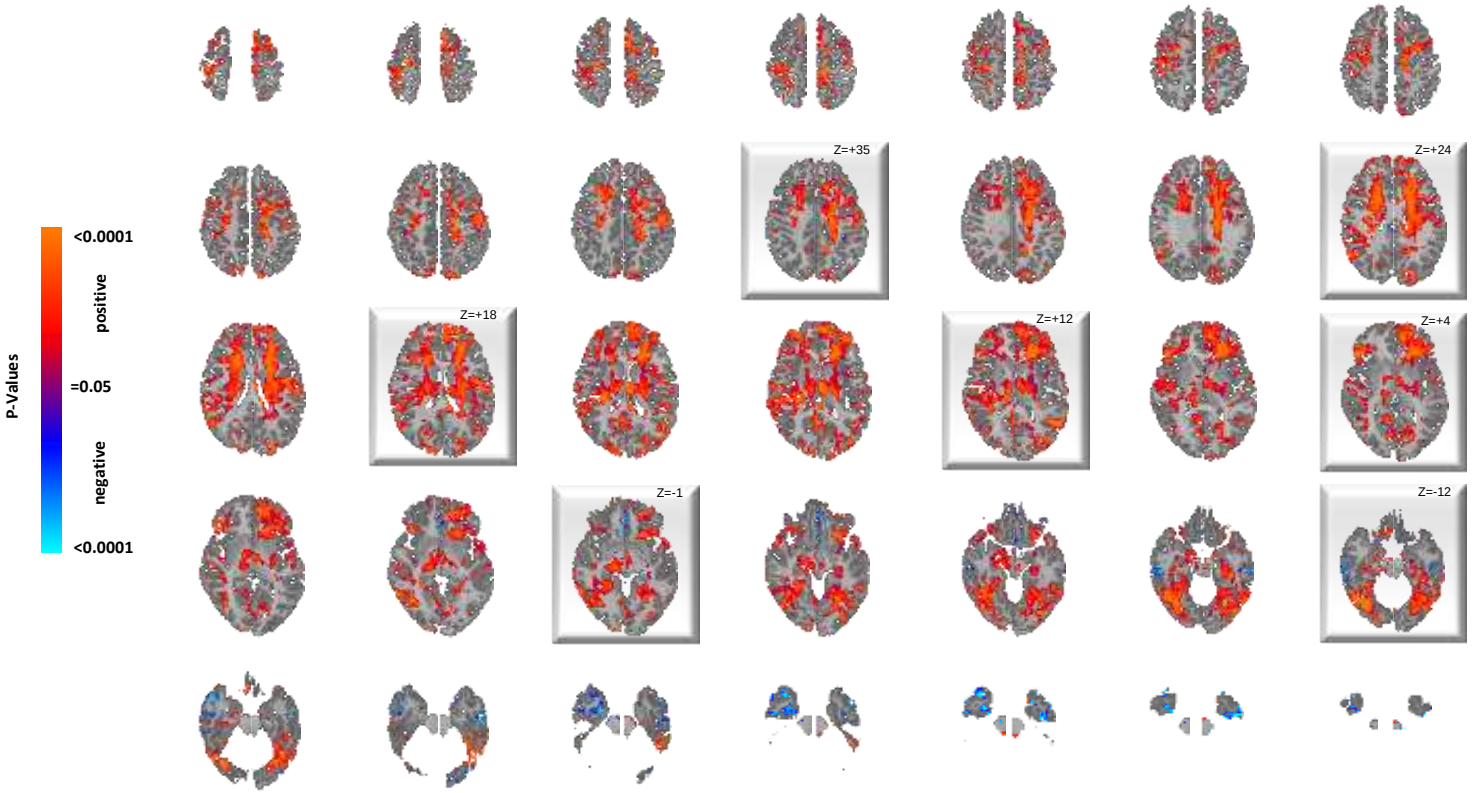

Supplementary Figure S34. Correlation of rCBF with ADOS Total Scores while Excluding ASD Participants Taking Any Psychotropic Medication
This map shows in all slices the statistically significant correlations of ADOS Total scores with rCBF values, while covarying for age and sex, in a subset of the ASD group (N=28, 21 males, 7 females, mean age 23.0 years) who were not taking any psychotropic medications at the time of the MRI scan, displayed at a threshold of P<0.05 after FDR correction for multiple comparisons. Red and blue voxels represent, respectively, significant positive or inverse correlations of ADOS Total scores with rCBF values in the ASD group. Highlighted slices (with their z-level Talairach coordinates) are those displayed in Figure 1 of the main text.

ACCEPTED MANUSCRIPT

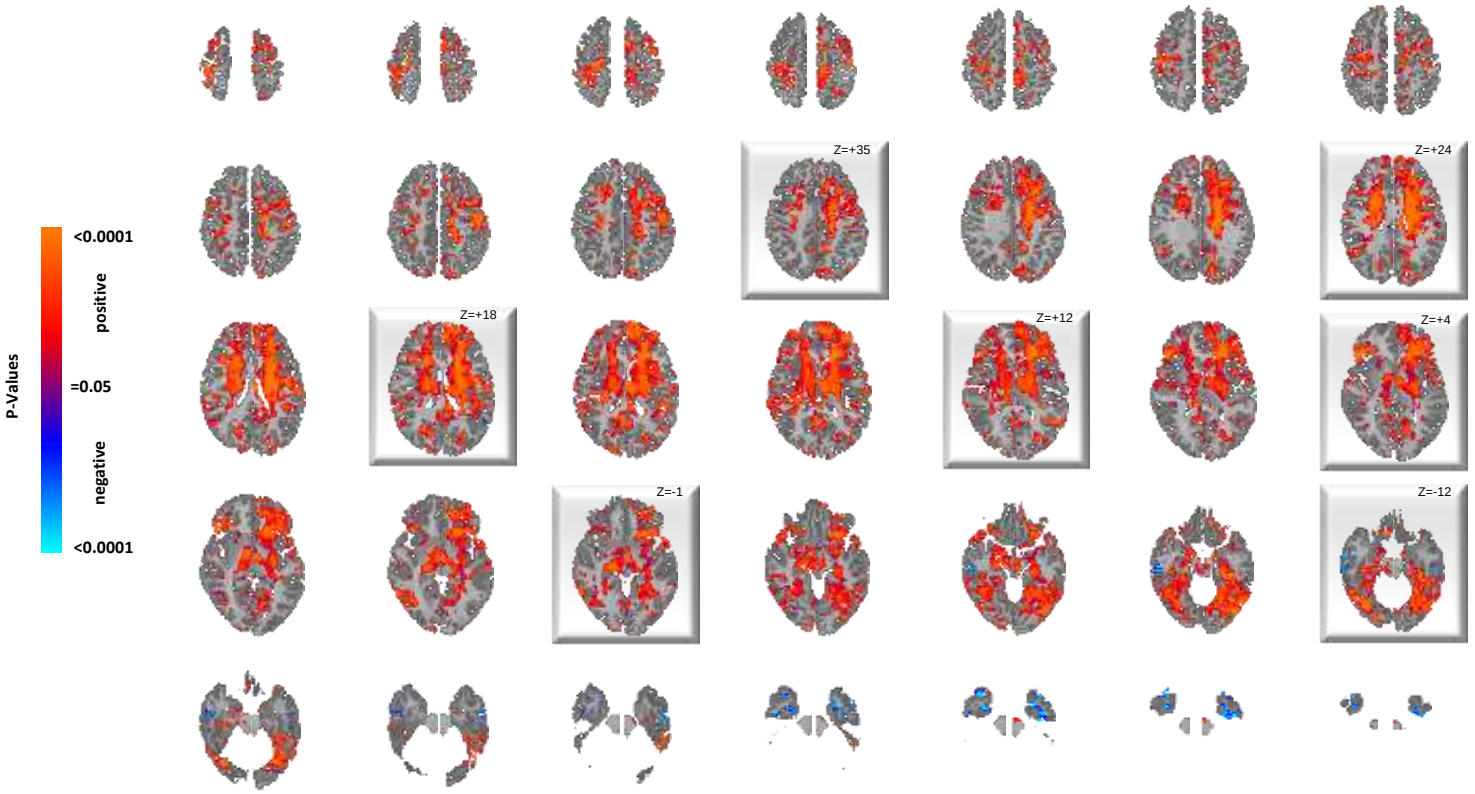

Supplementary Figure S35. Correlation of rCBF with ADOS Total Scores while Covarying for the Use of Any Psychotropic Medication
This map shows in all slices the statistically significant correlations of ADOS Total scores with rCBF values, while covarying for age and sex, for all participants in the ASD group (N=41, 30 males, 11 females, mean age 24.9 years) while covarying for age, sex, and the use of any psychotropic medication at the time of MRI scan, displayed at a threshold of P<0.05 after FDR correction for multiple comparisons. Red and blue voxels represent, respectively, significant positive or inverse correlations of ADOS Total scores with rCBF values in the ASD group. Highlighted slices (with their z-level Talairach coordinates) are those displayed in Figure 1 of the main text.

ACCEPTED MANUSCRIPT

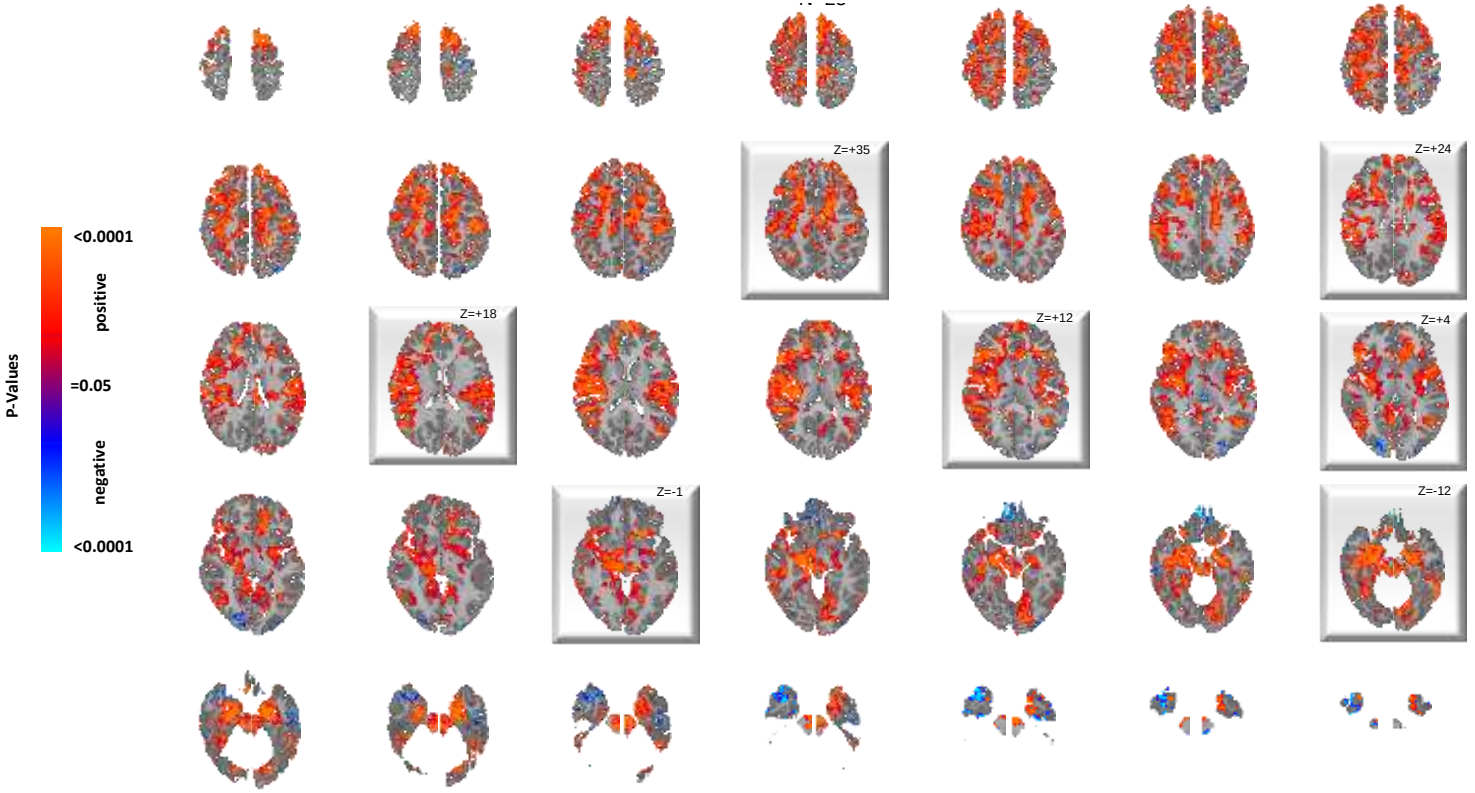

Supplementary Figure S36. Correlation of rCBF with SRS Awareness Scores while Excluding ASD Participants Taking Any Psychotropic Medication
This map shows in all slices the statistically significant correlations of SRS Awareness scores with rCBF values, while covarying for age and sex, in a subset of the ASD group (N=25, 19 males, 6 females, mean age 25.1 years) who were not taking any psychotropic medications at the time of the MRI scan, displayed at a threshold of P<0.05 after FDR correction for multiple comparisons. Red and blue voxels represent, respectively, significant positive or inverse correlations of SRS Awareness scores with rCBF values in the ASD group. Highlighted slices (with their z-level Talairach coordinates) are those displayed in Figure 1 of the main text.

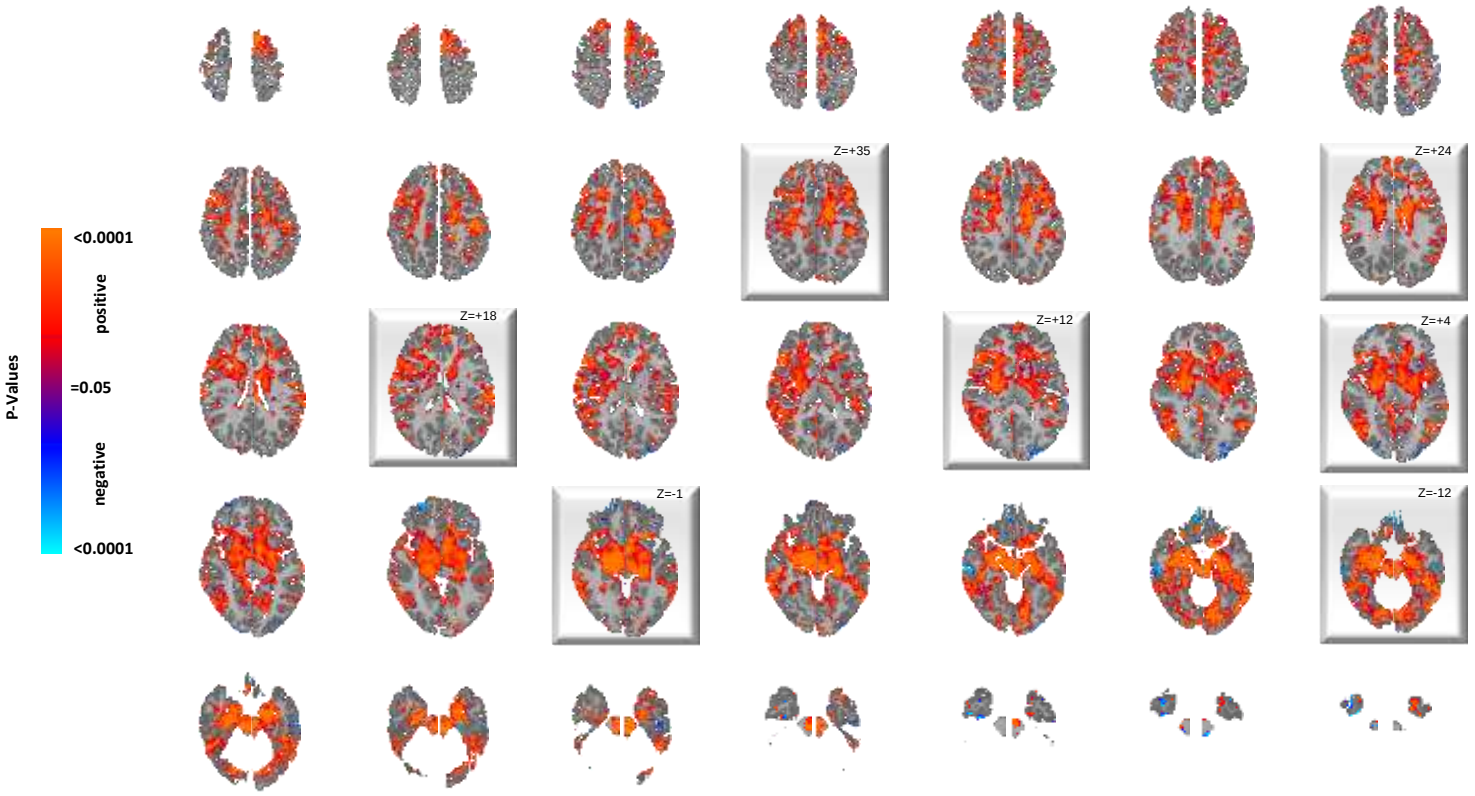

Supplementary Figure S37. Correlation of rCBF with SRS Awareness Scores while Covarying for the Use of Any Psychotropic Medication
This map shows in all slices the statistically significant correlations of SRS Awareness scores with rCBF values, while covarying for age and sex, for all participants in the ASD group (N=38, 27 males, 11 females, mean age 26.4 years) while covarying for age, sex, and the use of any psychotropic medication at the time of MRI scan, displayed at a threshold of P<0.05 after FDR correction for multiple comparisons. Red and blue voxels represent, respectively, significant positive or inverse correlations of SRS Awareness scores with rCBF values in the ASD group. Highlighted slices (with their z-level Talairach coordinates) are those displayed in Figure 1 of the main text.

ACCEPTED MANUSCRIPT

Supplemental Materials Section 6c:

Total Cortical Gray and White Matter Volumes Added to Base Model

ACCEPTED MANUSCRIPT

ACCEPTED MANUSCRIPT

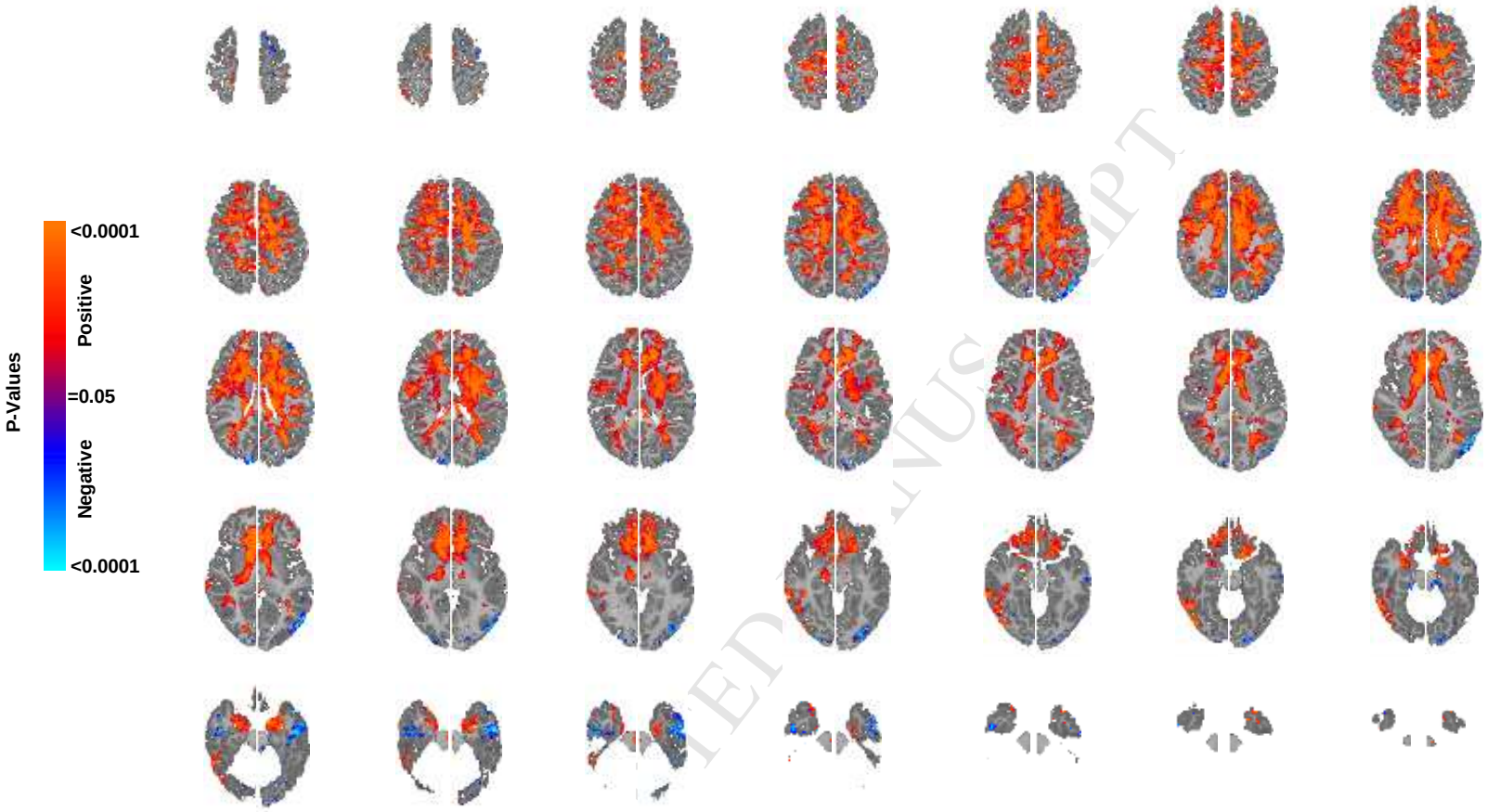

Supplementary Figure S38. Effects of Diagnosis on rCBF while Covarying for Total Cortical Gray Matter Volume
This shows the statistically significant differences in rCBF values between the ASD group and TD controls for all slices while covarying for age, sex, and total cortical gray matter volume, displayed at a threshold of P<0.05 after correction for multiple comparisons. Voxels in red indicate significantly increased rCBF, and blue voxels reduced rCBF, in ASD relative to controls.

ACCEPTED MANUSCRIPT

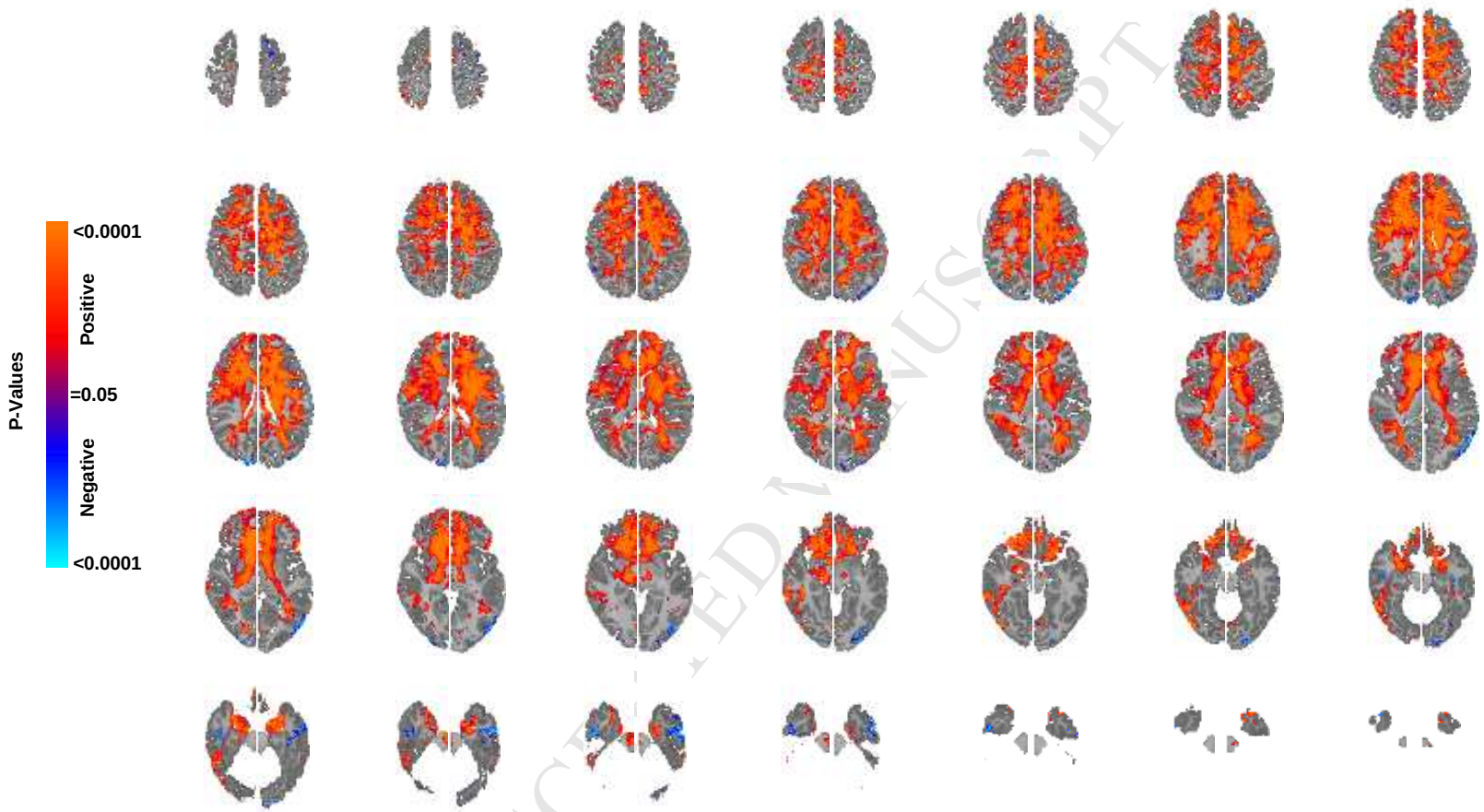

Supplementary Figure S39. Effects of Diagnosis on rCBF while Covarying for Total White Matter Volume
This shows the statistically significant differences in rCBF values between the ASD group and TD controls for all slices while covarying for age, sex, and total white matter volume, displayed at a threshold of P<0.05 after correction for multiple comparisons. Voxels in red indicate significantly increased rCBF, and blue voxels reduced rCBF, in ASD relative to controls.

ACCEPTED MANUSCRIPT

Supplemental Materials Section 7:
Primary Analyses Separately in Youth and Adults

ACCEPTED MANUSCRIPT

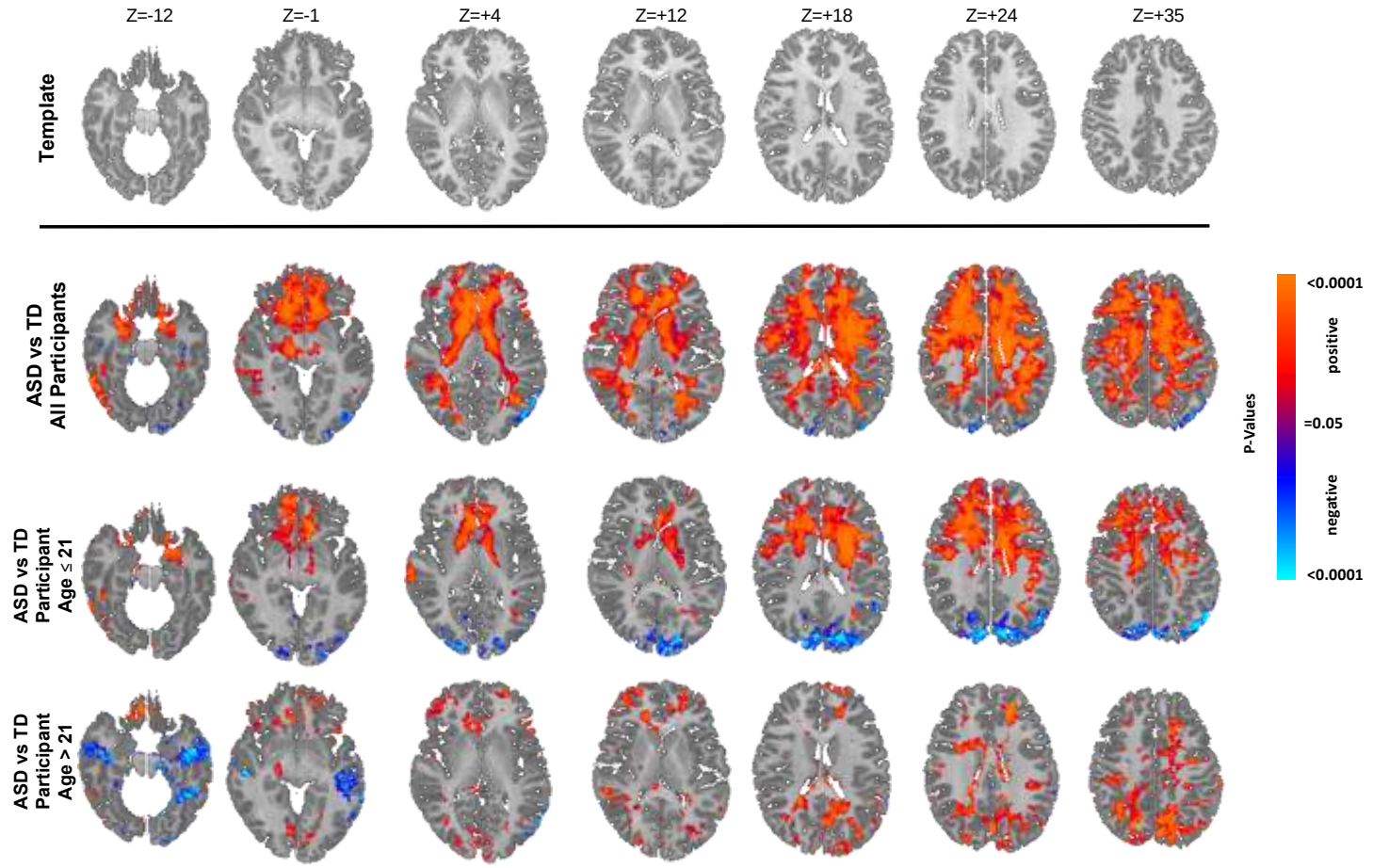

Supplementary Figure S40. Main Effect of Diagnosis Within Different Age Groups

This shows the statistically significant differences in rCBF values between the ASD group and TD controls while covarying for age and sex, separately in youth (≤21 years) and adults (>21 years), displayed at a threshold of P<0.05 after correction for multiple comparisons. Voxels in red indicate significantly increased rCBF, and blue voxels reduced rCBF, in ASD relative to controls.

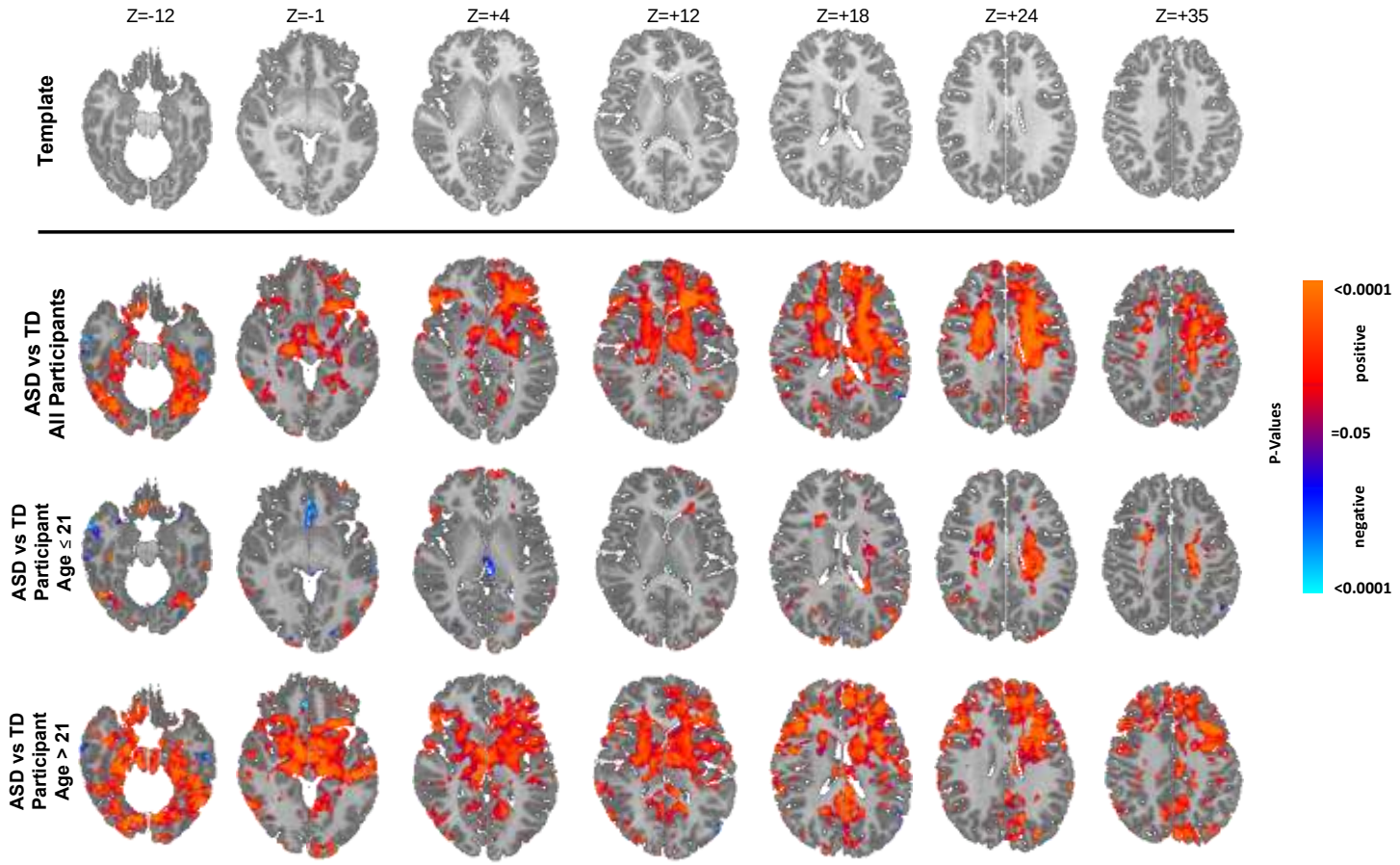

Supplementary Figure S41. Correlation of rCBF with ADOS Total Scores Within Different Age Groups

Red and blue voxels represent, respectively, significant positive or inverse correlations of ADOS total scores with rCBF values separately in youth (≤ 21 years) and adults (>21 years) of the ASD group, after FDR correction for multiple comparisons.

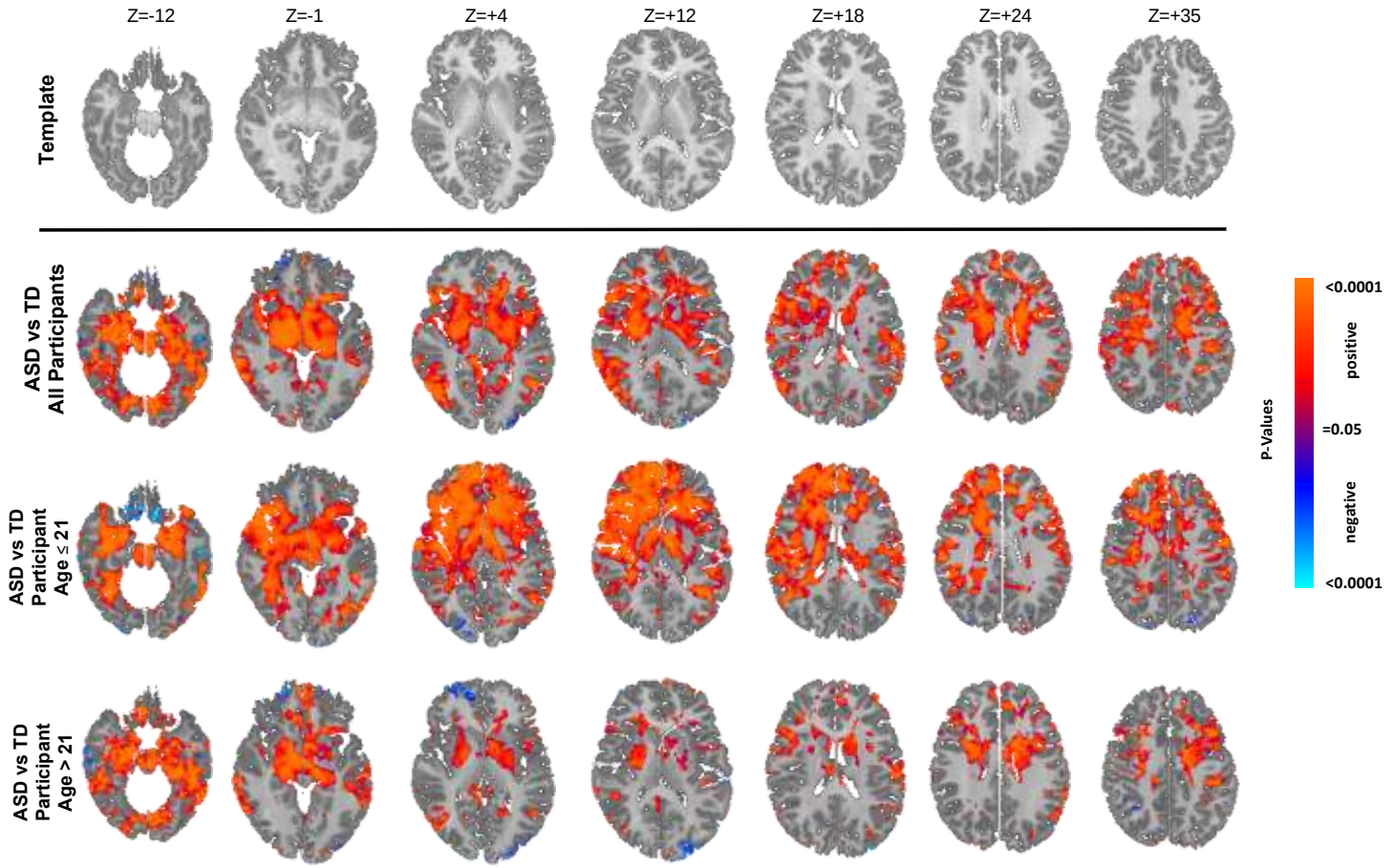

Supplementary Figure S42. Correlation of rCBF with SRS Awareness Scores Within Different Age Groups

Red and blue voxels represent, respectively, significant positive or inverse correlations of SRS Awareness scores with rCBF values separately in youth (≤ 21 years) and adults (>21 years) of the ASD group, after FDR correction for multiple comparisons.